3D Electron Beam Lithography for Biomedical Applications

By

Khodr Maamari
B.S., University of Illinois at Chicago, 2012
M.S., University of Illinois at Chicago, 2014

THESIS

Submitted in partial fulfillment of the requirements
for the degree of Doctor of Philosophy in Electrical and Computer Engineering
in the Graduate College of the
University of Illinois at Chicago, 2015

Chicago, Illinois

Defense Committee:

Vitali Metlushko, Chair and Advisor
Jeremiah Abiade, Mechanical and Industrial Engineering
Michael Stroscio, Electrical Engineering
Michael Cho, Bioengineering
Ernesto Indacochea, Civil and Materials Engineering

ACKNOWLEDGMENTS

I would like to express the deepest appreciation to my committee chair Professor Vitali Metlushko. He continually and persuasively conveyed a spirit of adventure in regard to research and scholarship, and an excitement in regard to teaching. Without his supervision and constant help this dissertation would not have been possible.

I would also like to express my sincere gratitude to my committee members, Professor Jeremiah Abaideh, Professor Ernesto Indacochea, Professor Micheal Cho, and Professor Michael Stroscio for providing their valuable time and guidance.

Immeasurable appreciation and deepest gratitude for my parents, Jamal and Waad Maamari, for their endless support, continuing encouragement, and advising. Without your help, none of my achievements would be possible. Also my sisters, Diana and Zeina Maamari, for their help and support through my entire life.

Very special thanks to the Head of the Electrical and Computer Engineering Department Professor Rashid Ansari, and the Director of Undergraduate Studies, Professor Vahe Caliskan, for their help, support.

ACKNOWLEDGMENTS (Continued)

I would also like to thank the Nanotechnology Core Facility Director Dr. Antonio DiVenere for his help and support. The lab manager, Dr. Seyoung An, for all the training, assistance, and consultation that he provided. The graduate research assistant Albert Colon for his help and support. Last but not least, I would like to thank all my family members and friends for all their support.

KM

TABLE OF CONTENTS

TABLE OF CONTENTS (Continued)

TABLE OF CONTENTS (Continued)

LIST OF FIGURES

LIST OF FIGURES (Continued)

LIST OF FIGURES (Continued)

LIST OF FIGURES (Continued)

LIST OF FIGURES (Continued)

LIST OF FIGURES (Continued)

LIST OF FIGURES (Continued)

LIST OF FIGURES (Continued)

FIGURE **PAGE**

NOMENCLATURE

AFM	Atomic Force Microscopy
AM	Additive Manufacturing
CAD	Computer Aided Design
CAGR	Compound Annual Growth Rate
DNA	Deoxyribonucleic Acid
DUV	Deep Ultra Violet
EBL	Electron Beam Lithography
EHT	Extra High Tension
FDA	Food and Drug Administration
FE	Field Emission
FIB	Focused Ion Beam
IR	Infrared
MEMS	Micro-Electro-Mechanical Systmes
MIBK	Methyl IsoButyl Ketone
MW	Molecular Weight
NCF	Nanotechnology Core Facility
PDMS	Poly-Di-Methyl-Siloxane
PMMA	Poly(Methyl MethAcrylate)
POF	Plastic Optical Fiber
PR	Photoresist
RPM	Round Per Minute
SEM	Scanning Electron Microscope
SNR	Signal to Noise Ratio

NOMENCLATURE (continued)

SOG	Spin On Glass
STM	Scanning Tunneling Microscope
TE	Thermionic Emission
TFE	Thermionic Field Emission
TPA	Two Photon Absorption
UIC	University of Illinois at Chicago
UV	Ultra Violet
VLSI	Very Large Scale Integration
XUV	Extreme Ultra Violet

SUMMARY

Three dimensional fabrication has recently been the main focus for a wide variety of research. Most techniques available in the market is limited to the materials that could be used and/or to the resolution that could be achieved. These techniques are not capable of fabricating structures with high resolution, below 100 nm. A new state of the art high aspect ratio 3D fabrication technique has been developed based on the electron beam lithography system (EBL) available at the Nanotechnology Core Facility at University of Illinois at Chicago. This new 3D method allows to fabricate structures with a resolution on the order of magnitude better than those available now in the market, such as 3D printers. The process requires a multiple parameter optimization, including exposure dose modulation, the number of the resist layers; thermal processing etc., and requires not only knowledge of electron beam interaction, electron backscattering, but also the understanding of physics and chemistry of the resist on the nanoscale. There are only a handful groups in the world that are capable of fabricating high aspect ratio 3D nanostructures with resolution on the order of few nanometers. This new 3D approach paves the road for future research that requires high aspect ratio 3D nanostructures especially those aimed for biomedical applications.

CHAPTER 1

INTRODUCTION TO 3D PRINTING

Three dimensional (3D) fabrication has been a hot topic for a lot of researchers and industrial manufacturers for its wide usage and high importance. Over the years, researchers have developed various techniques that enable them to fabricate complicated 3D structures. 3D fabrication is also known as additive manufacturing (AM). Additive manufacturing are automated process where the user can first design a structure using computer aided design (CAD) software. Then, this software translates the virtual design to a machine language. Since the structure will be fabricated layer by layer, the software usually converts the design into multi-layers [1], [2], [3]. The more layers a machine can fabricate at a certain height, the higher vertical resolution it could achieve. As of April 2013, Marketsandmarkets listed on its website that "the AM is a potentially growing market in every manufacturing sector with a global additive manufacturing market of $1,843.2 million in 2012 and is expected to grow at a [compound annual growth rate] (CAGR) of 13.5% to reach $3,471.9 million by 2017" [4]. With the presence of 3D fabrication, it is possible to create complex structures with no limits on creativity. However, the designer should be aware of the physical aspect of the structure, since some structures might not be physically stable even though on the software the design looks stable. In the following paragraphs, different 3D printing techniques are presented with their advantages and limitations.

1.1 3D Printing

3D printers were first being used in industry due to their high cost and because they are relatively large sized equipment. They were and still being used to create rapid prototypes and for research purposes. There is a wide variety of materials that could be 3D printed such as powdered metals, plastics, polymers, food, etc. However, some printers are specialized for only one material either because it is not equipped to print other materials, or to avoid cross contamination. One of the main reasons why 3D printing has become one of the major topics in the industry production is because it allows the user to fabricate any structure by using a CAD software, which is easy to use and doesn't require a lot of training. After the user designs the structure, the computer translates the design to the machine language and the machine starts to execute the orders. Its operation is similar to the operation of a regular printer. The material deposited should be either in powder form or viscous liquid so it can easily flow from the printer head also known as gun nozzles. After the material is deposited it is cooled down in order for it to solidify and become ridged [5]. However, some materials requires post processing for it to harden such as powdered metal. During the deposition, the nozzle is moved along the x-axis and the y-axis to deposit the first layer. Then the stage, where the deposition is taking place, lowers in a fraction of a millimeter in the z-axis to perform the deposition of the second layer. The following images represent how the 3D printing functions.

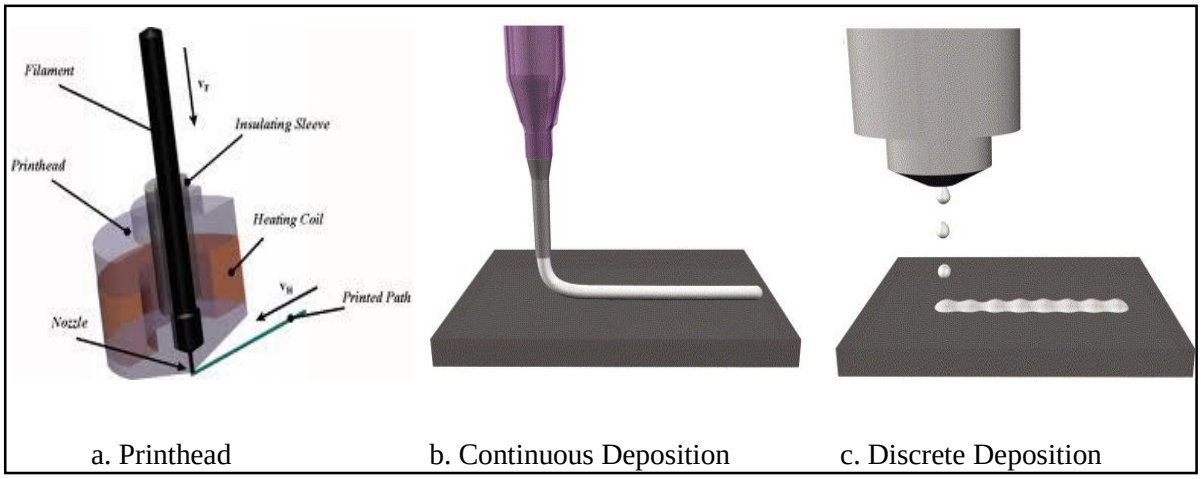

a. Printhead b. Continuous Deposition c. Discrete Deposition

Figure 1. A representation of 3D Printer printhead for continuous and discrete deposition.

As can be seen in figure 1, the filament is heated in order to melt the material passing through it using a heating coil. The insulating sleeve protects the heated material from being exposed to the outside environment. The enclosing body is called the printhead. In addition, there are two different deposition methods: continuous deposition, as shown in figure 1b, where the nozzle squirts the material continuously and discrete deposition, as shown in figure 1c, where the nozzle squirts droplets of the material which then combine to form a continuous layer.

Some of the materials that are mainly being used are plastics, wax and foundry sand. The size of the 3D printers is getting smaller and smaller, and reached the size of a copier machine. There is a wide variety of applications were 3D printers can be used. These applications ranges from engineering, construction, architecture, aerospace, to dentistry, human tissue replacement, to fashion, and much more. Even though 3D printers seems user friendly; however, the user should have a deep understanding of the whole process and not just the software used for the designing

process. For example, on a CAD software an angle could look like a 90 degree turn; however, in reality after the printing is done, it looks more like a curve turn instead of a sharp angle. On the Wall Street Journal Guth says that "one issue is that certain details on design, such as a flowing cape, that look fine on a computer screen are tricky for printers to handle" [6]. Moreover, the materials used and the process involved in depositing these materials often limits the resolution of the 3D printers. One of the commercially available 3D printers can reach around 16 µm in layer thickness and an accuracy of 20 µm for structures that are below 50 mm [7]. However, such printers are usually expensive and require special environment to operate. This is one of the main drawbacks why 3D printers are not currently being used in order to fabricate structures on the sub-micron feature size.

1.2 3D Fabrication Using Laser Lithography

3D fabrication using a laser source started as a theory predicted by Maria Goeppert-Mayer in her doctoral dissertation in 1931 [8]. However, the first experimental results that were able to prove this theory occurred 30 years later. 3D fabrication using a laser source is mostly known as two photon absorption (TPA). TPA is a process in which the photoresist (PR) absorbs two photons and changes its physical state from liquid to solid, due to a chemical reaction[9], [10], [11]. A photon is a quantization of energy. It can be examined as a particle with zero rest mass that carries energy. This energy, when present, is then absorbed by the photoresist which allows the electron to be excited to a virtual energy state. When a second photon is absorbed by the photoresist the electron gains more energy and is excited to a second energy state. At this point, there is enough energy to create a chemical reaction. The component in the photoresist that absorbs this energy is called initiator. The initiator is required to initiate the chemical reaction. Once the initiators receive

the required energy, they start to form bonds with neighboring initiators to form radicals. Another component of the photoresist is called monomer. Monomer is a Greek word that stands for one part and when it is chemically bind with another chemical it becomes a polymer which stand for many parts. The monomers are usually in the form of acrylic groups where carbon atoms are bonded together with a double bond. The radicals break the bond between the carbon atoms and create another radical at the end of each monomer, which then combines with another monomer. This chain reaction, also known as polymerization, continues until the chained radical meets another neighboring radical. Polymerization takes place only when the energy absorbed is sufficient to excite the electrons within the initiators. Polymerization propagates randomly in space and can't be controlled where to terminate. It automatically stops when two radicals meet each other. This is one of the limitations that doesn't allow us to reach high resolution feature sizes. In addition, the speed of this chemical reaction is directly "proportional to the square of the photon density at each position in the resin" [12] (Maruo, p132-134). Polymers are usually solid in nature, so when the resist is exposed to photons it changes from liquid to solid state. The source of the photons is usually a laser beam; however, there is no unique laser source. As long as the photons can supply enough energy to initiate the chemical reaction then the laser source could be used. Different laser sources has been tested to get better resolution such as, near infrared (IR laser), deep ultraviolet (deep UV), extreme UV (XUV), He-Cd laser, Ti:sapphire, etc. Moreover, there is more than one type of photoresist that could be used. For example: in [12], the resin used was SCR-500 from Japan Synthetic Rubber Company Ltd. The laser source was a mode-locked Ti:sapphire laser with 790 nm oscillating wavelength, pulse width of 200 fs, repetition rate of 76 MHz, and peak power of 50 kW. The spiral wire's width fabricated by Shoji was around 1.3 μm. "[The] spatial resolution of the [method] proposed is limited by the radical diffusion and growth

of polymer chains outside the illuminated region" [12] (Maruo, p132-134). In two photon absorption technique, it turned out to be that the resolution of the 3D structure fabricated is not only limited by absorption and light diffraction but also by the spherical aberration which imposes the main limitation. In addition, theoretically the initiation of the chemical reaction should start where the laser beam is focused; however, the experimental results show that the light absorption was present in non-focused points which furthermore limits the resolution.

There are two methods to create 3D structures using TPA. In both methods, the user creates the design in a CAD tool which then is translated by the computer to the hardware controlling the laser and the stage.

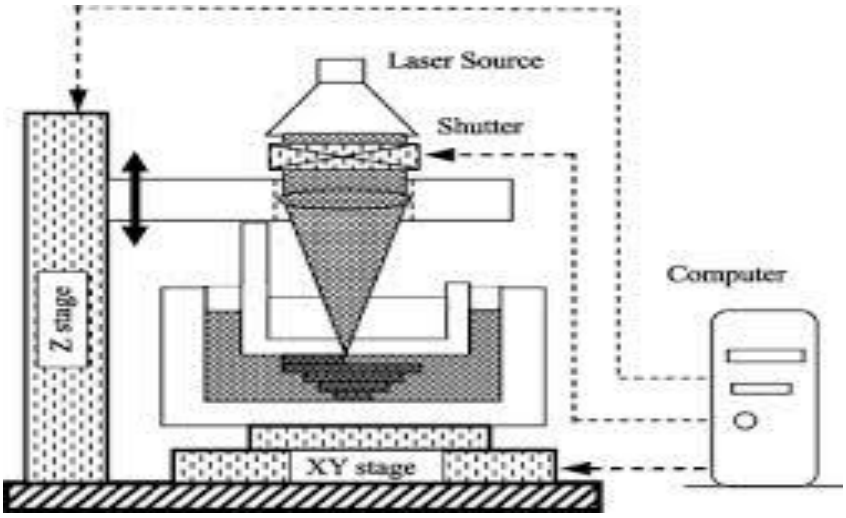

Figure 2. 3D laser fabrication schematic diagram.

Shown in figure 2 is the setup for a 3D laser fabrication which consists of a computer connected to the stage, lenses and shutter. Lenses have been used in order to focus the laser at a sharp point with small dimensions [13]. The smaller the dimensions the higher the resolution. When the lens is moved, the focal point where the light rays converges is moved accordingly. One way to achieve 3D structures is by moving the lens, which limits the resolution to how fast the laser converges at the new spot desired. Another way to achieve 3D structure is by moving the stage. In order to move the stage precisely, a piezoelectric stage is used. A piezoelectric is a material that changes its physical structure when biased by electric voltage or vice versa. It can be controlled along the x, y and z axis depending on the bias. Other stage control could be used to get a higher precision movement, such as laser controlled stages; however, price increases almost exponentially when trying to achieve higher precision. Whether it's the movement of the stage or the lens, we are limited to the chemical lateral solidification of the resin which can't be controlled precisely. So another way has been used to achieve better resolution, which is exposing the photoresist layer by layer. First, the stage is moved all the way to the top of the photoresist chamber, which is usually made from glass. It will then be lowered until a thin layer of photoresist is present which will then be exposed. Second, the stage lowers to a certain distance so that a fresh layer of the photoresist is covering the previous layer and then this new layer is exposed and so on. In this process the resolution is limited to the thickness of the new layer photoresist which overlaps the previous layer. The photoresist is viscous in nature due to its chemical composition, so it is almost impossible to get a thin submicron layer of photoresist by just lowering the stage. The depth resolution reported by Ikuta et al. is limited to 5 um [14], which is not desired when trying to fabricate precise features on the nano-scale. The thickness of the new layer can't be controlled and is relatively thick since it is not being spun. If the photoresist is being spun, it could

reach a thickness of sub-micrometer range, but still this thickness is relatively high if you are trying to achieve high resolution features. Moreover, the laser beam could lose energy before reaching the focal point so more power has to be delivered. When more power is supplied, solidification on the glass chamber could occur and form an opaque layer that blocks the laser from reaching its destination and limits the re-usage of the glass chamber. Moreover, the photoresist is not reusable since it is being solidified in the areas where the laser is out of focus which limits the resolution and increases the chemical wastes. Another proposed method is single photon absorption where the energy supplied by one photon is enough to initiate the polymerization. This method turned out to be cheaper due to the availability of lower cost laser source. However, resolution limitations remain the same as two photon absorption. In most cases, the feature size and resolution of machining are around 0.43 um [12]. According to theoretical analysis, the best resolution is around half of the laser wavelength. "One of the reasons for the limited resolution is the diffraction limit of the laser beams in the far field, where the target surface from the optical element is greater than the optical wavelength" [15] (Li, p 735-755) which is given by Abbe's equation:

$$d = \frac{\lambda}{2n\sin\theta} \tag{1.1}$$

where d is the diameter of the smallest beam spot, λ is the wavelength of the laser used, n is the index of refraction of the medium through which the beam travels to reach its target and θ is the angle divergence of the beam. In order to get a better resolution, different laser sources has been tested such as "deep ultra violet (DUV, ArF 193nm), extreme ultraviolet Xe or Sn plasma systems with a 13nm wavelength, and near infrared lasers" [15] (Li, p 735-755). One issue with these sources is that they are expensive, have relatively low power, and unstable in intensity. Multiple

lenses has been used to focus lasers and reduce the diameter; however, this process is limited by the lens physical characteristics in which it can't focus the laser into a smaller diameter. The smallest beam size achieved was in 2001 by Lo and Wang, who were able to demonstrate 128 nm resolution fabrication [16]. Moreover, the resolution and the spot size of the focused point also depend on the distance between the laser and the photoresist, and the shape of the tip of the laser beam. The diffusion of the resin also affects the resolution of the photoresist being used. On the other hand, laser fabrication could be done without vacuum and doesn't require a lot of time to fabricate a high aspect ratio structures.

1.3 3D Fabrication Using Focused Ion Beam Lithography

Focused ion beam (FIB) lithography, was developed as a tool for high resolution lithography. FIB then was extended to accomplish other tasks such as 3D lithography [17], [18]. Spin on glass (SOG) and PMMA resists are typical photoresists for FIB lithography. Thickness of photoresist depends on the spin speed which could range from few nanometers to few millimeters. The source of energy used in FIB is usually ions. Those ions hit the surface of the resist breaking the bonds in the polymers to create monomers, which are then dissolved using a specific developer. In [19], a Gallium ion (Ga+) source was used. The minimum feature Jun et al. could obtain was around 114 nm which is on the order of magnitude higher than that achieved by the electron beam lithography (EBL) which is around 25 nm. However, the photoresists turned out to be more sensitive to FIB then EBL which makes the patterning faster. When the dosage required decreases the beam would spend less time on a specific area which makes the fabrication faster. According to [19], the sensitivity of photoresist using EBL was around 500uC/cm^2 while the sensitivity of photoresist using FIB is around 1uC/cm^2. However, it is almost impossible to achieve smaller

features than EBL due to the size of the ions being used. Moreover, there is a risk of ion implementation during FIB lithography which makes it highly undesirable since it introduces impurities in the resist or the substrate.

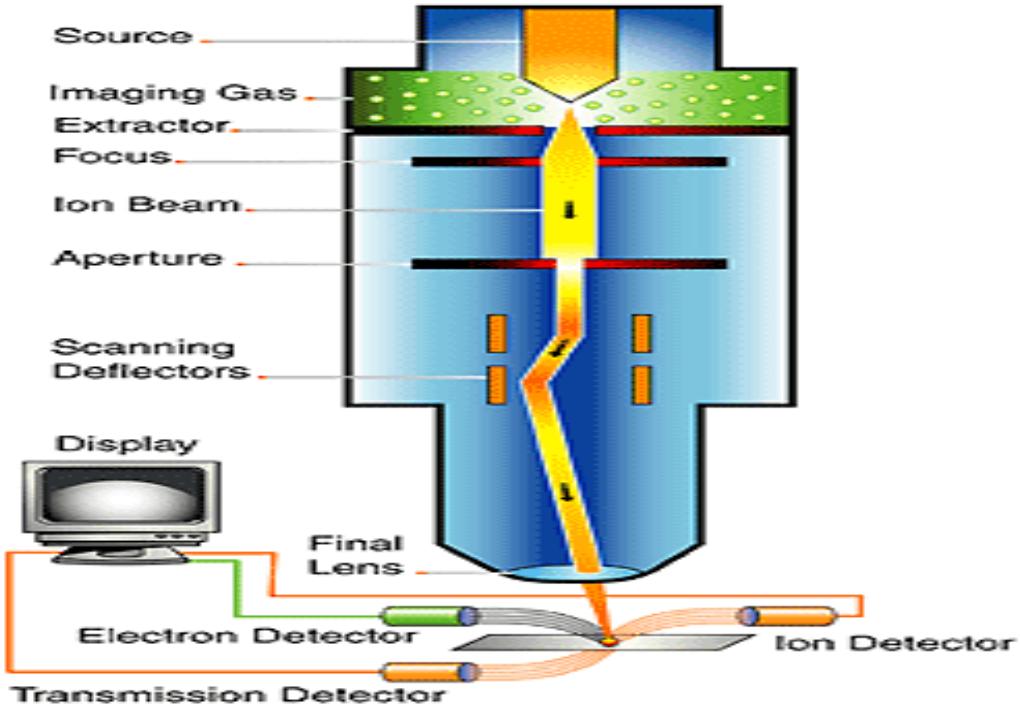

Figure 3. Focused ion beam lithography apparatus.

Shown in figure 3 is the apparatus used for FIB lithography which consists of a source, in this case is Gallium ions, imaging gas chamber, and extractor as the initial stage of producing the

Gallium beam. Following the extractor are the focusing lenses, aperture, and scanning deflectors which control the size and raster scan of the beam. The apparatus as well as the stage are controlled by a computer which also can display an image of the substrate by using electron, transmission, and ion detector.

1.4 3D Fabrication Using Atomic Force Microscopy:

Atomic force microscopy (AFM) is mainly used in order to obtain high resolution images on the scale of a fraction of a nanometer [20]. Due to the diffraction limit of light, optical microscopy is almost thousand times much worse in resolution compared to an image obtained from an AFM. It uses a cantilever with a sharp tip, around 15 nm in diameter, to probe the surface roughness. AFM is used not only for scanning images, but also is being used in biological applications such as arranging DNA molecules. Recently, researchers are trying to use AFM to fabricate 3D nano-structures. A heating element such as a resistor is fabricated on top of the cantilever. Then the tip of the cantilever is brought into contact with the photoresist. Bias is applied to heat the tip of the cantilever till it reaches the same temperature of evaporation of the resist. The resist then starts to evaporate in the point of contact. Another way to control the thickness of remaining photoresist to be heated by the AFM tip is by controlling the spring constant of the cantilever. By biasing the cantilever, the spring constant changes which causes the deflection of the cantilever tip. This method can obtain sub-micron features however feature size can't be precisely controlled due to thermal reflow from tip of cantilever to the photoresist. In addition, the tip could collect contamination from the sample which could result in increase in the diameter of the tip hence lower resolution. Moreover, during fabrication of the AFM tips, the diameter of the tip is not precisely controlled.

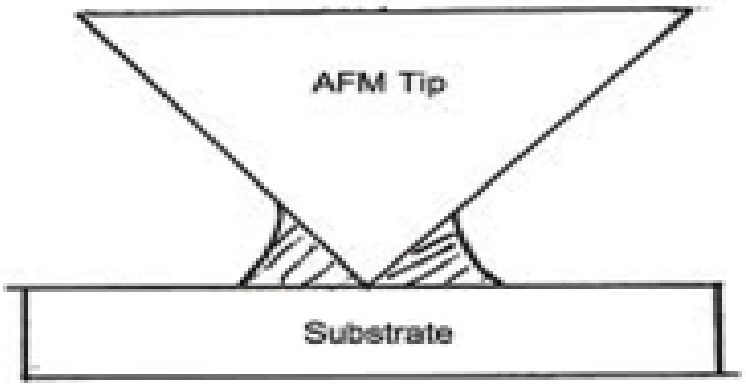

Figure 4. Atomic Force Microsocpe tip-sample interaction.

Shown in figure 4 a schematic diagram of an AFM tip and the possibility of stickness of the material on the substarte to the AFM tip.

1.5 3D Fabrication Using Bottom Up Approach

Another approach to build a 3D structure is to build it atom by atom. The first technique which enabled scientist to position atoms in certain locations was discovered by IBM scientists in April 1990. Using a scanning tunneling microscopy they were able to move each atom separately on a metal surface. The technique was demonstrated by assembling the atoms one by one to spell the letters “I-B-M” [21]. However, the technique of placing one atom on top of the other hasn’t been demonstrated yet. Even though with such technique we will be able to obtain really high resolution by building one layer of atoms on top of another layer of atoms. However, it takes enormous amount of time which makes it impractical. Another approach was to shift a

photolithography mask slowly during ultra-violet exposure. With this approach the minimum feature is around 1 um, and it is extremely difficult to create a complex 3D structure.

CHAPTER 2

ELECTRON BEAM LITHOGRAPHY

2.1 Introduction to Electron Beam Lithography

Electron beam lithography (EBL) uses a beam of electrons to directly write on the surface of a sample. It is capable of creating patterns with extremly high resolution on the order of few nanometers which is highly desired for current and future integrated circuits [22],[23],[24]. It does not require a mask to transfer the pattern to the sample. The user designs the template to be written using a CAD tool and then the EBL system excutes the design. Even though several improvemnets has been done to enhance photolithography such as liquid immersion, phase-shift masks and optical proximity correction, the next-generation lithography technique of EBL offers the best resolution. Early on, electron microscopes were being used to perform the task of an EBL system. However, nowadays there are more advanced, specialized systems which are used mainly for EBL but could also perform the task of electron microscopes with a resolution of less than 25 nm. An EBL system is a complex equipment which will be discussed in the following paragraphs.

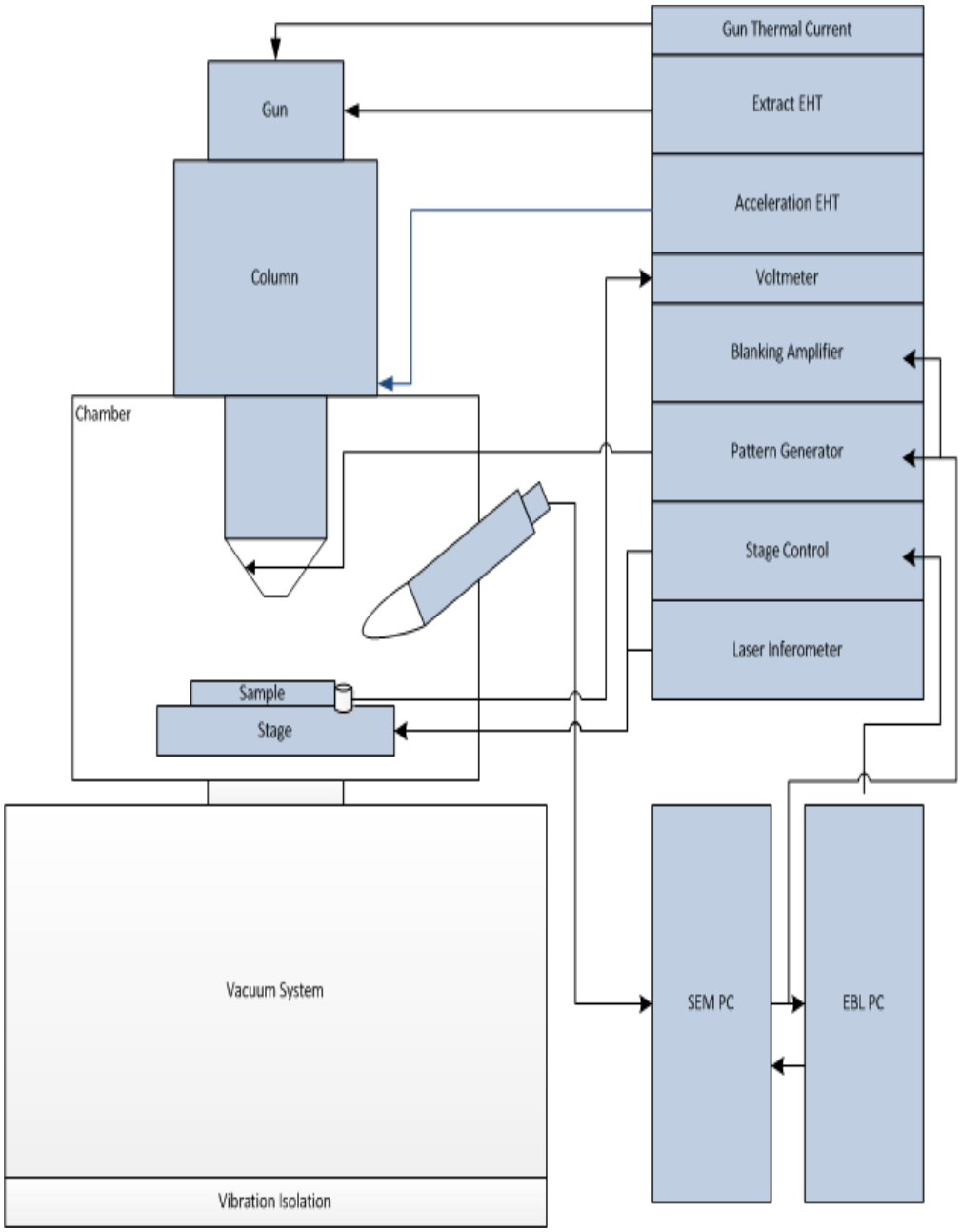

Figure 5. Electron beam lithography system schematic diagram.

2.2 Vacuum Requirement

Vacuum chamber is an essential component of an EBL system. An electron is a very small particle with a mass of 9.109 x 10^{-31} kg. It can be easily thrown off its course when it collides or interacts with the electron clouds surrownding a molecule [25]. There are about 2.4811x10^{25} molecules present in a one cubic meter at atmospheric pressure. This causes the electrons to undergo enourmous amount of collisons and cause them to deflect from their path and lose their energy and momentum. If the vacuum pressure is brought down to 1x10^{-5} Torr, there would be around 3.260x10^{17} molecules which is 8 order of magnitude less than that present at atmospheric pressure, 760 Torr. The distance travelled by an electron without colliding with the surrounding atoms or molecules is known as the mean free path (*l*). It relates to pressure according to the following formula from kinetic gas theory:

$$l = \frac{RT}{\sqrt{2}\pi d^2 N_A P} \tag{2.1}$$

where R is the univeral gas contant 8.31446 J/mol.K , T is the temperature in Kelvin, d is the diameter of the gas molecule in meters, N_A is the Avogadro's number, and P is the pressure in Pascal. In order to do a mean free path comparison, a pure nitrogen gas (N_2) enviroment can be examined knowing that normal air consists approximately 78% of N_2. Another estimation that has been done was to consider the size of an electron to be the same size of the gas molecule. It turns out that at atmospheric pressure, the mean path is around 0.1 nm compared to that in high vacuum level (10^{-5} Torr) which is around 7 m [26]. This is 70 billion times larger mean free path. This allows the vast majority of electrons to make it to their target without obsticles.

Moreover, high potentials are used in the electron gun. In order to prevent arcing and to protect the electron gun from being damaged, an insulating medium is required. The best insulating medium in this case is vacuum. The electrical breakdown of air is about 3kV/mm [27]. In high vacuum, it can be raised to 10 times higher to 30kV/mm [28]. This is an important factor in a higher power (potential) equipment. This is another important reason why EBL system requires a vacuum chamber.

In order to reach high vacuum, multiple vacuum pumps are used due to the fact that each type of pump has its own efficiency. Roughing pumps which are usually piston type are used to pump down to 10^{-3} Torr, and turbo-molecular pumps are used to pump down to higher vacuum: 10^{-5} – 10^{-7} Torr. Moreover, an ion pump is capable of reaching pressures as low as $7.5x10^{-9}$ Torr which required so that the filament doesn't get damaged. In order to reach such high vacuum level a bake-out procedure is required. During the bake-out, the walls of the chamber are heated up to an elevated temperature which help to vaporize materials and release gasses that remain in the system, such as water vapor. Even though high temperatures are prefferd during bake-out, the bake-out temperature can't exceed the temperature that the equipment can tolorate. This procedure helpes in achieving lower pressures faster since less amount of material has to be pumped out of the system.

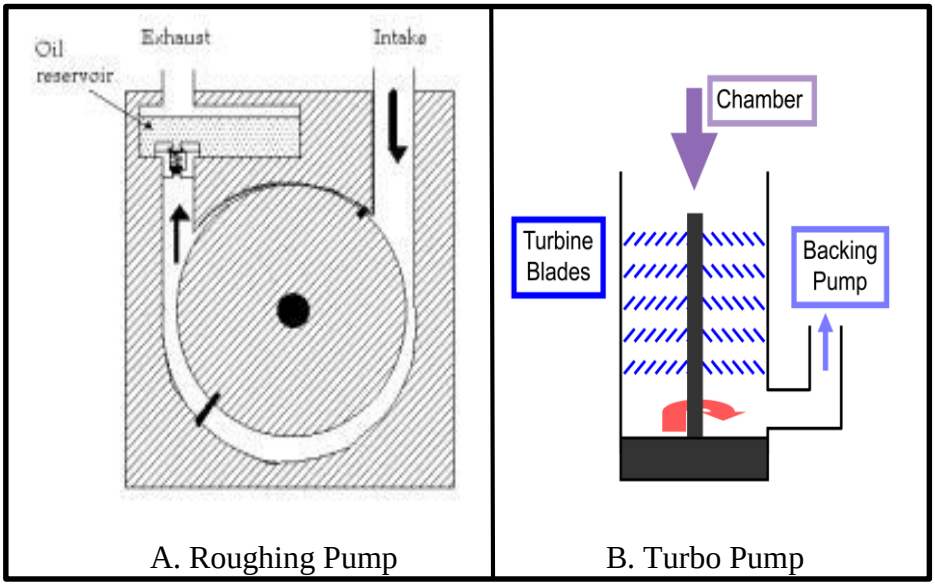

Figure 6. Representation of a Roughing pump and a Turbo pump.

The down part of the vacuum systems is that it contributes to one of the reasons why electron beam lithography is more expensive than other lithography methods, which usually can be done in a clean room at atmospheric pressure.

2.3 Electron Duality

Electrons exhibit both wave and particle properties. Electrons behave as particles in both photoelectric effect and scattering. On the other hand, electrons are affected by diffraction which gives it the wave phenomenon.

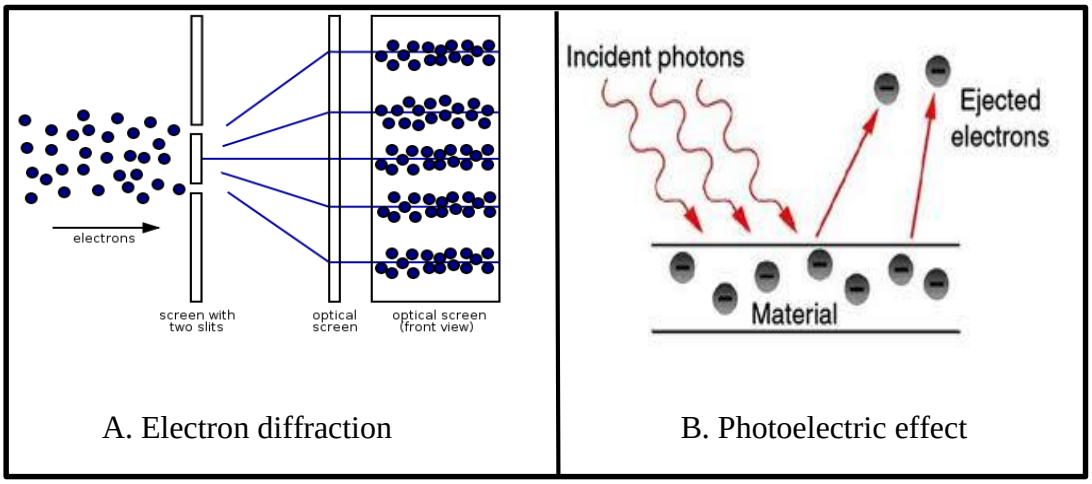

Figure 7. Electron duality, diffraction and photoelectric effect.

In order to calculate the wavelength of an electron, the deBroglie equation is used:

$$\lambda * p = h \tag{2.2}$$

where h is the Planck's constant 6.626 x 10^{-34}kg·m^2/s, p is the momentum of an electron, and λ is the wavelength of an electron.

Moreover, the momentum of an electron can be related to electron volts, which is the amount of energy that an electron gains in the presence of an electric field of 1 Volt:

$$p = \frac{V * q}{c} \tag{2.3}$$

where V is the voltage, q is the electron charge 1.602x10^{-19} C and c is the speed of light 2.9979x10^8 m/s.

A typical scanning electron microscope (SEM) accelerated by 10 kV leads to an electron with a wavelength of 0.124 nm. This means an electron has a much lower wavelength than ultra

violet (UV), deep UV, and even XUV light. With such a low wavelength, the theoretical resolution of an EBL is much better than any other lithography techniques.

2.4 Electron Emission

Electron beam lithography or Scanning electron microscopy requires an electron source which is the most vital part in an electron gun. Electron emission involves giving enough energy to an electron so that it can overcome the binding potential, or work function (ϕ), and escape from the surface of a material.

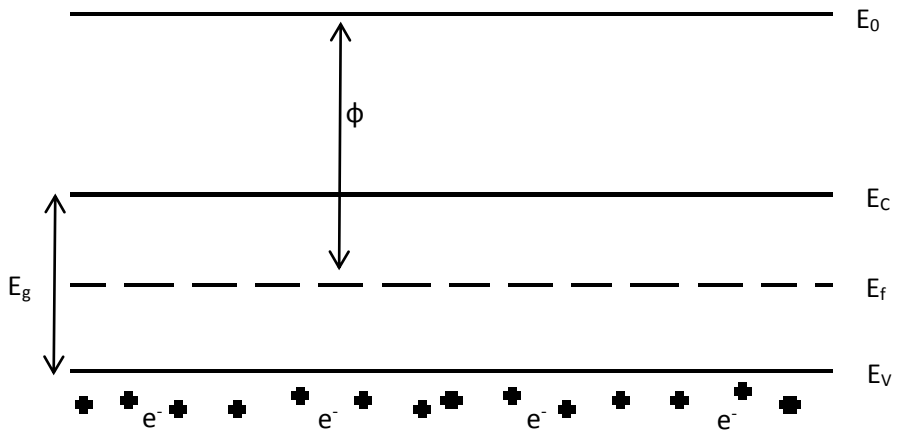

Figure 8. Energy band diagram of a semicoductor.

Figure 8 is an example of an energy band diagram for a semiconductor material. The area below E_v, the valence band energy, is where most of the electrons in a given material are present. The Fermi energy level, E_f, is a hypothetical energy level of an electorn such that at thermal equilibruim this energy level whould have 50% probability of being occupied. E_c is the conduction band where the electrons conduct in a material. E_g is the energy gap between E_c and E_v, which usually defines whether a material is semiconductor or insulator. The vacuum level, or free energy state, is that above E_o. At this energy level, the electron is no longer bounded to the material. In order to excite an electron from the Fermi energy to the vacuum level, a sufficeint energy is required which is known as the work function.

In order to have a stable electron beam, the electron sources must provide a simple and consistent source of electrons. These sources can be either thermionic emission or field emission sources.

2.4.1 Thermionic Emission

Thermionic emission (TE) is the emission of electrons using heat. By heating the material, electrons gain enough thermal energy to overcome the barrier and escape to the vacuum energy level [29], [30]. The energy of an electron is related to temperature by the Boltzmann constant ($k = 8.617398 \times 10^{-5}$ eV/K):

$$E = k*T \tag{2.4}$$

where T is the temperature in Kelvin (K). For example, at 2700 K, electrons will have energies of about 0.23 eV [31].

Tungsten is a good example of a thermionic source. For many years tungsten was used as a thermionic source because it could tolerate high temperature without metling or evaporating. Electrons are emitted from the tungsten wire by running a current through it. Due to the resistance of the material, it heats up giving enough energy to the electrons to escape to vacuum level. When tungsten is placed in vacuum, there will be few particles to carry away the heat from the filamnet. In this process, the filimant heats up much faster than when placed at atmospheric pressure. Moreover, placing the filamnet at low pressures helps in maintaining the temperature at a constant value since there are fewer external influences affecting it. In addition, high vacuum helps maintaining the filament in good conditions since there are less air molecules interacting with it which for example could cause oxidation. Thermionic sources are not only used for EBL, but also for various systems such as electron beam evaporators. Thermionic sources are known for being easily constructed and embeded in a system.

The emission flux which is the amount of electrons emitted from a thermionic source can be expressed by the Richardson-Dushman equation:

$$J = AT^2 e^{\frac{\Phi}{kT}} \tag{2.5}$$

where J is the current density emitted and A is a material constant. For tungsten, A is 60 A/cm^2K^2 and the work function (Φ) is 4.5 eV. The current is quadratically related to temperature, so a small increase in temperature would increase the current quadratically. This relationship holds true for tungsten for temperatures ranging from 2500 K to when it melts at 3100 K. Even though the relation is quadratic, but there is always a limit to which the current will saturate and then the

material starts to melt. Moreover, even though higher temperatures provide more electrons, but they also sacrifice filament lifetime. At 3 to 4 A, tungsten runs at 2500 to 2700K [31].

The shape of the filament is an important factor which determines the overall size of the beam and the beam current. If the emission is fine and focused, then less area for the column is needed for focusing the electrons to form a narrow beam. However, having a focused beam emission doesn't eliminate the need of the magnetic column since electrons are negatively charged particles and repel each other causing a wider beam size. Moreover, when the beam is focused, it maintains a higher current density, and requires less demagnification by the column. Narrower electron beam also results in less energy spread, which is comparable to monochromatic light. When the electron beam is narrow, most of the electrons will have the same kinetic energy which means a constant wavelength.

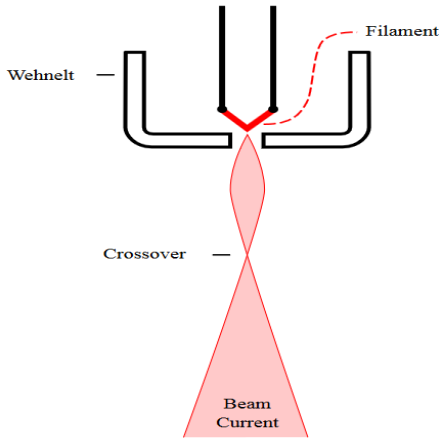

Figure 9. Schematic representation of a Wehnelt Cup.

A Wehnelt cylinder is a cap that surrounds the electron source. It is used to confine the electrons after they are emitted from the source [32]. It is usually kept at a negative voltage bias typically between -200 Volts to -300 Volts. The electrons are then pulled toward the anode part of the electron gun through a small hole at the bottom of the cap, the hole is acts as a filter to eliminate unfocused electrons and usually as a circular shape virtual source.

2.4.2 Field Emission

Field emission (FE) deffers from the thermionic emission in the process by which electrons gain their energy. Field emision uses an electric field that is strong enough to help the electrons tunnel through the barrier and make it to the vacuum level [33]. Mainly used sources are tungsten tips sharpened to a needle point as shown in the figure:

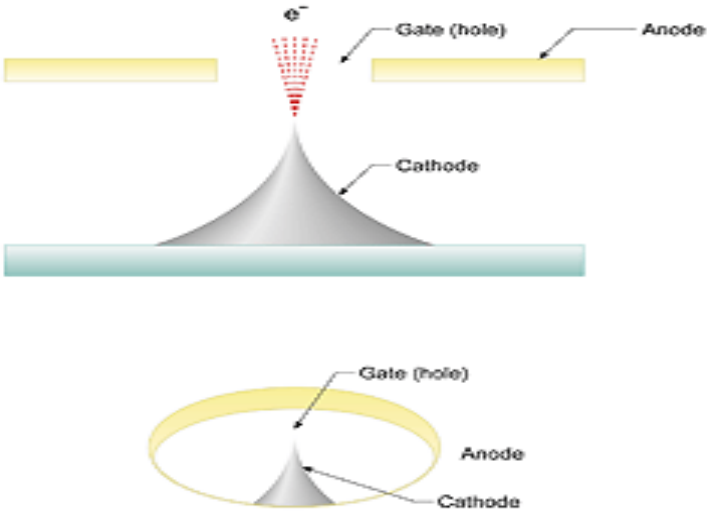

Figure 10. Schematic representation of a field emitter.

When high electric fields are applied, the energy barrier bends allowing the electrons to tunnel a shorter distance. For the process to be more effceint, extremly sharp tips are used. Tungsten is one example of materials that can be shaped to very sharp points, where the tip can be sharpend to a single atom [34],[35]. Sharp tips also allows a better control of the electron emission. Field emitters use voltage as the extraction force. The cathode is usually reffered to as the suppressor, and the anode is reffered to as the extractor. No heat is required which makes it desirable for varoius amount of applications. Electron microscopes are a good example where field emitters are used as the souce of electrons since no heat is required. However, the current field emitters were not being used in EBL because the current is not as stable as a thermionic emission.

A combination of both, thermionic and field emitters, is known as Mueller-emitter-based sources which are being used in newer equipments. These sources operate at a high temperature and requires an extraction voltage. They are known to be stable for several months because the heat drives off gasses that might interfere with a cold source. Mainly used thermionic field emission (TFE) sources are tungsten tips coated with zirconium dioxide, which is used to lower the work function of the material [36].

There are three critical parameters that are needed to be to optimized: the size of the virtual source, its brightness, and the energy spectrum of the emitted electrons. The aim during electron beam lithography to is to obtain a really small electron beam spot. In order to achieve this small size beam spot, the beam must be narrowed as much as possible starting from the source. This is why it is really important to obtain a small size virtual source to help reduce the amout of demaginification the magnetic lenses has to provide in order to form a small beam spot at the target. Another important factor is the brighness of the source, which is related directly to current

measured in amperes per square centimeter per steradian. The brighter the electron source the higher the current that it emits. Current is also related to dosage, which in terms determine the writing time of a specific pattern in an EBL. The energy spead also plays an important role in order to obtain a focused beam. An electron beam with wide energy spread is very similar to white light. White light is composed of a combination of electromagnetic radiations with different wavelengths. When passed through a lens, each electromagnetic radiation will have its own focal length. So in order to obtain a small beam spot, it is highly desirable to focus a combination of electromagnetic radiations with wavelength that have almost the same length which leads us to the monochromatic light. This is why if the electron beam consists of electrons that have almost the same wavelenght, it will be easier to obtain a small beam spot. However, due to the repulsive interaction of the electrons with each other, the beam spread becomes wider as the electrons are accelerated down through the column. This is also known as the Boersch effect [37].

2.5 Electron Beam Formation

After the electrons are emitted from the source, they start to move in random direction in vacuum. In order to accelerate the electrons down thorugh the column, extra-high tension (EHT) is required through the gun. The electron source is usually the cathode, and the aperture where the electrons exists is the anode. In electron beam lithography, EHT can range from 0 to 100kV [38]. EHT could also be increased up to 200kV in tunneling electron microscopes. Higher voltages provide more energy to the electrons. This energy might be required due to the type of the photoresist being used which could be thick and/or requires high energy to initate the process that changes the state of the photoresist. Even though high voltages tend to provide a small beam spot; however, electrons will not only pierce deep into the photoresist but might also might cause

damage to the substrate. Moreover, if the vacuum level inside the column is not high enough, arcs could occur which could damage the system. This is why most of the equipments come with safety features to warn the users during a gun break down to prevent the damage of expensive parts.

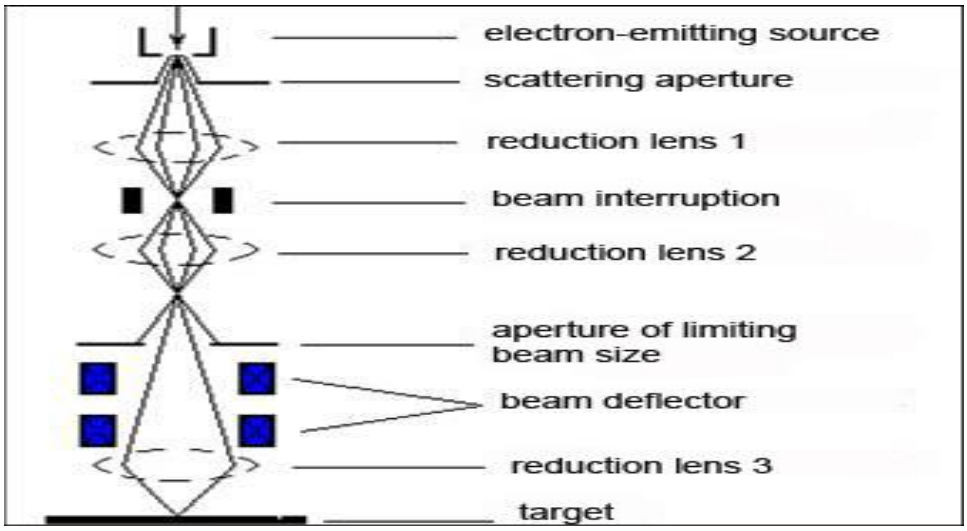

Figure 11. Stages through which the electron beam is formed and focused.

2.5.1 Aperture

After the electrons are extracted from the source they pass through the aperture. An aperture is a small hole located at a distance really close to the beam source. The shape and size of an aperture varies in order to form a wide variety beam shapes [39], [40]. Manily used shapes are cirlces and squares with size ranging from 20 µm to 120 µm. In order to limit the effect of space

charge caused by electron-electron repulsion, they are place close to the source. The main purpose of the aperture is to block the electrons that were not tightly focused, which are also known as stray electrons. Moreover, it insures that most of the beam will incident normally on the sample. When the aperture size increases, more electrons passes through and hence higher the current. Calibration is required when changing between one aperture size and the other, to insure that the aperture is in the correct position. In order to prevent damaging the apertures from contamination deposites, heat maybe applied in order to provide thermal energy to the contaminants which causes them to evaporate. Otherwise, apertures must be cleaned or replaced every few months because contamination degrades the resolution of the system. Apertures that are made from platinum usually have longer life span since they can be heated to orange hot without deformation in shape. This causes most of the contaminants to be released from the aperature.

2.5.2 Beam Blankers

In most designs the patterns are not continuous, which means the beam has to be stopped and started where there are discontinuities. This process has to be done with the least amount of time since the design template might have a lot of discontinuities [41]. Mechanical shutters could be one approach to achieve this step. However, mechanical shutters are not fast enough which could cause over exposure or shift in the design pattern. Moreover, the electron source and the acceleration voltage cannot be cycled on and off quickly due to high instant power that could melt some parts of the equipment. So in order to overcome these obsticles, an electrostatic deflector is used. An electrostatic deflector is a pair of plates that are electricaly controlled in order to provide fast response time. When the plates are energized, the beam is deflected off its perpendicular path down the column. So the beam itself is not actually being turned on and off, it is just being deflected

when there are no patterns to be written. The blankers must be positioned precisely close to the focal point of the beam; otherwise, streaks can occur on the sample when the beam is deflected off its axis. In higher energy systems multiple beam blanking systems is usually used since the electrons might carry enough energy to overcome the electrostatic field of a single beam blanker [36]. However, there is a minimum time interval for which the beam can be blanked and this time determines the minimum dosage the equipment can achieve.

2.5.3 Electron Lenses

When the electrons are extracted and accelerated, they interact with each other causing the beam to diverge at the edges. When the beam then passes through the aperture, depending on the size of the aperture some of the diverging electrons will get blocked. However, to be able to obtain high resolution lithography, the beam needs to be finer and thinner. In order to accomplish that, lenses must be used to converge the beam to a small spot. Furhtermore, electron beam trajectory can be considered like the light rays, and the ideas of converging and focal points are almost the same. However, optical lenses are transperant to electron beam, so they can not be used to focus the beam. Instead, electromagnets are used as lenses. Electrons are charged particles ($q = 1.60217657\times10^{-19}$ C) and in the presence of magnetic field, a magnetic (Lorentz) force will be exerted on them. This force depends on the magnitude of the magnetic field (B), the speed of the electron(v), and the direction in which the electron is traveling. The relationship is given by Lorentz equation:

$$F = q(vxB) \tag{2.6}$$

This magnetic field helps in bending the electrons inward and converge them to a focal point. Electromagnets are coils of insulated wires, usually copper, wrapped around a highly permeable material, such as iron, to concentrate the magnetic field.

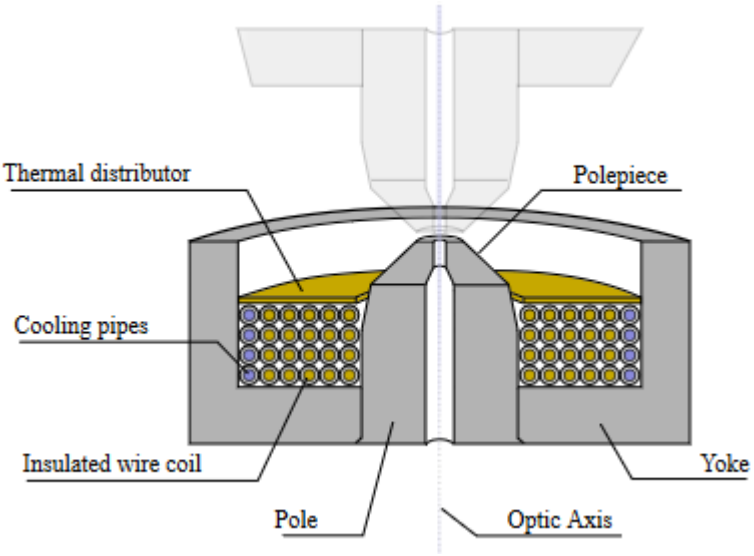

Figure 12. Cross-section representation of an electromagnet in an EBL system.

Even though these lenses tend to focus the beam to a small spot as an optical lens can do to light; however, they are not as good as optical lenses in terms of aberrations. There are two types of aberrations: spherical aberrations and chromatic aberrations. Spherical aberrations are caused by a difference in power between the inner and outer areas of the lens. Chromatic aberrations occur because electrons of different energies (i.e., wavelengths/color) are focused to

different image planes. Solutions have not been found yet to correct these types of aberrations. One method of reducing these aberrations is by confining the electrons to the center of the lenses by reducing the convergence angle of the system. This method causes a huge reduction in the beam current since a large number of electrons will be filtered out. Some electrostatic lenses are used in the earlier stage of the column, close to the gun, because these lenses cause more serious aberrations than the magnetic lenses. The overall goal of the lenses is to condense the electron emission into a relatively parallel, or collimated, beam.

2.5.4 Stigmators

After the electrons passes through the electromagnetic lenses and electrostatic lenses, the beam will have an elliptical distortion known as astigmatism. Astigmatism occurs when the energy spread of the electrons is wide causing each part of the beam to be focused at a certain focal length. It could also occur due to the fact that the lenses are not perfectly constructed around the circumference of the lenses. Stigmators are special type of lenses that are used to fix this issue. These special lenses have 4 or to 8 poles arranged around the optical axis.

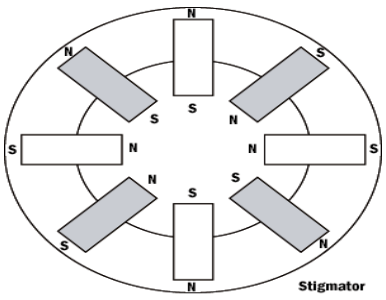

Figure 13. Schematic representation of a stigmator.

In order to furthermore enhance the shape of the beam, two or more stigmators can be used. These stigmators change the shape of the beam along the x-axis and the y-axis in order to get the circular beam spot. This step is not done automatically, the user has to pick a particle on the substrate and then manually do the corrections until a circular beam spot is obtained. This step is critical since not only it determines the shape of the electron beam but also the size of the beam [42]. In an EBL system, the user can adjust the stigmators along the x-axis and along the y-axis separately. However, a change along the x-axis could result in a change in the y-axis and vice versa, so the changes are not independent of each other.

2.5.5 Scanning

After the beam is confined by the lenses, it continues to flow until it incidences normally to the sample. However, the beam must be scanned across the surface of the sample in order to provide an image in an SEM mode or to write a pattern in EBL mode. In order to scan the electron beam across a certain surface, deflectors needs to be used. In a typical EBL system, two deflectors are used. First deflector tilts the beam towards another position on the sample. However, this deflector introduces an angle between the beam and the sample. This is why another deflector is needed to correct the beam back to being normally incident on the sample. Even though deflecting the beam causes aberrations and enlarges the beam diameter, EBL still results in a high resolution lithography. The extent to which the electron beam can be deflected without drastically reducing the quality of the beam is known as the write field area. Beam deflectors can be either electrostatic plates or magnetic coils. Electrostatic plate deflectors tend to cause more distortion to the beam compared to electromagnets, but they can perform at a much higher speed than electromagnets. High speed deflection is more desirable during electron beam lithography since most patterns gets complicated and takes really long time to write. Due to the fact that electromagnetic coils can’t

respond to high frequencies of charging and discharging a combination of both electrostatic and magnetic deflectors should be used. Magnetic deflectors are usually used for long-range deflection; on the other hand, electrostatic deflectors are used for short-range and high-speed deflections. The deflectors are usually placed at the end of the column of a system, so most of the time the final lenses are covered with ferrite in order to minimize the field interactions from the deflectors.

2.5.6 Stitching

The electron beam can deflect at a limited angle beyond that angle the amount of aberration and distortion are unacceptable for high resolution lithography. So, in order to be able to scan the whole sample, the sample must be moved along the x-axis and y-axis. This movement of the stage is really critical since an overlap in a pattern could cause a short circuit or a discontinuity could cause an open circuit [43]. This is why the stage is controlled by two different method. The first method is the coarse movement which is usually used to move a stage for relatively long distances. This movement is controlled using servos which are electric motors that involve error-feedback via encoders to allow for precise position control. Due to the mechanical nature of the servos, they are not accurate enough to move the stage alone. Since EBL deals with features on the nanoscale, another type of motors are used which are known as piezoelectric motors. Piezoelectric material is a material that changes its physical shape upon applying voltage to the material and vice versa. These type of motors can cause fine movement of the stage. So when writing a pattern using an EBL, first the deflectors are used along the write field. Then, the piezoelectric motors are involved to move the sample in fine movements. Finally, the servos are used in order to move the stage at large distances. The servos use laser beam as the feedback mechanism, where the laser reflects back for a mirror placed on the stage and the difference between the wavelength of the incident

and reflected wave determines the distance travelled by the stage [44]. The laser sources are usually expensive and requires precise alignment when installed.

CHAPTER 3

ELECTRON BEAM INTERACTION

When the electron beam strikes the surface of the sample, it doesn't penetrate the sample in a linear trajectory. Instead, the electrons start to interact with the atoms that form the sample. When these electrons, also known as primary electrons, collide with atoms within the specimen they release part of their energy to the sample. When there is a change in the momentum or energy loss from the primary electrons, this energy is then converted to another form of energy. Depending on the type of interaction, there might be more than one energy phenomena produced which when detected could give information about the sample under examination [45]. These forms of energies are also known as events.

3.1 Introduction to Electron Scattering

When the primary electrons interact with the atoms of the sample, part of its energy is transformed and/or the direction of propagation changes. This is also known as the scattering effect. The scattering effect forms a three dimensional space region which is known as the interaction volume. Electron scattering can be classified into two different categories: elastic scattering and inelastic scattering. Elastic scattering, also known as backscattering, is when an electron losses part or no energy during an interaction with an atom, but its direction is changed. Inelastic scattering, also known as forward scattering, is when an electron losses significant amount of its energy, but has its direction remains unchanged. The overall shape of the interaction volume is determined by these scattering events.

3.2 Elastic Collision

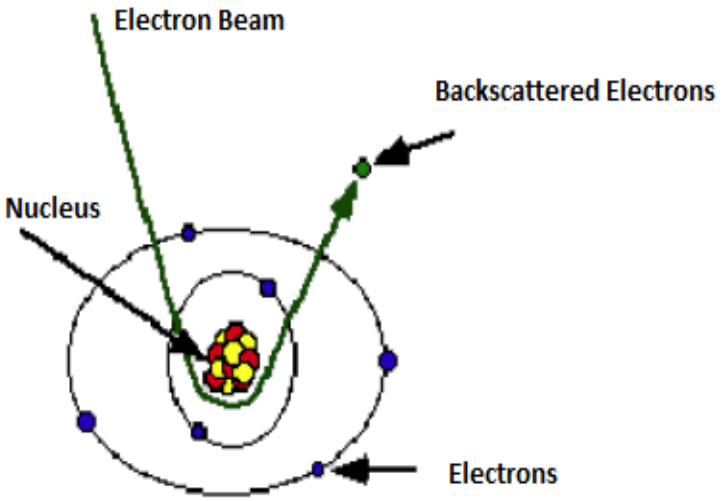

Figure 14. Illustration of an elastic collision between an atom and an incident electron.

Figure 14 represents the elastic collision of an electron with an atom, where the primary electron is travelling really close to the nucleus of the atom. The mass of the nucleus is much higher than that of an electron, which causes the electron's kinetic energy to remain almost unchanged after its interaction with the nucleus. However, the electron's momentum changes causing a change in its direction of propagation. The angle between the primary electron and the backscattered electrons could reach up to 180^{o} [46]. After an elastic collision, the primary electron is backscattered. These electrons are now called the backscattered electrons. The difference between the energies carried by the primary and backscattered electrons can be measured in several

volts; however, this amount in energy is insignificant since the primary electrons carries an energy that is thousands of volts. Atomic particles are usually treated in terms of probabilities since it is almost impossible to simultaneously obtain the position and energy of such particles as stated by the Heisenberg Uncertainty Principle. Hence, scattering events should also be described in terms of probabilities. The probability for large deviations in the trajectory, after an elastic collision, is directly related to the atomic number of the target and inversely proportional to the primary electron's energy.

$$Q_{>\phi_o} \propto \frac{Z^2}{E^2} \tag{3.1}$$

This equation, which is given by [47], show that the probability (Q) in which an electron deviates more than a given angle (ϕ_o) is directly proportional to the atomic number (Z) of the sample and inversly proportional to the electron's energy (E). It shows that a sample with high atomic number will cause a greater degree of deviation to the primary electorns. On the other hand, primary electrons with high energy are less likely to be deflected than those with low energies. If the deflected angle is large enough such that the electron escapes the surface of the specimen and reaches the detector, then the number of electrons detected will have a strong dependence on the atomic number of the sample. With such information we can dertermine the type of an unknown sample [47].

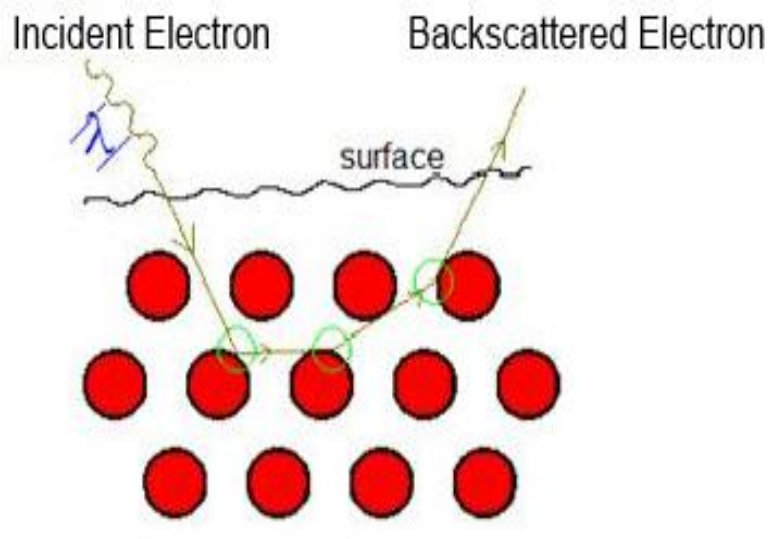

Figure 15. Illustration of a primary electron undergoing 3 elastic collisions and escaping the sample's surface.

Elastic scattering also gives information about how much energy is available for inelastic scattering. If a primary electron encounters elastic scattering near the surface of the target and then escapes from the specimen, as shown in figure 3.b, then this electron is not capable of transferring any energy to the specimen. So, no more effect will result from this electron which can be a good indicator to how the interaction volume would look like.

3.3 Inelastic Collision

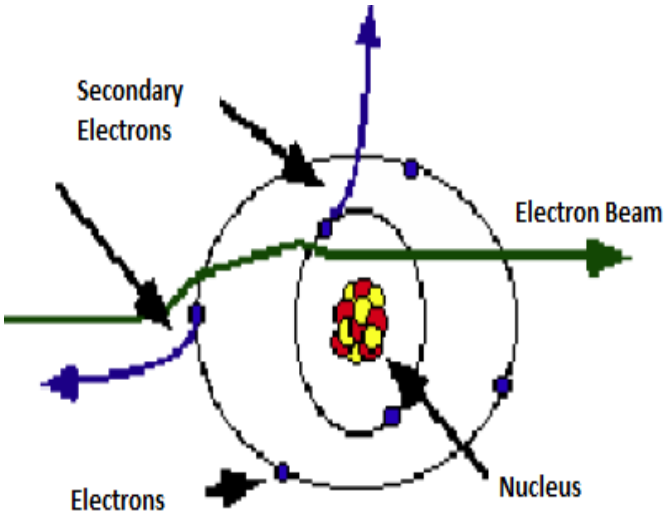

Figure 16. Illustration of an inelastic collision between an atom and an incident electron.

During an inelastic scattering, the primary electrons exchange a significant amount of its energy with the specimen; however, the direction of propagation remains almost unchanged. This type of interaction would result in an energy spectrum that could give more information about the sample or help in predicting the size of the interaction volume. Depending on the quantum state of each atom involved in the collision, there will be a different type of energy trading. Plasmon excitation, phonon excitation, conduction band electron excitation, ionization of inner shell

electrons, Bremsstrahlung or continuum x-rays are some effects that can give us important information about the specimen.

3.3.1 Plasmon Excitation

Plasmon excitation is one of the highest probable energy transform during an inelastic collision. A plasmon is a quantum of plasma oscillation which is just like photons and phonons which are quantization of electromagnetics and mechanical vibrations respectively. This phenomena occurs due to the exciting waves in the free electron gas. This form of energy is usually uninformative due to the fact that the plasmon scattering affects the entire region where the interaction took place [f]. The energy exchange is also very small typically ranging between 5 to 30 Volts. This event is similar to dropping a rock in a pond of water. The center of the pond feels the oscillation immediately; however, the waves continues to affect the whole pond.

3.3.2 Phonon Excitation

Phonon excitation occurs when the primary electrons exchanges energy with the bonded atoms, also known as the crystal lattice, that form the substrate. The primary electrons cause a faster structural vibration which causes the sample's temperature to increase. This effect doesn't cause damage to most of the materials since the heat increase is around 10 degrees Celsius and is usually dissipated without causing any change in the crystal lattice. However, there are some materials which can't tolerate such temperature increase and gets damaged due to the amount of energy exchanged. Materials that have weak ionic bonding are highly prone to damage due to the fact that the amount of heat exchanged increases the vibration of the atoms causing the bond to

break, which leads to the diffusion of ions throughout the sample. In order to reduce such effect, the beam's energy can be reduced or the beam can be slightly unfocused causing the energy to dissipate in a wider area.

3.3.3 Conduction Band Electron Excitation

Conduction band electron excitation occurs when the electrons in the conduction band gain enough energy to escape to the vacuum level. When the electron beam strikes the surface of a sample, some of the primary electrons interact with the electrons in the conduction band of the specimen, which are not strongly bonded to the atoms. Hence, a small energy transfer from the primary electron causes these electrons to escape to the vacuum level. The amount of energy required to excite these electrons to the vacuum level is around 1 to 50 volts. These electrons are then called secondary electrons.

3.3.4 Ionization of Inner Shell Electrons

Ionization of inner shell electrons occurs when the primary electrons delivers sufficient energy that causes electrons that are tightly held in the inner atomic shells to escape to the vacuum level. When the atom loses its electron, it becomes ionized and unstable causing electrons in the higher energy levels to lose their energy and drop to the lower energy level causing it to become stable. When the electrons drop from the higher energy level to the lower energy level, it emits energy in the form of x-rays.

3.3.5 Bremsstrahlung or Continuum X-rays

Bremsstrahlung or continuum x-rays are energy spectrum caused by the interaction of the primary electrons with the strong coulomb field of an atom. These x-rays are generated with energies all over the spectrum which is only limited by the primary electron beam energy. Since energy is neither created nor destroyed, and the since the energy delivered to the sample is mainly from the primary electrons, the Bremsstrahlung can't have energy that is greater the primary electrons. Hence, when the continuum x-rays are detected, then the energy of the primary electrons can be determined. On the other hand, this effect causes noise in measurements when measuring the characteristic x-rays. Moreover, Bremsstrahlung carries enough energy to excite electrons in the inner shells of an atom causing it to be ionized, which is usually referred to as fluorescence.

Other effects of inelastic collisions are cathodoluminescence and Auger electrons [49]. Cathodoluminescence is an optic and electromagnetic phenomena which occur when an electron impacts a substrate producing long-wave radiation in the visible, IR and UV spectral range. This effect is the opposite of the photoelectric effect in which an electron is emitted after the absorption of photons. Cathodoluminescence could be due to the intrinsic property of the material, or could be caused by an impurity that is present in the sample. Auger electrons are electrons that loses energy to go from a higher state to lower state causing an emission of an electron from the same atom [50]. This occurs because the energy difference between the higher state and lower state is sufficient enough to cause an electron in a higher energy level to escape to the vacuum level.

3.4 Secondary Electrons

Secondary electrons travel at a typical speed equivalent to less than 5 volts, thus traveling at a distance not too far from where it originated. However, some of the secondary electrons which are generated within 5 nm of the sample's surface are capable of escaping the surface of the sample and reaching the detector. These electrons are the main reason behind obtaining high resolution SEM images. Moreover, because not all electrons are held to an atom at the same energy level, there could be secondary electrons with higher velocities equivalent to 1000 volts. These secondary electrons are known as fast secondary electrons which mainly have trajectories normal to the incident electrons. Even though the number of such electrons is small with respect to the number of primary electrons, they can still degrade the quality of the beam that is striking the surface. In order to minimize this effect, the samples are usually coated with a thin layer of metal such as gold or chromium in order to increase the conduction/covalent bond ratio, which would reduce the effects due to fast secondary electrons and provide a higher resolution image.

3.5 Interaction Volume

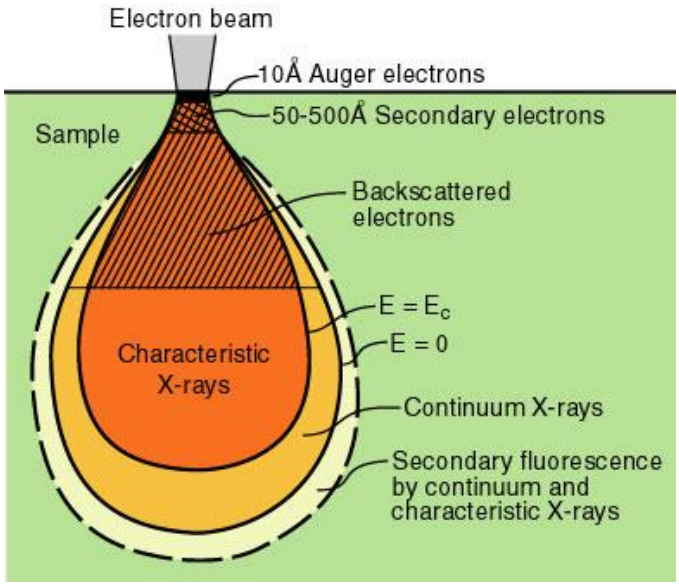

Figure 17. Schematic diagram of an interaction volume.

The resolution of electron beam lithography is usually limited to both elastic and inelastic collision because backscattering electrons can carry enough energy to expose the resist in unwanted areas. The shape of the interaction volume is what limits the resolution in an electron beam lithography. An interaction volume looks very similar to an eye drop with the tip towards the top surface of the sample. The shape of an interaction volume not only depends on the nature of the sample, but also on the electron beam's energy, angle of incidence. An electron beam that is accelerated at a high voltage will gain more energy and can penetrate the sample much deeper

than an electron beam that is accelerated at a lower voltage. During an interaction, an electron can travel distances that ranges between 1 to 5 μm. The depth and width of the interaction volume can be predicted with by the following Potts formulas [51]:

$$depth(\mu m) = \frac{0.1E_o^{1.5}}{\rho} \tag{3.2}$$

$$width(\mu m) = \frac{0.077E_o^{1.5}}{\rho} \tag{3.3}$$

Where E_o is the acceleration voltage measured in keV, and ρ is the density of the substrate measured in g/cm^3. In order to get better approximations about how the interaction volume could look like, Monte Carlo simulations can be used. Monte Carlo simulations are a broad class of computational algorithms that is based on repeated random sampling obtained from numerical results [52]. These simulations where named Monte Carlo simulations because it is just like playing and recording the results in a real casino. However, in order to simulate an electron beam interaction with the sample, around one thousand electron interaction needs to be considered which consumes significate amount of time and requires intensive calculations to simulate [53]. Shown in figure 3.d are Monte Carlo simulations at 10 kV and 20 kV:

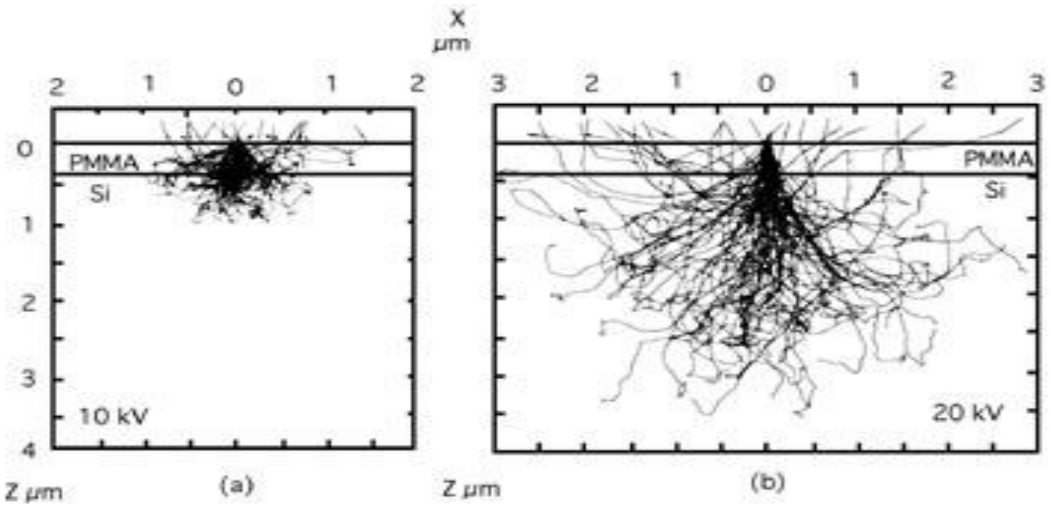

Figure 18. Monte Carlo simulation diagram.

In order to evaluate how different parameters can change the size and shape of the interaction volume several experiments have been performed. When the beam's total energy is increased, keeping everything else the same, the electrons were able to penetrate to a greater depth. This can be explained by the amount of energy that the primary electrons carry which is much larger than the amount of energy that these electrons exchange with the atoms. So, by the time the primary electrons loses all their energy, they would have interacted with more atoms hence a greater penetration depth. However, the overall shape of the interaction volume at a high beam energy remains almost unchanged.

In order to evaluate the influence of the atomic number of the substrate on the interaction volume, the beam's energy was kept the same and the different metal such as aluminum, gold and

copper were examined. In a given volume, substrates with high atomic numbers caused more elastic scattering and higher average scattering angle compared with those with lower atomic numbers. Since the elastic scattering is more probable in high atomic number samples, the electron trajectory tends to deviate from its original path hence causing the shape of the interaction volume to change drastically.

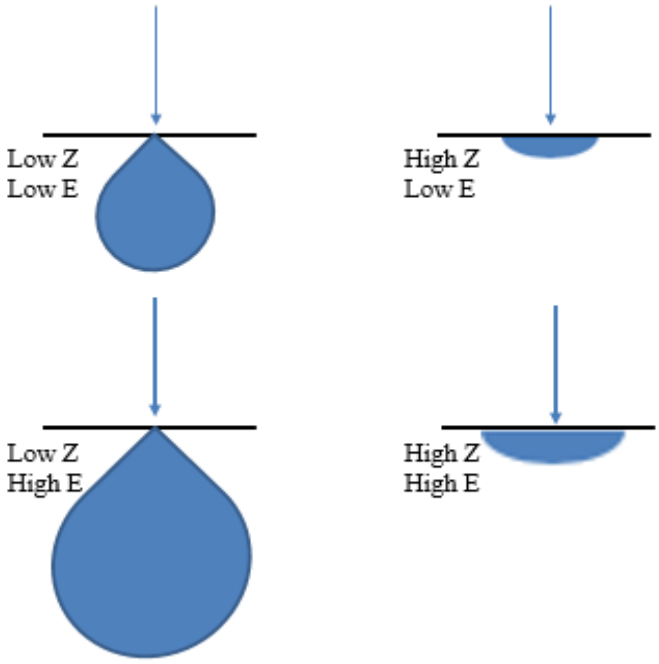

Figure 19. Interaction volume shapes representation in different specimens.

Another parameter that could affect the interaction volume is the angle of incidence of the electron beam. As the angle of incidence is deviated away from the normal plane to the surface, the interaction volume becomes smaller and asymmetrical. This happens due to the fact that a small change in angle from an interaction is sufficient to allow the electrons to escape the surface of the sample.

3.6 Proximity Effect

A positive resist consist of long molecular chains known as polymers. When these polymers are exposed to an electron beam, the electrons will exchange energy with these polymers causing them to break into smaller chains, also known as monomers. Due to the change in the chemical composition, the solubility and etch rate of the resist increases. This is why it is important to know the 3D shape of the interaction volume in order to avoid multiple exposure of the resist in unwanted regions [54]. A mean free path of an electron can reach up to 10 μm when accelerated with high potential energies. This thickness is typically on the order of magnitude the thickness of the resist (55). This penetration causes the electrons to interact not only with the resist, but also with the substrate. The backscattering of electrons is what causes the proximity effect. Moreover, when the primary electrons strikes the surface the resist, part of the energy that is dissipated causes the generation of secondary electrons which are also responsible for exposing the resist. However, secondary electrons have low energy ranging between 2 to 50 eV which means they can travel short distances on the order of a few nanometer. So, their contribution to proximity effect is rather small. In order to achieve high resolution feature sizes on the order of few nanometers, both forward and backscattering should be taken into account during the design process and determining

related parameters such as dosage. The proximity effect is considered the main limiting factor that limits the resolution of the electron beam lithography. Proximity effect correction is one way of achieving a higher resolution.

3.7 Energy Profile

Energy profile plays an important role in proximity effect. So, predicting the profile created by the exposure of a resist by an electron beam at a point or pixel can help in reducing the proximity effect. This type of exposure is also known as point spread function. Even though dosage plays an important factor in exposing the resist; however, the energy density profile does not depend on dosage [56]. "This profile [can be] approximated by the sum of two Gaussian distributions representing the forward and the backscattered electrons:

$$f(r) = C_1 e^{-(r/B_1)^2} + C_2 e^{-(r/B_2)^2} \tag{3.4}$$

Where C_1, C_2, B_1, and B_2 are constants and r is the distance from the point of electron incidence" [57] (Chang, 6). However, this equation can be rewritten in the following format:

$$f(r) = \frac{1}{1+\eta}\left(\frac{1}{\pi\alpha^2} e^{-(r^2/\alpha^2)} + \frac{\eta}{\pi\beta^2} e^{-(r^2/\beta^2)}\right) \tag{3.5}$$

Where η represents the percentage of the backscattered energy to the forward scattered energy, α represents the scope of the forward scattering, and β represents the scope of the backwards scattering. Since the probability of finding an electron somewhere in space after exposing the resist is equal to one, it is safe to state the following normalization equation:

$$\int_0^{\infty} f(r) 2\pi r dr = 1 \tag{3.6}$$

However, the double Gaussian function turned out to "be insufficient for expressing the energy density profile, and a more complex functions are needed" [58] (Murali, 37-62). These functions do not take into account the composition of the substrate, wether it is mono-layer or multi-layer. In order to obtain a more accurate modle, an exponentail term was added to the double Gaussian model in order to take into account the type of substrate being used [59]:

$$f(r) = \frac{1}{1+\eta_1+\eta_2}\left(\frac{1}{\pi\alpha^2}e^{-(r^2/\alpha^2)} + \frac{\eta_1}{\pi\beta^2}e^{-(r^2/\beta^2)} + \frac{\eta_2}{24\pi\gamma^2}e^{-\sqrt{r/\gamma}}\right) \tag{3.7}$$

These models are simplified versions of the energy distribution. The energy distribution is three dimentional; however, these equation only represents the two dimensional version of the profile. In order to take into acount the third dimension, the dependence of the energy profile to depth must be known. Even though equations that take into acount the third dimension are more acurate; however, it consumes enormous amount of computational time which makes it almost impractical. Moreover, measuring the three dimensional energy profile is not an easy task since some feature sizes are below 10 nm [56]. Instead, in order to get an estimate of the three dimensional profile, Monte Carlo simulations can be used taking into account that majority of the electrons will encounter elastic scattering in order to reduce the computational time.

3.8 Exposure Estimation

Exposure estimation is also important to take into account when trying to do proximity effect correction. The equations previously mentioned, represents the energy profile point by point. However, in order to reduce exposure time, electron beam lithography usually exposes in a continuous fashion rather than point by point. In order to take the continuity into account, a convolution between the energy profile and dosage is performed as follows [60]:

$$E(x,y) = f(r) * d(x,y) \tag{3.8}$$

Where E(x,y) represents the energy delivered by the electron beam to the resist, f(r) is the energy profile as described earlier, and d(x,y) is the dosage delivered by the beam at certain point. Patterns are usually made of small pixels, so convolving large patterns with the point exposure profile will lead to long computational time. In order to make computation more efficient primitive shapes can be used.

3.9 Dose Modification

The third type of proximity effect correction is the modification of dosage. Each pixel in a large pattern should have a specific dosage corresponding to it so that proximity effect is reduced. The problem with this approach is that it requires extensive computations since it has to define the correct dosage for each pixel. It is similar to the previously proposed equations for proximity effect correction in the sense that they both use exponential functions; however, when determining the

dosage the calculation is done in reverse to those done in exposure estimation. The equation can be described as follows:

$$E_i = \sum_{j=1}^{N} R_{ij} Q_j \text{ with } R_{ij} = \frac{\overline{\Delta V_f}}{t}\left(\frac{1}{\pi\alpha^2} e^{-(r_{ij}^2/\alpha^2)} + \frac{\eta}{\pi\beta^2} e^{-(r_{ij}^2/\beta^2)} \right) \tag{3.9}$$

Where Q_j is the dosage assigned to a pixel j, N being the number of pixels, and r determines the distance between the centers of two pixels. Since calculations in matrix format are easier to solve, this equation can be rewritten as follows:

$$[E_i] = [R_{ij}][Q_j] \tag{3.10}$$

In order to obtain a proximity effect correction, the matrix equation needs to be solved. Even though solving this equation leads to a close proximity effect correction; however, it only takes into account the pixels being exposed and requires intensive calculations when dealing with large patterns. “Solving this set of equations with matrix operations will provide a proximity effect corrected pattern. However this scheme will not be a perfect correction since only the exposed pixels are considered in this equation. With dose modification, it is possible to achieve superior proximity effect correction” [61]. The main disadvantage is that it may require large computation times when dealing with large patterns.

CHAPTER 4

ATOMIC FORCE MICROSCOPE

In order to characterize the samples that are fabricated using the 3D electron beam lithography an atomic force microscopy (AFM) is required. Due to the limits on the wavelength of the optical microscopy, it is almost impossible to characterize samples using optics on the nano-scale. Furthermore, a scanning electron microscope (SEM) provides high resolution planar two dimensional imaging; however, it provides a really low lateral resolution that makes it almost impossible to accurately analyze 3D nano-structures without damaging the sample [62]. So in order to characterize the 3D EBL samples accurately, an AFM needs to be used.

4.1 Introduction

An AFM is a very high-resolution type of scanning probe microscopy almost 1000 times better than the optical microscopy. It can characterize samples with resolution on the order of fractions of a nanometer. It was developed by Greg Binning, Calvin Quate, and Christopher Greber in 1986, and was commercially available in 1989. Prior to the development of the AFM, was the invention of the scanning tunneling microscope (STM) which was also developed by Greg Binning and Heinrich Rohrer in 1980 at IBM Research in Zurich [63]. This invention earned them Nobel Prize in Physics in 1986, since scientist were then able to visualize and study nanostructures which was almost impossible prior to the STM. An STM uses an extremely sharp tip that ends with a single atom. When approached to the surface of the sample, there will be tunneling current from the probe to the sample. Depending on the intensity of this tunneling current, it is able to determine the distance between the tip and the sample. This is a wonderful technique that works for

conductive surfaces; however, it might not work for non-conductive samples since there no path of the current to flow. On the other hand, the AFM uses a cantilever tip to feel the surface of the sample which enables the gathering of the information about the sample's structure. So, there is no conductivity requirement to get a topographic image of a sample using an AFM.

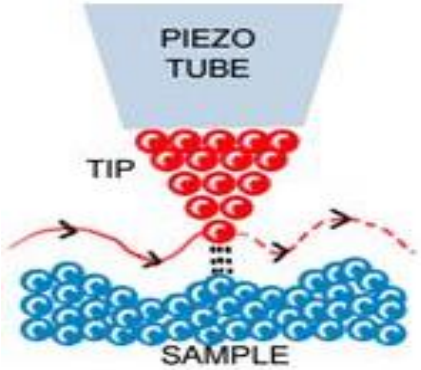

Figure 20. Illustration of a Scanning Tunneling Microscope.

Since an AFM uses a sharp tip for imaging, the tip's radius of curvature should be on the order of few nanometers in order to obtain high resolution images [64]. The tip is usually fabricated by using an anisotropic etching of silicon substrate by potassium hydroxide.

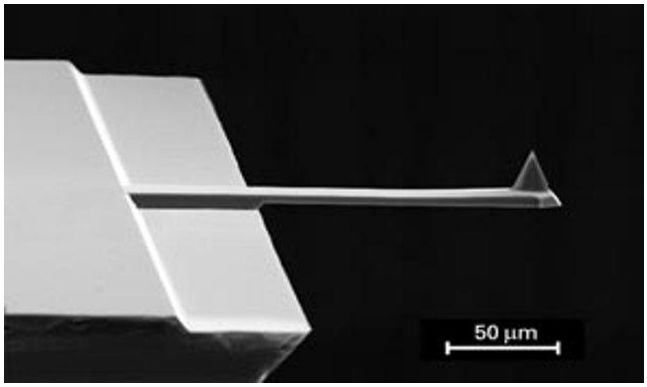

Figure21. An SEM image showing an AFM Tip.

When the cantilever tip is brought to the vicinity of the sample, forces start to interact with the tip causing a deflection in the cantilever. When the tip is far away from the sample 10-100 um there is no interaction between the two. When the tip approaches the sample on a distance of few microns it encounter electrostatic forces and long-range interactions from adsorbed molecules such as polymer brush [65]. When the tip is brought furthermore closer to the sample at a distance of nanometers to atomic distances, the forces encountered are Van der Waals, capillary forces, chemical potential, magnetic forces, solvation forces (from water layering) [66]. These forces causes the tip to deflect. The amount of deflection gives information about the specimen. The deflection is detected by using a laser source where the laser shines on top of the cantilever and reflects back to the detector.

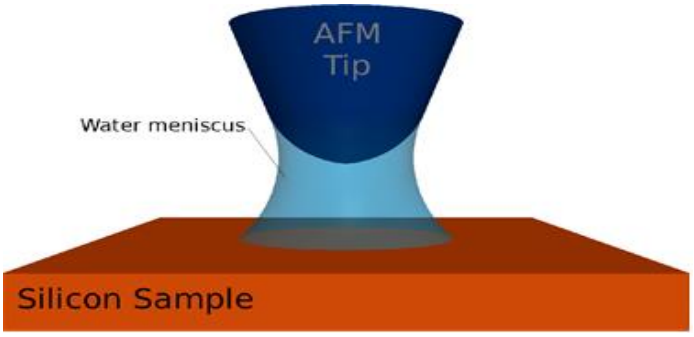

Figure 22. Water meniscus interaction with an AFM Tip.

4.2 Atomic Force Microscope Detectors

An AFM uses a solid state laser that shines laser on top of the cantilever and reflects onto a dual diode photodetector illustrated in the image below.

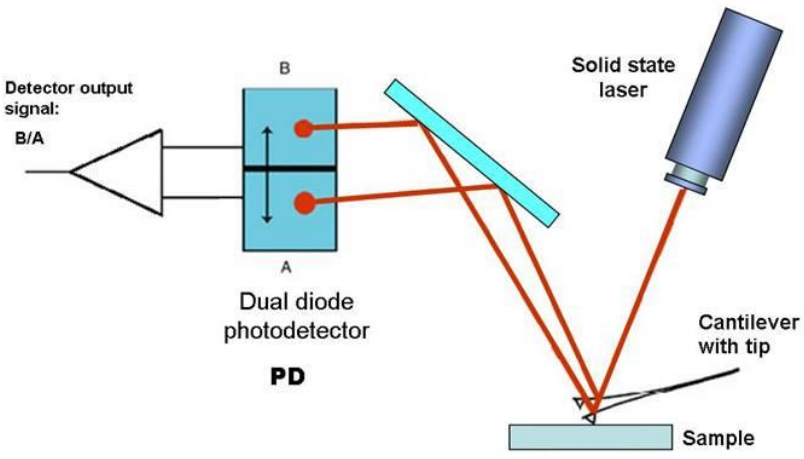

Figure 23. Schematic diagram representing an AFM system.

A photodiode is a type of photodetector that is able to sense photons and translate them into voltage or current depending on the application. The difference between photodiodes and regular semiconductor diodes, is that photodiodes requires photons as a source of energy for the electrons to be excited to the conduction band. The photons must not be blocked by any material before they are absorbed by the sensitive material of the device [67]. Photodiodes can be designed in order to absorb certain electromagnetic wavelengths such as UV, x-rays, monochromatic visible light, etc. The response of these diodes plays an important role in determining the scanning speed of an AFM. Furthermore, the signal to noise ratio (SNR) is also an important factor that determines the resolution of an AFM image. A typical diode is fabricated using a PN junction; however, in order to increase the response time of the diode a PiN junction is used. Moreover, a diode can be operated in several modes such as: photovoltaic mode, photoconductive mode, avalanche breakdown, etc.

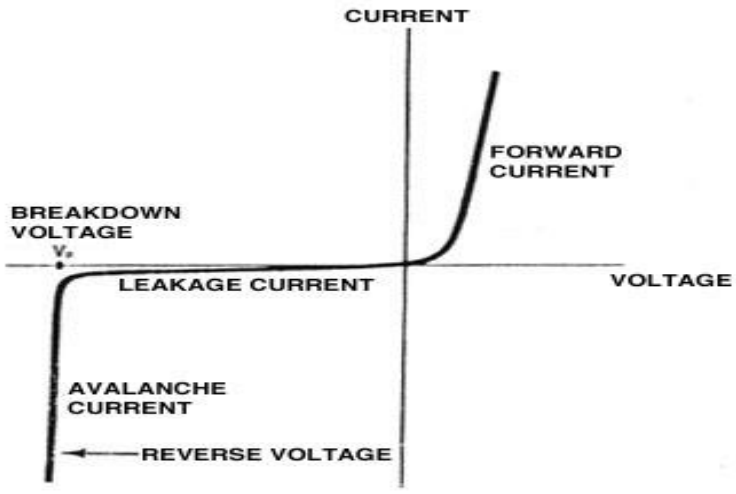

Figure 24. Illustration of current versus voltage relationship in a diode.

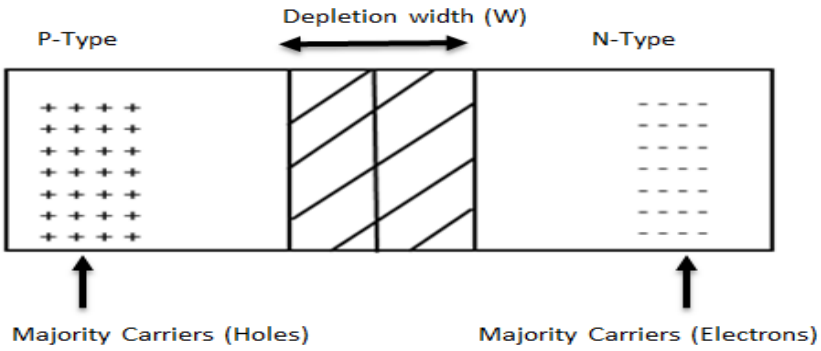

Figure 25. A cross-section of a PN junction.

The PN junction is fabricated by doping a substrate with another element. For example, doping a silicon wafer with Boron causes the region to become P-type, since Boron is an element in group 13 in the periodic table which means it has one electron less than a silicon atom, which is in group 14. On other hand doping a silicon wafer with Phosphorous cause the region to become N-type, since Phosphorous is an element in group 15 in the periodic table which means it has one electron more than a silicon atom. When a PN junction is formed, the electrons on the N-type region, also known as majority electrons, starts to repel the electrons on the P-type, also known as minority electrons. Similarly, the majority holes on the P-type region starts to repel minority holes on the N-type region. This phenomena causes a built-in electrical field and a built-in potential that affects the transport of electrons when biased. The equations for the current, built-in voltage, depletion width and capacitance are listed below.

The following equation represents the current in a diode:

$$J = q\left[\frac{D_N}{L_N} N_{P0} + \frac{D_P}{L_P} P_{N0}\right](e^{\frac{qV_A}{kT}} - 1) \tag{4.1}$$

Where q is the electron charge, D_N and D_P are the diffusion coefficients of electrons and holes respectively, L_n and L_P are the mean free path of the electrons and holes respectively, N_{P0} and P_{N0} are the donor and acceptor concentrations at the p-side and n side respectively, k is Boltzmann's constant, and T is the temperature in Kelvin.

The built-in voltage can be represented using the following formula:

$$V_{bi} = \frac{kT}{q} \ln\left[\frac{N_D N_A}{ni^2}\right] \tag{4.2}$$

Where q is the electron charge, k is Boltzmann's constant, and T is the temperature in Kelvin, N_D and N_A are the concentration of the donor and acceptor respectively, and n_i is the intrinsic carrier concentration in the semiconductor, a typical value for silicon is 10^{10} cm^{-3}.

The depletion width in a diode can be represented using the following formula:

$$W = \frac{2K_s\varepsilon_0}{q}(V_{bi} - V_A)\left(\frac{N_A + N_D}{N_A N_D}\right)^{1/2} \tag{4.3}$$

Where ε_0 is the permittivity, V_{bi} is the built-in potential and V_A is the applied potential.

The capacitance in a PN junction can be represented using the following formula:

$$C = \left[\frac{q\varepsilon s}{2\left(\frac{1}{N_A} + \frac{1}{N_D}\right)(V_{bi} - V_A)} \right]^{1/2} \tag{4.4}$$

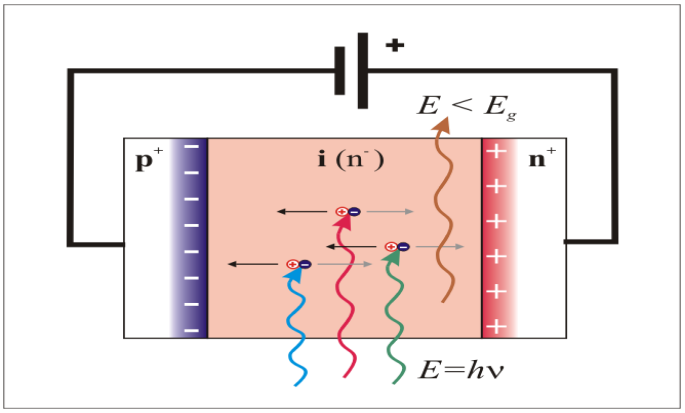

Figure 26. Photoelectric effect in photodiodes.

The depletion region in a P-i-N is much wider than that in a PN junction. This allows more photons to be absorbed.

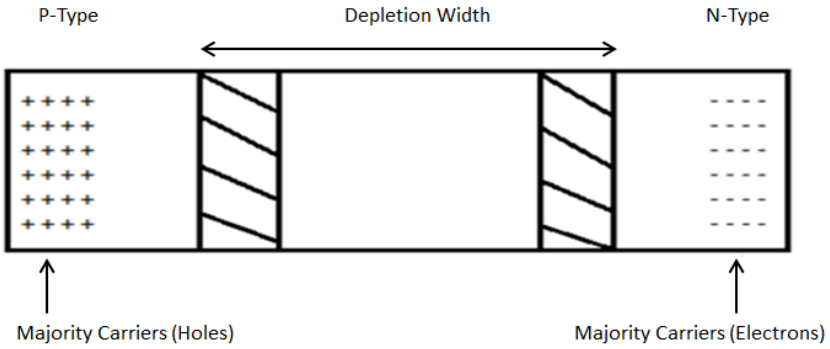

Figure 27. A cross-section of a PiN junction.

The depletion width in a P-i-N diode can be represented as follows:

$$W = \left[\frac{2K_s\varepsilon_0}{q} \left(\frac{N_A + N_D}{N_A N_D} \right) * V_0 + d^2 \right]^{1/2} \tag{4.5}$$

Where d is the width of the depletion region.

The following formula represents the depletion width at the N-type region:

$$X_n = \frac{(N_A * W + N_D * d)}{N_A + N_D} \tag{4.6}$$

The following formula represents the maximum electrical field before breakdown:

$$E_m = \frac{q * N_D * (X_n - d)}{K_S \varepsilon_0} \tag{4.7}$$

The following formula represents the break down voltage of P-i-N diode:

$$V_0 = \frac{E_m * (W + d)}{2} \tag{4.8}$$

The following formula represents the capacitance inside a P-i-N diode:

$$C = \frac{K_S * \varepsilon_0}{X_N + X_P + d} \tag{4.9}$$

The origin of the x-axis is at the p-i junction. The capacitance of a p-i-n junction will be the result of the series connection of the capacitances of each region.

In the photovoltaic mode, there is no potential difference applied on the diode. This will restrict the current to flow out of the diode which causes a built-in voltage. The photovoltaic mode is usually used as the basis for solar cells. On the other hand, in the photoconductive mode the diode is usually operated in reverse bias where the n-type region is biased with positive potential while the p-type is biased with negative potential. The reverse bias causes the depletion width to increase which in terms reduces the junction's capacitance. The current that flows through a diode in the reverse bias mode is usually known as Dark current, which is almost independent of the photocurrent. Depending on the spectral distribution, the photocurrent is directly proportional to the intensity of the illuminance. With the reduction in capacitance, the delay time decreases; however, the electronic noise increases causing noise in the measurement analysis.

4.3 Imagining Modes

The two main modes of operation for an AFM are the static mode and the dynamic mode. The static mode uses amplitude modulation in order to detect the surface's topography. The

cantilever is dragged on top of the sample, when the cantilever is deflected the laser reflecting back from the top of the cantilever is also deflected which is then recorded by the detector. However, in the dynamic mode it uses frequency modulation in order to detect the surface's topography. The cantilever is oscillated at a frequency close to its resonance frequency. When the cantilever is brought into the vicinity of the sample, forces start to act on the cantilever causing a change in either in the amplitude of oscillation, frequency of oscillation, or in the phase of oscillation. This change is then recorded by the detector and translated to an image about the sample's topography.

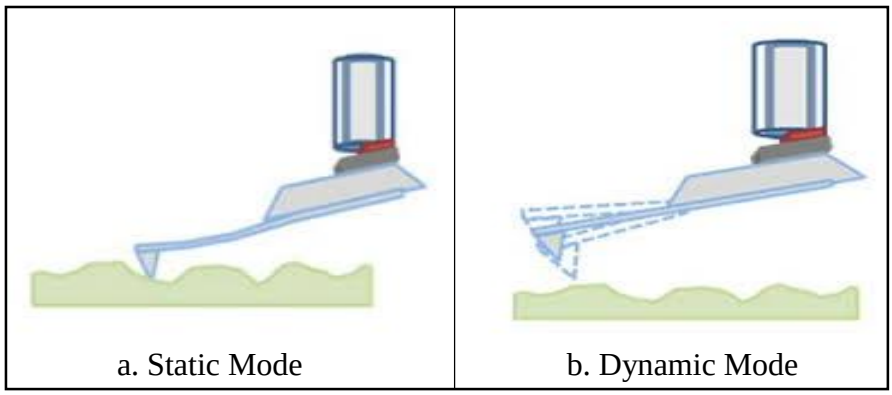

Figure 28. Representation of static and dynamic mode in an AFM.

4.3.1 Static Mode

The static mode, which is also known as the contact mode, is mainly used when the sample is ridged. It uses low stiffness cantilevers in order to avoid damaging the sample's surface from causing scratches. The force between the tip and the sample's surface is kept constant and using

the amplitude modulation method, a change in topography is detected. When the tip is brought to a close distance with respect to the sample, forces act on the tip causing it to snap-in to the surface. Since these forces could cause damage to the tip, a sample with an overall repulsive forces are usually preferred. However, there is still a possibility that the tip might still damage the sample's surface. The tip may also collect debris from the sample causing more noise on the measurements.

4.3.2 Dynamic Mode

The dynamic mode is also known as the non-contact mode or tapping mode. It is mainly used when the substrate is soft. The cantilever oscillates at or close to its resonant frequency and when brought really close to the sample's surface, around 10 nm or below, the forces acting from the sample on the tip cause the oscillating frequency to change. Typical oscillating amplitude ranges from few picometers to several nanometers. A feedback loop is usually used to maintain the same oscillating amplitude or frequency, and any change detected would be related to the sample's topography.

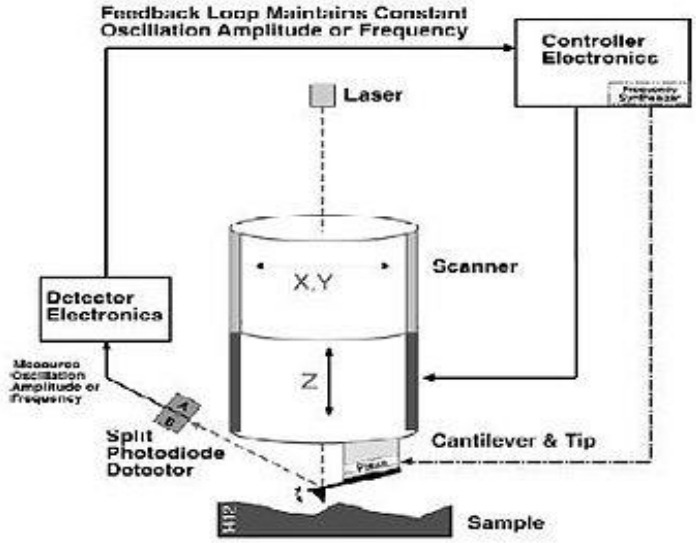

Figure 29. Illustration of the feedback loop in an AFM system.

The benefit of using non-contact mode is that the sample and AFM tip do not degrade after couple measurements which is not the case during contact mode. This is usually preferable when measuring soft sample such as biology samples and organic thin films. On the other hand, if the sample is rigid, contact mode is preferred due to the presence of few monolayers of absorbed fluid such as water on top of the sample since the tip will pass through the water layer and contacts the sample's surface. In tapping mode, the tip will oscillate on top of the sample; however, due to the presence of a monolayer of water on top of the sample the tip will oscillate on top of the fluid instead of the sample. Even though this effect might be uniform throughout the sample; however, it might degrade the image resolution.

As mentioned earlier, in dynamic mode operation there are two types of modulation: frequency modulation and amplitude modulation. Frequency modulation takes the advantage of a change in frequency in order to characterize the sample. This mode usually requires stiff cantilever tips since they provide high sensitivity [68]. Moreover, using this mode, scientists were able to obtain the first atomic resolution image [69]. In order to eliminate most of noise sources and get a high resolution AFM image, the system can stored in a high vacuum chamber. However, vacuum is not an essential requirement to operate an AFM. Depending on the application a vacuum ambient might be required. Similarly, amplitude modulation takes the advantage of a change in oscillating amplitude in order to characterize the sample. Moreover, the change in phase gives information about the various material that the sample is composed of.

4.4 Disadvantages of Atomic Force Microscope

Even though an AFM is capable of providing a high resolution image; however, the scanning speed is extremely slow compared to that of an SEM [70]. An AFM can only scan samples with maximum height ranging 10 to 20 micrometer. In one pass, an SEM can scan samples with depth of millimeters. Moreover, the maximum scanning area of an AFM is around 150x150 micrometers, whereas, an SEM can scan a square of several millimeters. This disadvantage of an AFM can be resolved by using a stitching method. Where the total area of a sample is divided into smaller areas, imaged and then stitched together. However, this capability consumes a lot of time and is limited to the stage movement precision. An alternative to stitching is to use parallel probes, where multiple probes are placed parallel to each other separated by a certain distance. This method

increases the cost of the AFM; however, most industries prefer this method of imaging because it consumes less time and provides faster feedback.

There are several sources that introduces noise while scanning the surface of the sample during imaging. Noise could be introduced from vibration of the floor or sound waves that are close by the instrument. However, nowadays AFM are placed in acoustic chambers, which absorbs most sound frequencies, and on a vibration isolation table, which absorbs most vibration frequencies. There are also internal source of noise and that could be due to mechanical parts or to electronic components. The piezoelectric material, which is a material that changes physical shape when electrically biased and vice versa, could move slowly or deform permanently under the influence of mechanical stresses. However, this deformation is not perfectly controlled which means that a change in the x-axis could cause a change in the y-axis or z-axis and vice versa. Newer AFMs takes these noise sources into account and uses a closed loop-scanners or real-time correction software to eliminate these problems as much as possible. Alternative methods have also been used which separates the piezoelectric material for each axis. In other words, for each axis would be controlled by a different piezoelectric material rather than having all axis controlled by one piezoelectric material.

Another source of noise that is more severe when imaging using an AFM is the artifact from the tip of the cantilever used during imaging.

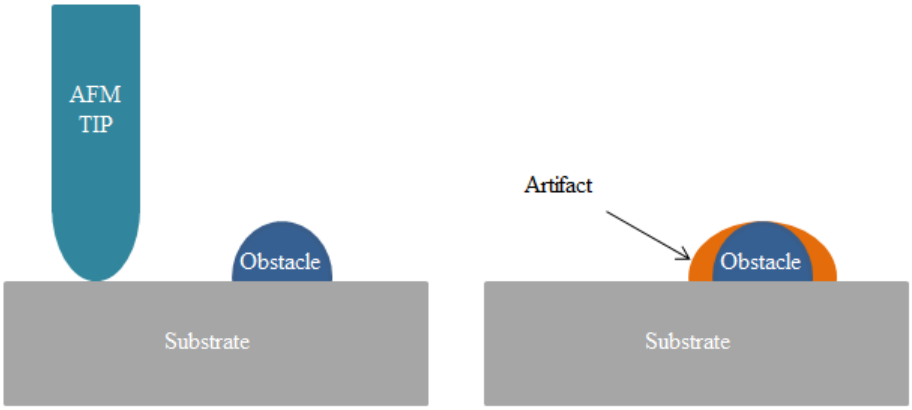

Figure 30. Illustration of an artifact in AFM imaging resulting from the tip's physical structure.

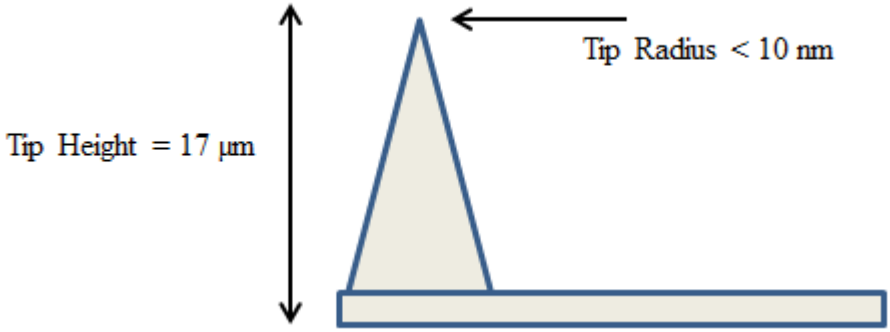

Figure 31. Schematic diagram representing typical dimensions of an AFM tip.

An AFM tip has a typical height of 10-15 micrometer and a tip radius below 10 nanometers. During scanning the tip may collect residue from the sample being imaged. This happens mainly in contact mode when the sample is not rigid. When the residue starts to collect on the tip of the

cantilever, the images become distorted and noisy, hence the tip must be replaced by a new one. Moreover, when the same tip is used for a long period of time it starts to become deflectable and the tip radius might increase, causing a distortion of the image.

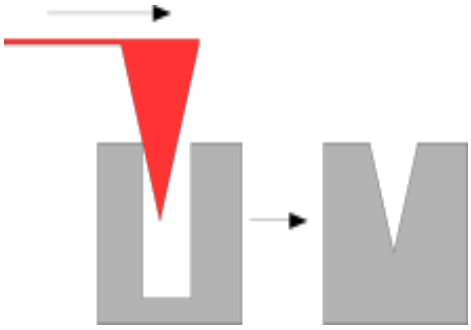

Figure 32. Illustration of an artifact in AFM imaging resulting from a steep sample topography

Another disadvantage comes from the physical shape of an AFM tip. The tips are triangular in shape making it almost impossible to image steep walls correctly. Even though, this could provide physical information about the tip itself; however, it doesn't provide the actual information about the depth and the overall shape of the structure [71]. On the other hand, imaging steep walls can provide information about the radius of curvature of the tip. Which is useful when trying to perform Young's modulus measurements since these measurements are directly related to the physical shape of the tip.

CHAPTER 5

POLYMERS

There is a wide variety of resists available in the market and each resist has its own unique properties. The choice of resist is highly dependent on the application it is being used for. The main parameters that need to be considered before purchasing a resist are: thickness, baking conditions, contrast, exposure source, and etch rate selectivity. The source of energy, that is required to expose the resist, is one of the main important parameters that determines the minimum feature size that can be obtained by the resist. For example, a much higher resolution can be obtained with an EBL compared to that using a UV light source. Moreover, there are resists that requires relatively high baking temperatures compared to other resists, which is usually not preferable in semiconductor industry. In this chapter few resists and polymers has been selected due to their outstanding properties and wide variety of applications.

5.1 Polymethyl Methacrylate (PMMA) Resist

PMMA which stands for polymethyl methacrylate is a standard electron beam lithography resist. Even though there is a wide variety of different electron beam resists with different properties, PMMA remains one of the highest resolution resist available [72]. PMMA is usually dissolved in solvents such as anisole, or chlorobenzene. PMMA dissolved in anisole is also denoted by PMMA A, while PMMA dissolved in chlorobenzene is denoted by PMMA C. Due to the environmental concerns that a PMMA C type resist could cause, the PMMA A type resist is more preferred. The viscosity of PMMA depends on the solvent that is formulated with.

For example, PMMA A resists has a viscosity slightly lower than those formulated in chlorobenzene, PMMA C. Typically, a resist with low viscosity has a lower thickness than those with higher viscosity. However, this difference in viscosity can be accommodated by using different spin speeds. So, in order to achieve a higher thickness, a low viscosity resist can be spun using a low rotational speed, expressed in round per minute (RPM). Similarly, a resist with high viscosity can be spun using high rotational speeds in order to achieve the same thickness as that of a lower viscosity resist. PMMA is represented by the following chemical structure:

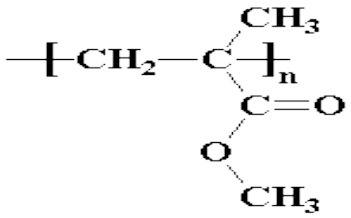

(5.1)

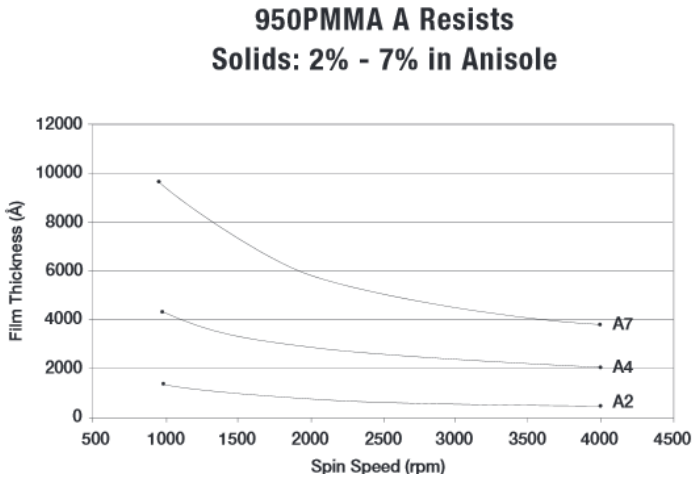

Figure 33. Film Thickness versus spin speed of a 950PMMA A resist.

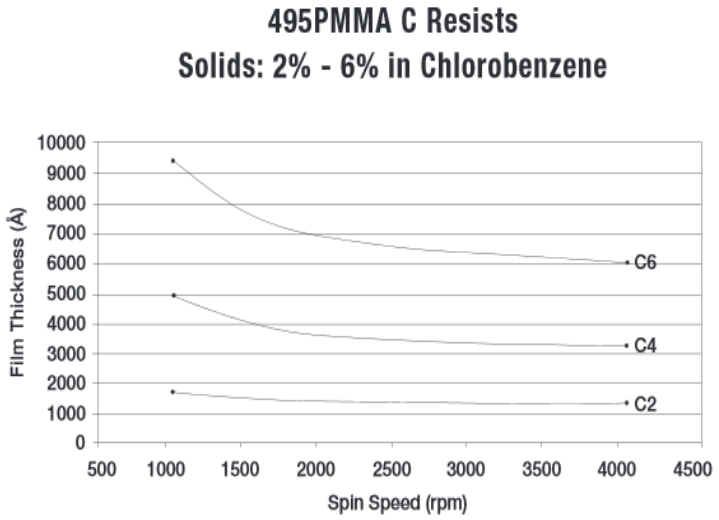

Figure 34. Film Thickness versus spin speed of a 950PMMA C resist.

The graphs above show that both resist can reach a thickness of 300 nm when the spin speed is 2000 rpm for 950PMMA A4 but on 4000 rpm for PMMA C4. Even though PMMA A type resists perform almost identically as those formulated with chlorobenzene, their compatibility with the layer underneath varies. For example, when spun on a phenol formaldehyde resin, a PMMA A type resist causes a spontaneous chemical reaction while a PMMA C type resist is more stable [73]. Moreover, PMMA resists also varies with molecular weights (MW). A significant factor that dictates the pattered features resolution. Generally, the molecular weights of PMMA can vary between 50 thousand all the way to 2.2 million. Although there is a variety of choices due to the different molecular weights, a 495,000 MW (495PMMA) and the 950,000 MW (950PMMA) are used most commonly. Molecular weight is an important factor to choose since it is directly related to the resolution of the patterned features. When

PMMA is exposed to electron beam with sufficient energy, the chemical bonds in the molecular chain starts to break. Then, the broken chains will be developed using a special developer, for PMMA it is MIBK, Methyl isobutyl ketone. The choice of MW weight is critical when fabricating bi-layer T-gate processes where the bottom layer should be more sensitive than then the top layer [74]. The difference in sensitivity will determine how much undercut can be obtained. Even though increasing dosage could lead to undercut, this method is usually not recommended due to the fact that PMMA at high dosages could crosslink, forming a negative resist.

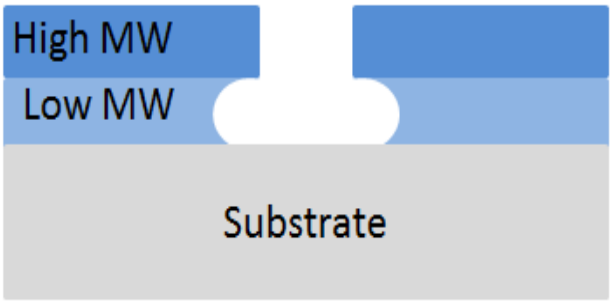

Figure 35. Schematic diagram of an undercut by using double layer resist with different molecular weights.

5.1.1 Applications of Polymethyl Methacrylate Resist

PMMA has been widely used in different applications and in different industries. Some of which are electronics, construction, fashion, medical devices, and furniture [75]. The

transparency of PMMA gave it a huge advantage for the usage in solar panels, lighting, signs and displays. Moreover, the high molecular weight of PMMA serve as a good replacement for bones [76]. The reason being is that it is biologically compatible and inert. When mixed with other polymers it possible to use it as a moldable dough which could harden in approximately 10 minutes [77].

PMMA are also used in alloplastic material for cranial bone reconstruction [78]. Plastic optical fiber (POF) usually use PMMAs as the inner material while fluorinated polymers are used as the covering material [79]. In particular fibers with relatively large diameters have PMMA as 96% of the cross section which in terms allow the transmission of light [80]. PMMA usually cause a 4% reflection of a normally incident light at the air-polymer interface. In the 1950s, early lenses were made from hard PMMA which are very similar to the hard lenses available today. PMMA are usually the result of annealing, a process that consists of successive heating and cooling. Annealing causes the PMMA to be much less toxic, and therefore making it suitable and safe for being used as lenses. Moreover, it can be molded with a high degree of precision [81]. Biodegradable polymers are important mainly due to the fact that they can be used in drug discovery systems and they can used in the fabrication of implants (fracture repairs, ligament reconstruction) and surgical dressings. However, there are other applications where non-biodegradable materials are in favor to be used such as artificial heart valves, contact lenses, and vascular grafts [82].

5.2 SU-8 Negative Resist

SU-8 is a well-known negative photoresist developed by IBM researchers in 1989. It is mainly used to obtain high aspect ratio structures with thickness more than 300 μm. However, it

could also be used as a thin film with thickness of sub micrometers. It is a mixture of an epoxy, a solvent, and a photoacid generator [83]. It is a very viscous polymer which makes it harder to handle compared with other less viscous photoresists. SU-8 is highly sensitive resist when exposed to UV-light with a wavelength of 365 nm. After the exposure and development of SU-8, it becomes very resistant to solvents, acids and bases and has excellent thermal and mechanical stability.

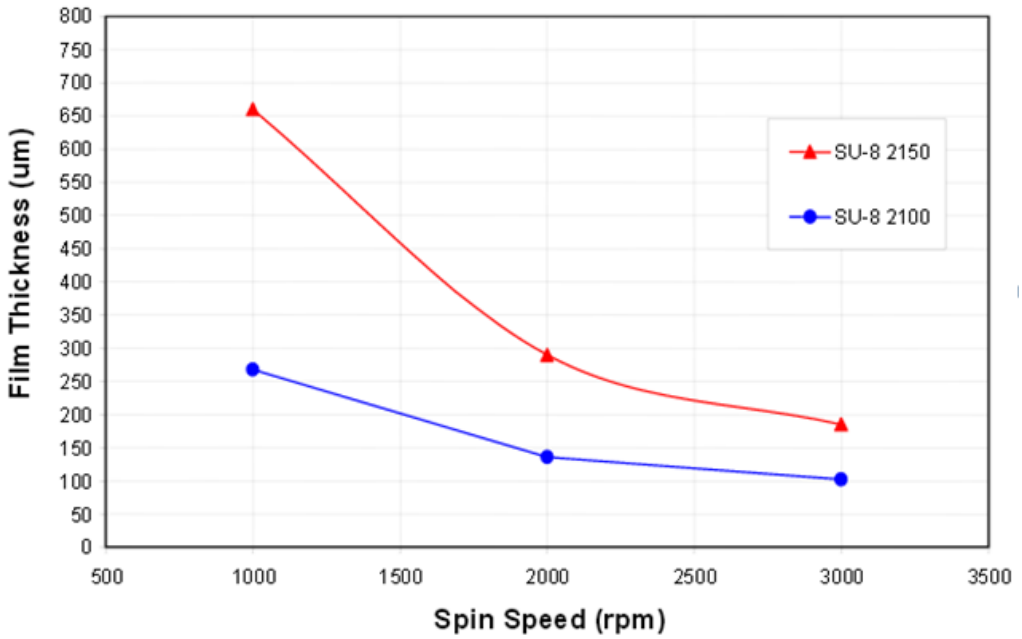

Figure 36. Film thickness versus spin speed of SU-8 2150 and 2100 resist.

5.2.1 Chemical Composition and Wafer Processing

In order to transfer the pattern from a mask to SU-8, several steps need to be followed. First, the substrate must be ultra-clean. For example, for silicon wafers it is highly recommended that the wafers undergo Piranha acid clean in order to remove any organic residues if any are present [84]. Piranha acid is really strong acid that needs to be handled with care. It is a mixture of sulfuric acid (H_2SO_4) and hydrogen peroxide (H_2O_2) usually to a ratio of 3 to 1 respectively. Then, the SU-8 is spun on top of the wafer. Due to the viscosity of the SU-8, spin speed should be slowly accelerated to reach the desired speed. After spinning, some of the photoresist build up on the edge of the substrate causing what is known as edge bead.

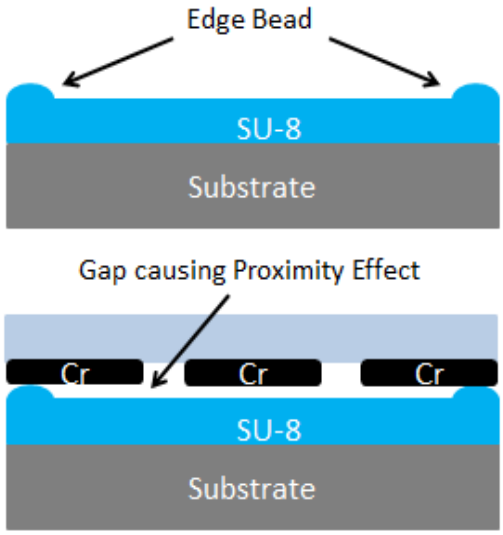

Figure 37. Illustration of edge bead and its effect on mask alignment in standard optical lithography.

The edge bead tends to cause a misalignment between the mask and the substrate and/or proximity effect. It is highly recommended to remove the edge bead before baking. Then, the wafer is baked for few minutes at around 65 degrees Celsius and then at 90 degrees Celsius from 30 min to 2 hours depending on the thickness of the film. This procedure is often referred to as prebake or soft bake. Then, the substrate is aligned with the mask and exposed with the required dosage. The cross-linking happens in two steps. First step is the formation of a strong acid which occurs during exposing. Second step is catalyzing the acid which occurs when heat is applied in a process also known as post exposure bake, during which the epoxy would cross link. Post bake requires heating the substrate at two different temperatures but at a less time compared to that of the prebake. After post bake procedure is performed, the resist is developed. Solvents based on ethyl lactate and diacetone are recommended along with strong agitation when developing high aspect ratio and/or thick film structure. Development time depends on resist thickness, agitation, dilution of solvent. Typical developing time ranges from 10 to 30 minutes.

5.2.2 Applications of SU-8

SU-8 has excellent mechanical properties, thermally stable, can resist a wide variety of chemical, and has high etch rate selectivity [85]. These properties gave it a huge advantage in fabricating microfluidic devices which could also be used for bioMEMS applications [86]. SU-8 is natively highly hydrophobic [87], which caused the use of external pumps to ease the flow of water in the microfluidic devices. Oxygen plasma has been used to modify the surface properties of SU-8 and make it hydrophilic [88]. However, with oxygen plasma the surface roughness increases. This enhancement enabled researchers to build lab-on-chip devices for biomedical

applications. Some of these devices are biosensors and membrane bioreactors, which could be used in clinical diagnostics [85].

5.3 Polydimethylsiloxane

Polydimethylsiloxane (PDMS) is an organic polymer mainly made from silicon. It has unique mechanical, chemical, optical properties which made it compatible for many microfluidic and optical devices. It is inert, non-toxic, and non-flammable. It can be prepared by mixing a base and a cross-linking agent, which are both viscous liquid until they are mixed together. The properties of this polymer are determined by the mixing ratios and curing methods used during the development process. PDMS chemical formula is $CH_3[Si(CH_3)_2O]_nSi(CH_3)_3$ where n is an integer number [89]. PDMS is represented by the following chemical structure:

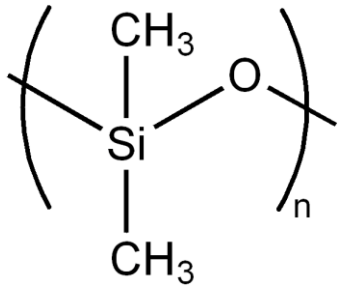

(5.2)

5.3.1 Applications of PDMS

PDMS is commonly used in microfabrication molds mainly because it changes state from being a liquid before curing into becoming an elastic solid after curing. The concentration of the cross-linking agent is an important factor that determines the rigidity of the polymer. If a high

concentration is added, the polymer could become hard solid. On the contrary, if few amount is added the polymer remains as a viscous liquid. PDMS can act as a rubber solid, so when mechanical forces are applied on it, it deforms permanently and then returns to its original state. PDMS is hydrophobic which makes it hard for water to penetrate its surface. This property made it highly favorable for microfluidic devices. However, it absorbs other chemicals through diffusion, but the chemicals can diffuse out from the other side easily as long as the concentration of the existing chemical is less on the other side. PDMS is considered transparent for a large electromagnetic spectrum. Depending on the mixture ratios, curing times, and temperature the refractive index of the bulk may vary. These properties made it an excellent candidate as a material to be used for lenses and waveguides. Since PDMS is considered inert to a wide variety of chemicals, it was used as a chemical sensor. Chemicals diffuse into the PDMS which causes a change in its optical properties, mainly its index of refraction. Even though it could be used in order to characterize the chemical and measure its concentration; however, it is relatively slow since it depends on the diffusion mechanism.

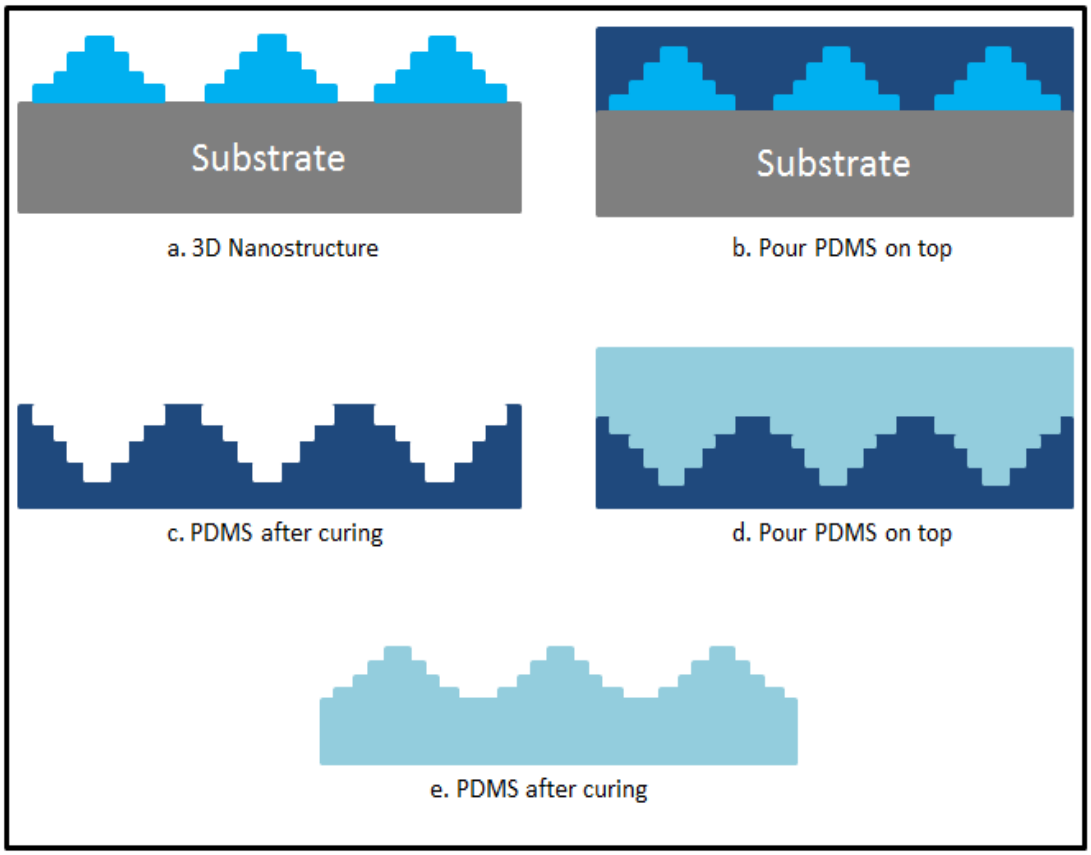

Figure 38. Illustration of the usage of PDMS as mold to duplicate 3D nanostructures.

CHAPTER 6

THREE DIMENSIONAL ELECTRON BEAM LITHOGRAPHY

6.1 Introduction and Applications

The interest in pattering thick resist is steadily growing due to its versatile applications. Patterning structures with height ranging from few microns to several millimeters is often referred to as high aspect ratio lithography. High aspect ratio lithography is necessary for but not limited to: electro-mechanical devices, interconnects for very large scale integrated circuits (VLSI), Fresnel zone plates, acoustic emission transducers, biomedical applications, etc. The main focus of this chapter will be fabricating high aspect ratio structures for biomedical applications. Cells in a human body interact with its surroundings; however, this sort of interaction is not fully understood. "The effects of topography and mechanical properties of surfaces on mammalian cell behavior, bacterial adhesion and biofilm formation have only recently been explored but remain largely unknown" [90]. In order to study the cell interaction with its surrounding, it is important to duplicate the exact structure and mechanical properties of a certain surrounding. One way of obtaining the exact structure is by sacrificing an animal and using its tissues as the 3D environment of the cell. However, sacrificing an animal's life for research purposes is not an easy task, and it would be much simpler if the topography and the mechanical properties of the scaffold could be duplicated without sacrificing an animal. This could be done by using various techniques such as 3D laser printing, 3D printers and other similar tools discussed earlier in Chapter 1. However, these fabrication methods are limited to low resolution and/or to the materials that could be used, which might not be FDA approved or

compatible for biomedical applications. On the other hand, PMMA which is the material used for our 3D EBL fabrication is FDA approved and its mechanical properties can be precisely controlled through thermal treatment. With 3D EBL high resolution can be achieved, below 25 nanometers. With a single layer of PMMA a 1:1 mimic of a real scaffold has been fabricated of different stages of a cancer cell topography, shown in figure 39. However, using a single layer resist limits the thickness of the resist to be 200 nm, which illustrates the need for an alternative method to fabricate high aspect ratio structures. Even though different resists might have a higher thickness; however, so far PMMA is the only electron beam resist that is FDA approved.

According to a research group at Weizmann Institute of Science, "HeLa cells, immortal cancer cell lines that divide indefinitely alleviating the need to sacrifice primary animal tissue for experiments, adhere to the extracellular matrix and like many other cell types on a microscope slide spread thinly to a diameter of ≈40 μm … but only a few μm in height" [91]. This illustrates the necessity of having a structure that has a depth on the order of few microns. In this chapter, multiple methods are proposed and demonstrated in order to obtain high aspect ratio 3D nano-structures.

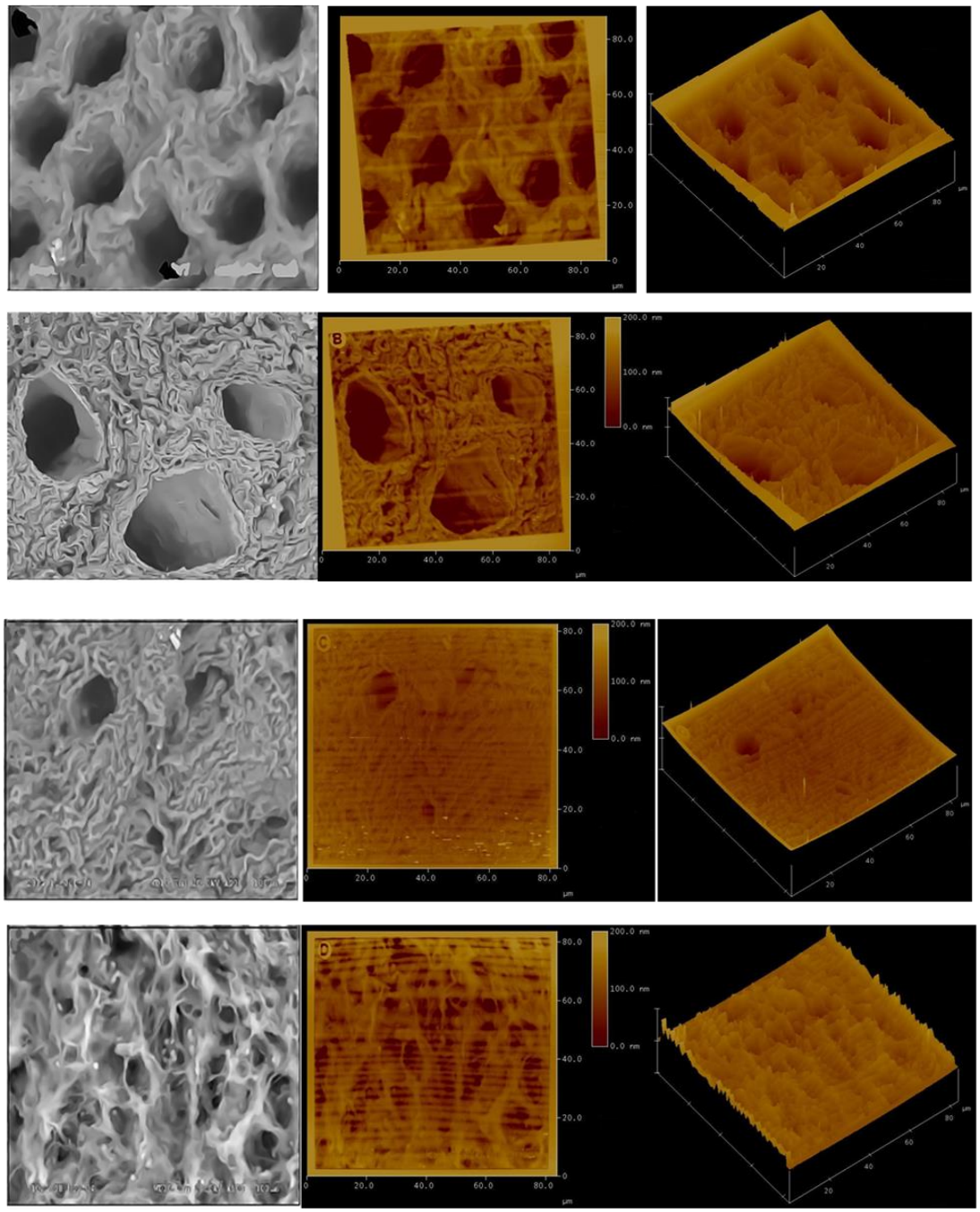

Figure 39. SEM image (on the left), AFM image (on the right) represent (from top to bottom): Normal topography, stage 1 colon cancer topography, stage 2 colon cancer topography, and metastatic stage topography.

6.2 Mix and Match Lithography

High aspect ratio structures can be fabricated by combining both optical and electron beam lithography. Two different approaches has been demonstrated in the following sections.

6.2.1 Mask Method

This method requires the use of two lithographic techniques simultaneously. Starting with a polished silicon wafer as a substrate, an ultraviolet (UV) sensitive resist, in this case AZ1518, is coated on the top surface. Even though this resist has a thickness of approximately 1.2 μm at 4000 rpm, photoresist thickness can range from 1 μm all the way to few millimeters depending on the type, viscosity and spin speed of the resist used. Following the standard lithographic procedure, the resist is then baked at the required temperature to solidify. Then PMMA, a resist which is sensitive to electron beam, is coated on top of the first resist, and then baked to solidify. After baking, 3D electron beam lithography is performed by modifying the dosage of the beam. The 3D structures would be obtained after developing the PMMA. There are several developers that could be used, however MIBK mixed with IPA with ratio 1 to 3 is preferred for better resolution. Following this step, an optical lithography mask is required to pattern the UV sensitive resist. The chromium portion of the mask will absorb the UV light; on the other hand, the UV light will pass through where chromium is absent. The mask must be precisely aligned with the patterned PMMA, then the substrate is brought into contact with the mask to minimize proximity effect and the substrate is exposed with ultra violet radiation (365 nm wavelength). Then, the exposed resist is developed using an AZ developer. With this approach, high aspect ratio 3D structures should be obtained; however, one problem arises in the process of aligning the optical mask to the patterned PMMA.

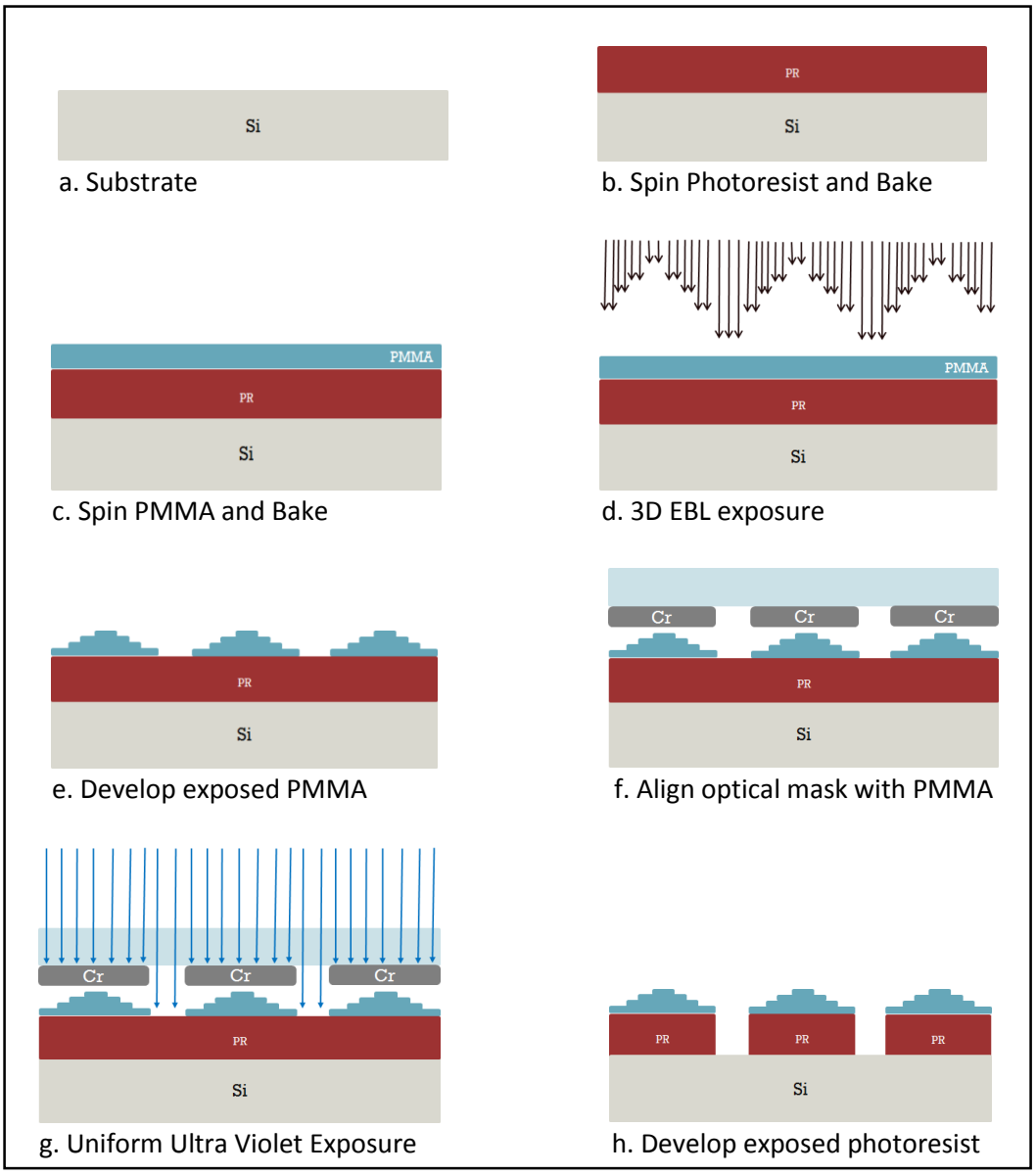

Figure 40. Illustrates the first approach of using both 3D EBL and photolithography to obtain high aspect ratio structures.

One disadvantage of this approach is that a small alignment mismatch will result in optical resist being exposed in unwanted areas. The optical resist below the PMMA will get exposed and then developed which will result in a different structure than the one desired. This would modify the mechanical properties, or the 3D PMMA structure could collapse to the substrate if there not enough optical resist to support it in position.

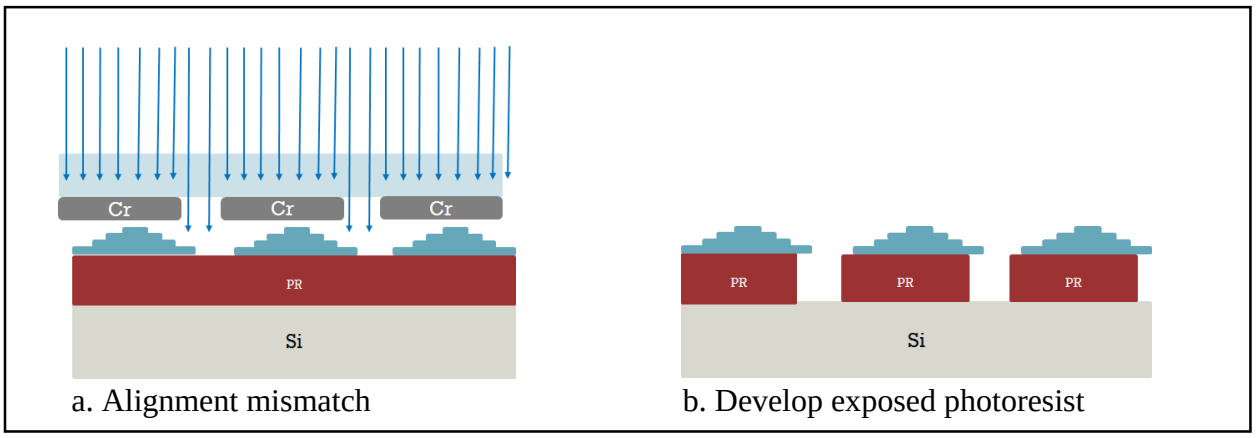

Figure 41. Illustrates the effect of misaligning the optical mask with the 3D EBL pattern.

6.2.2 Maskless Method

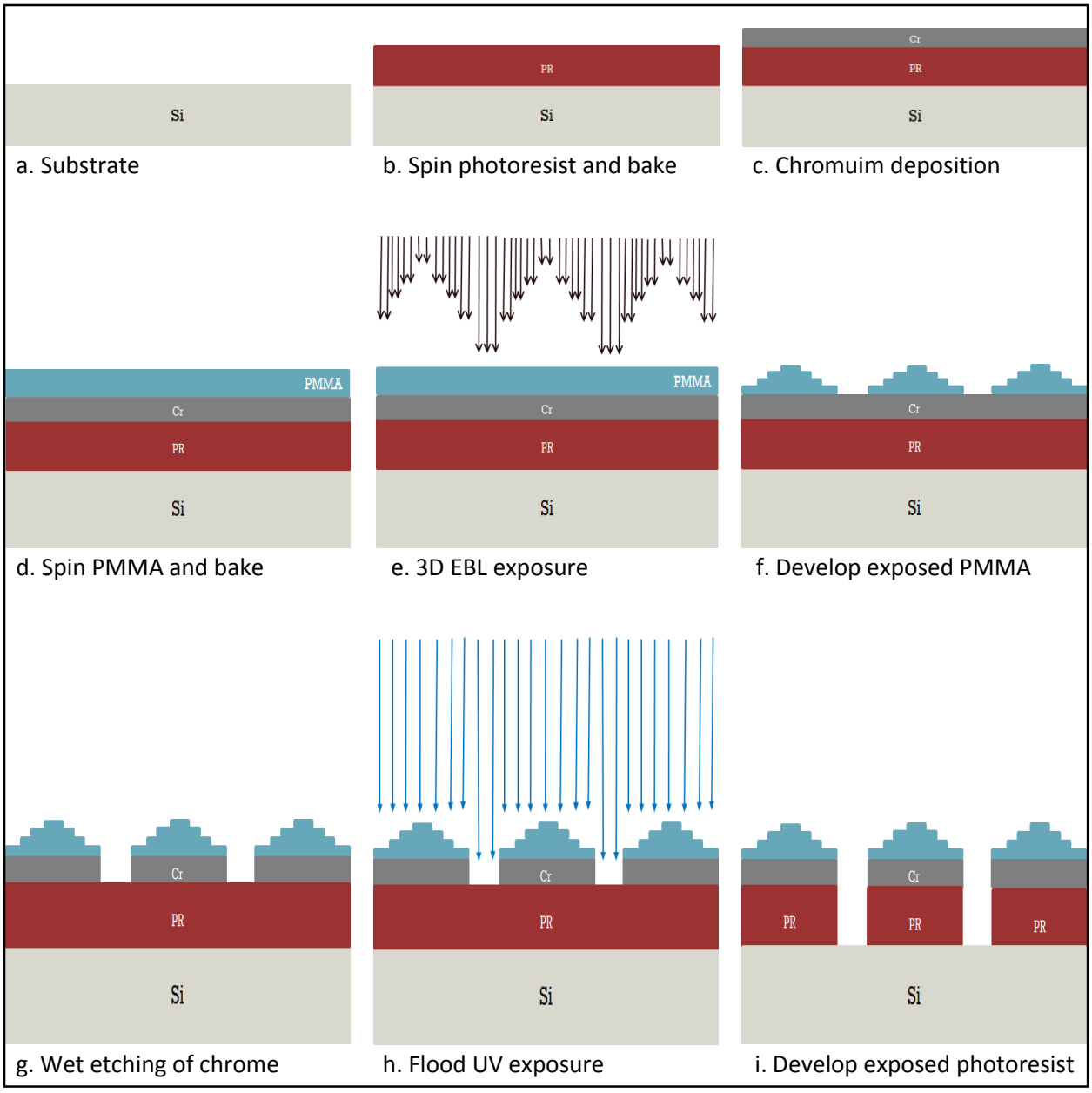

Figure 42. Illustrates the mask-less approach for combining optical lithography and 3D EBL

This approach substitutes the use of an optical mask, which could cost from few hundred US dollars to several thousands of US dollars depending on the quality and minimum feature size, by depositing a chromium layer. Starting with a polished silicon wafer, the photoresist is spun and baked until it solidifies. Then, using an electron beam evaporator, a 20 nm thick chromium film is deposited on top of the photoresist. The electron beam evaporator uses a filament as the source of electrons. The electrons are then extracted into vacuum and accelerated under high voltage, typically 10 kV. Since electrons are charged particles, their direction of propagation can be controlled precisely using magnetic field according to Lorentz's equation:

$$\mathbf{F} = q\mathbf{V}x\mathbf{B} \tag{6.1}$$

Where F is the force applied on the electron, q is the electron charge, **V** is the velocity of the electron, **B** is the magnetic field applied on the electron.

High vacuum should be reached in order for the chromium layer to be uniform. A typical pressure for electron beam deposition is below 10^{-7} Torr. Following the deposition of the chromium a 200 nm layer of PMMA is spun on top of the chromium, then baked. 3D electron beam lithography is then performed and the exposed PMMA is developed. Then using a wet etchant, the chromium which is not covered by PMMA is etched out. Then the optical resist is exposed to UV radiation, and then developed. The figure 34 illustrates the need of such technique.

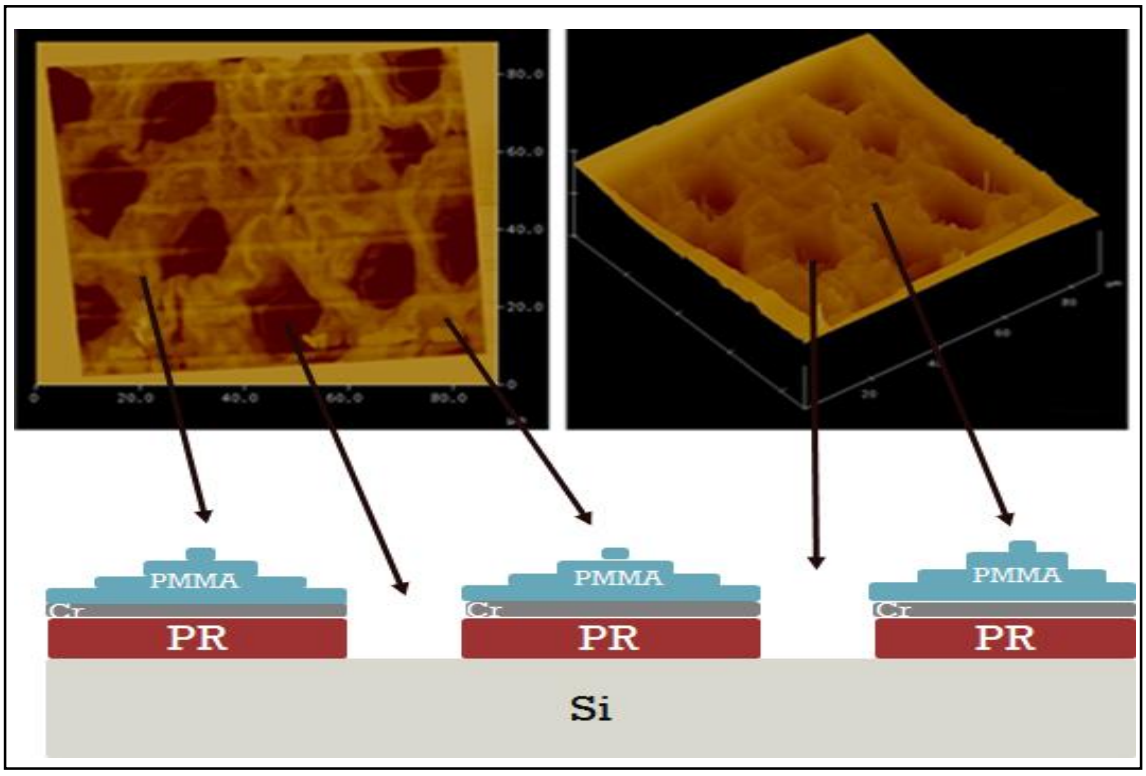

Figure 43. Shows the matching of scaffold topography with the fabricated structures.

Where the 3D PMMA in fig 43 represents the 3D structures of the scaffold and the holes would be on the size of a micron range deep.

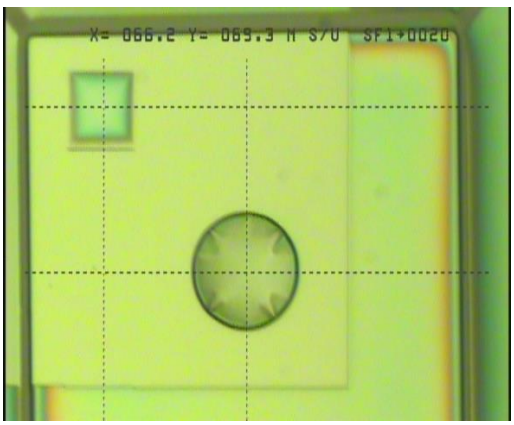

a. 3D Pyramid (200 nm) next to circular pillar (1.2 µm)

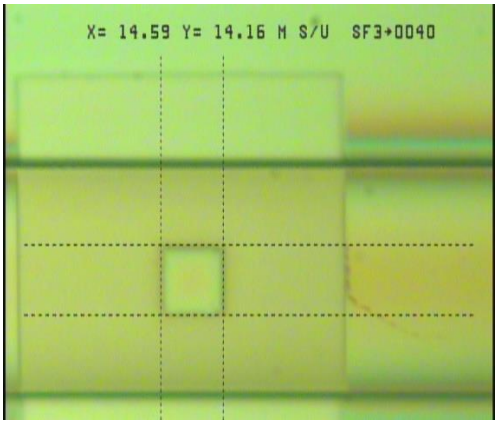

b. 3D Pyramid (200 nm) on top of bridge (1.2 µm)

Figure 44. Showing optical images of mix and match approach of 3D EBL and optical lithography.

Fig 44a shows a 3D Pyramid patterned using 3D electron beam lithography, while the circular structure was fabricated using optical lithography. On the other hand, fig 44b shows a pyramid which was fabricated on top of a bridge. The pyramid is patterned using 3D electron beam lithography, and the bridge was fabricated using optical lithography with chromium deposited on top.

6.2.3 Double Layer PMMA

An alternative method to obtain high aspect ratio structures is by using multi-layer resist. Starting with a polished silicon wafer, a layer of PMMA is coated on top then baked. Then, another layer of PMMA is coated on top of the previously baked PMMA, and then baked again at 180 degrees Celsius. Then, 3D electron beam lithography is performed and then developed. With this method, theoretically the thickness obtained should be twice as much as that of a single layer resist.

However, the actual thickness turned out to be less. Expected thickness was 400 nm, but the measured thickness was around 300 nm. Moreover, the bottom resist will be baked twice at 180 C which will affect its properties. This means that the baking time and temperature of both layers has to be recalibrated in order to avoid over baking of bottom resist. Temperature is a critical parameter that determines the dosage profile required to expose the resist and the developing time. If the temperature is not modified, the bottom layer will be baked twice and the resist would harden, and it would be difficult develop after exposure.

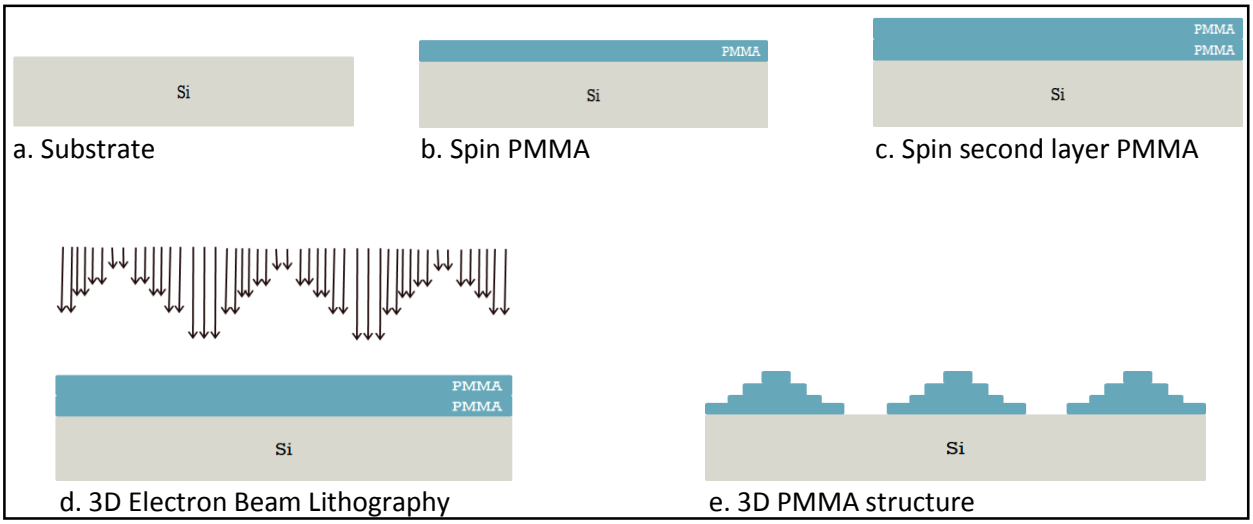

Figure 45. Illustration of double layer PMMA resist patterned using 3D EBL

6.2.4 Single Layer Resist 50 nm Developed (Results)

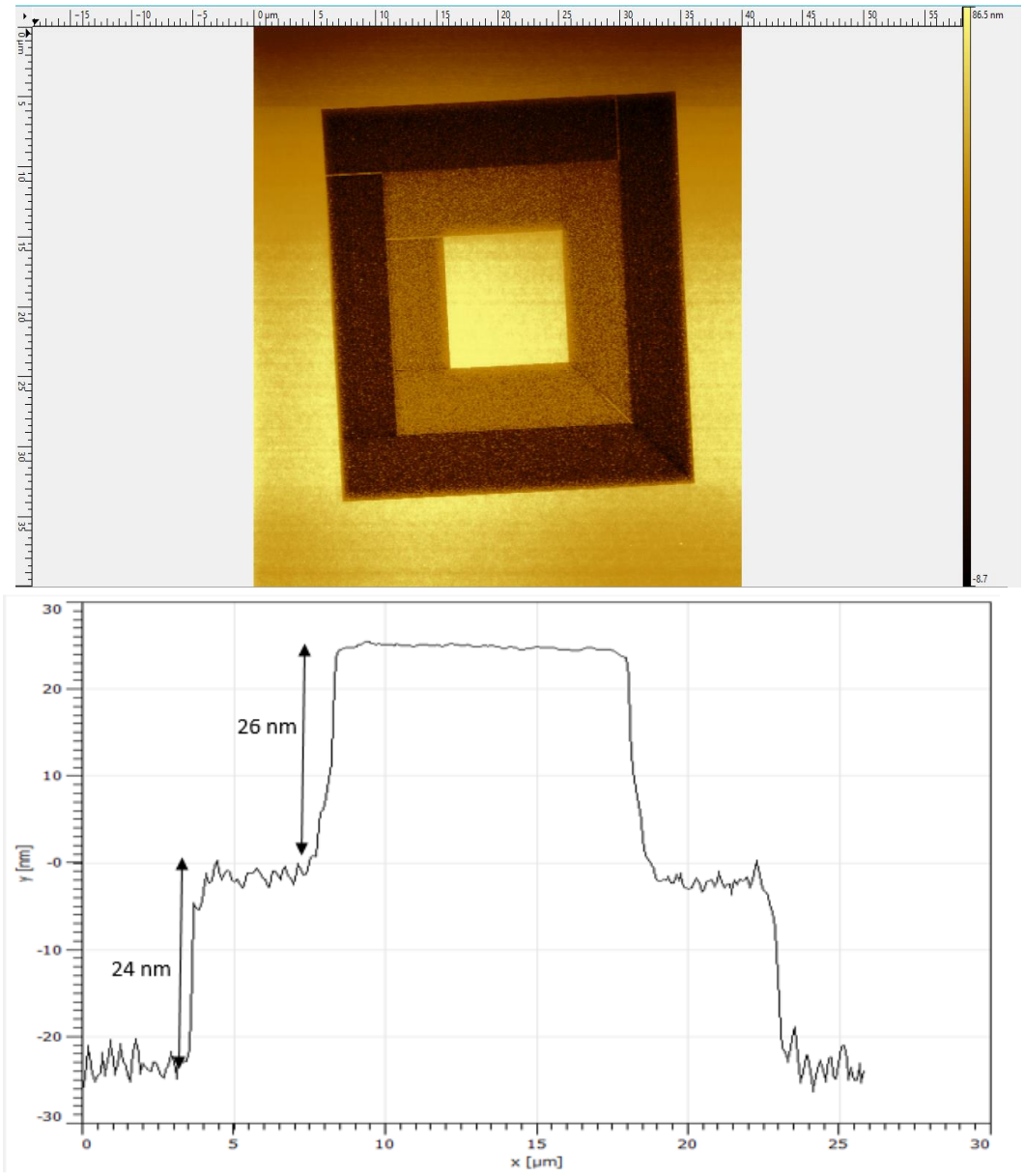

Figure 46. An AFM image (top) and a cross section (bottom) of a 2 step pyramid of a 200 nm thick resist developed thickness 50 nm.

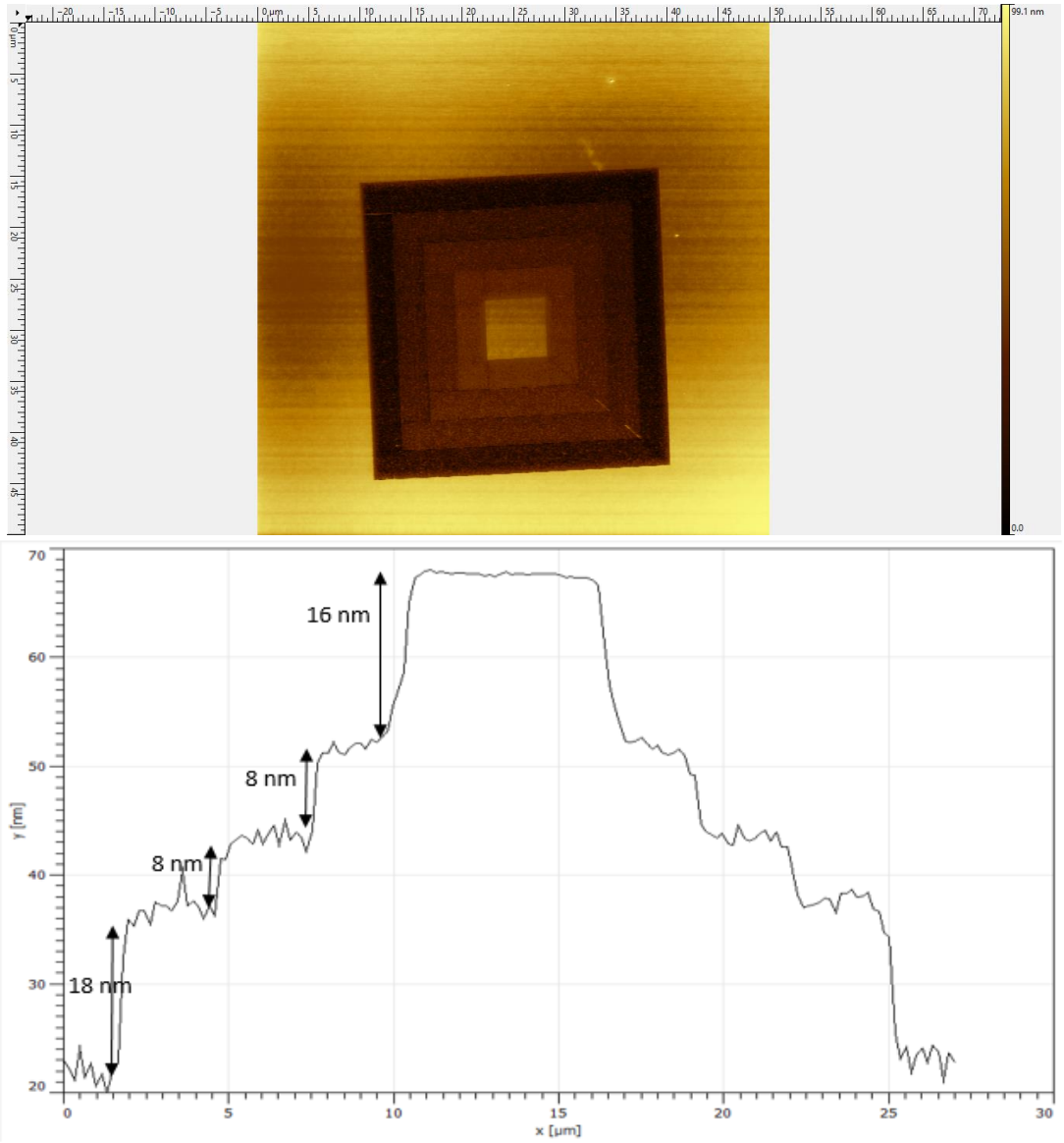

Figure 47. An AFM image (top) and a cross section (bottom) of a 4 step pyramid of a 200 nm thick resist developed thickness 50 nm.

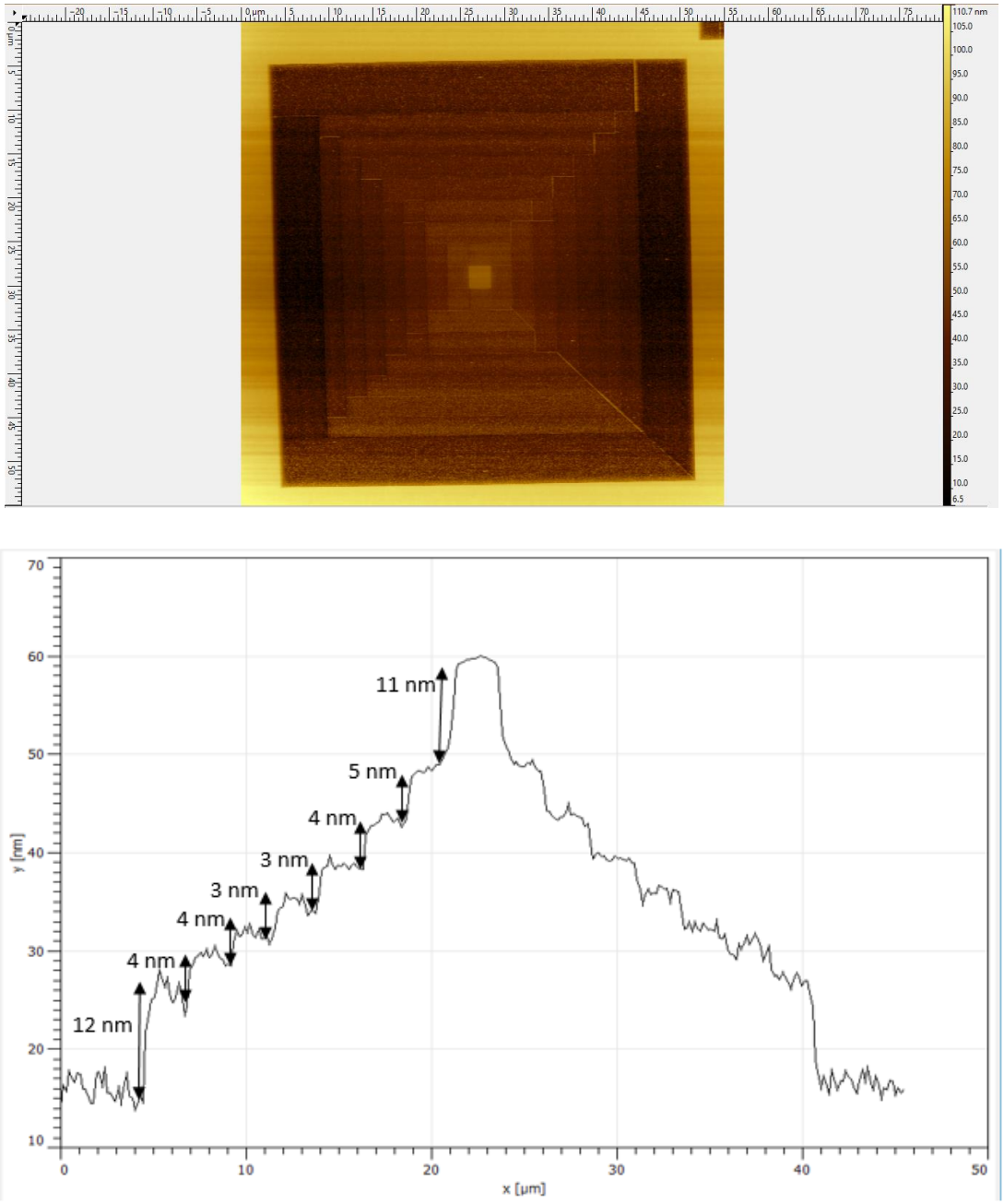

Figure 48. An AFM image (top) and a cross section (bottom) of an 8 step pyramid of a 200 nm thick resist developed thickness 50 nm.

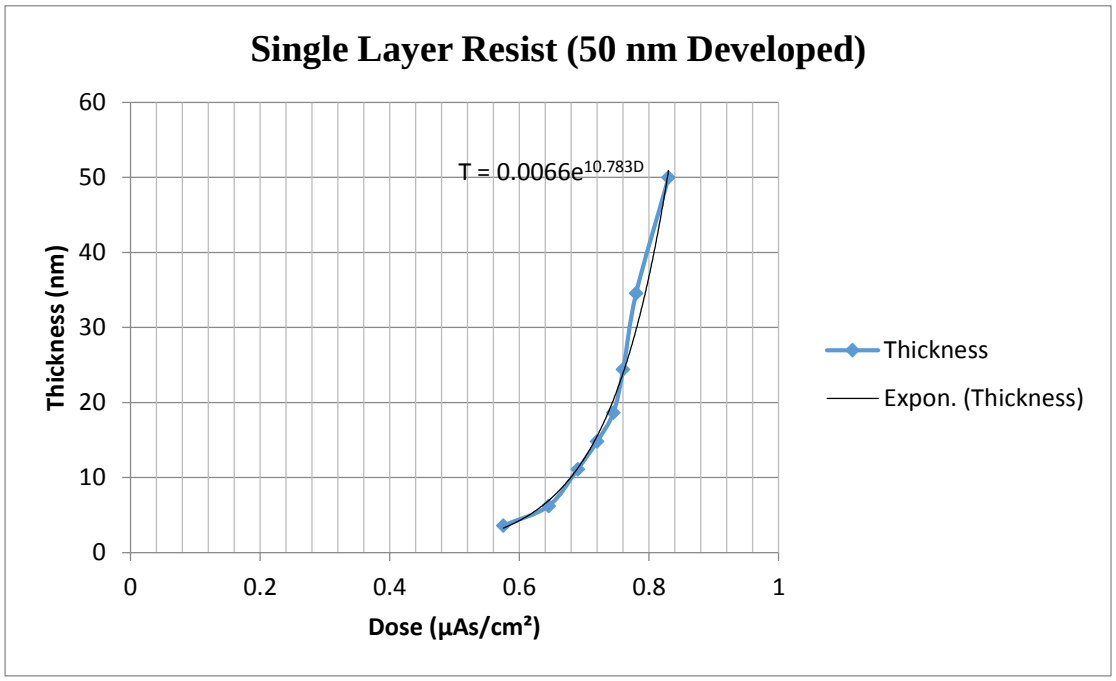

Figure 49. Thickness versus dosage relationship of a 50 nm developed resist

It turns out that the thickness is related to dosage exponentially according to the following formula:

$$T = 0.0066 * e^{(10.783 * D)}$$

Where T is thickness in nanometers and D is the normalized dosage in µAs/cm².

6.2.5 Double Layer Resist 60 nm Developed (Results)

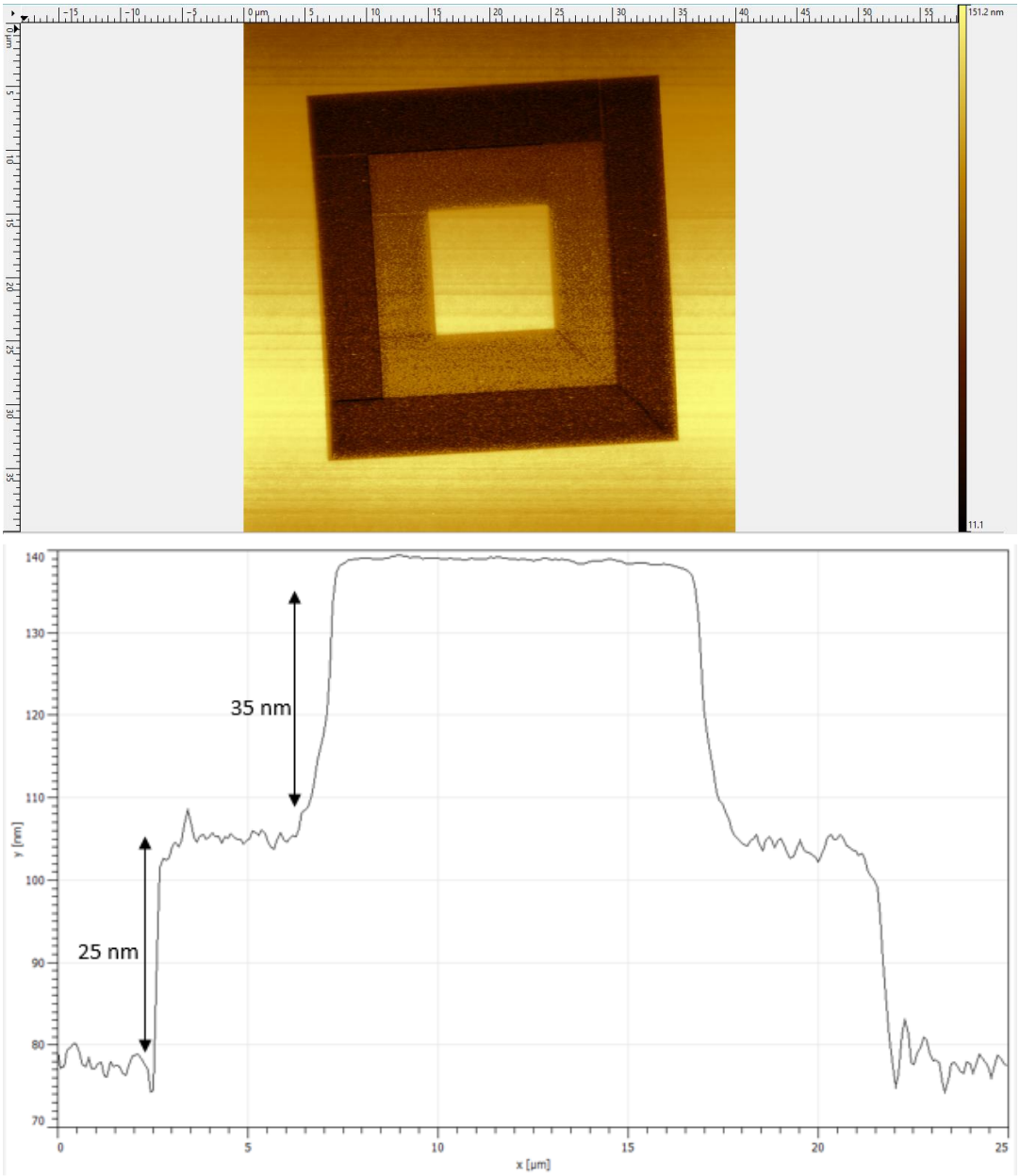

Figure 50. An AFM image (top) and a cross section (bottom) of an 8 step pyramid of a 300 nm thick resist developed thickness 60 nm.

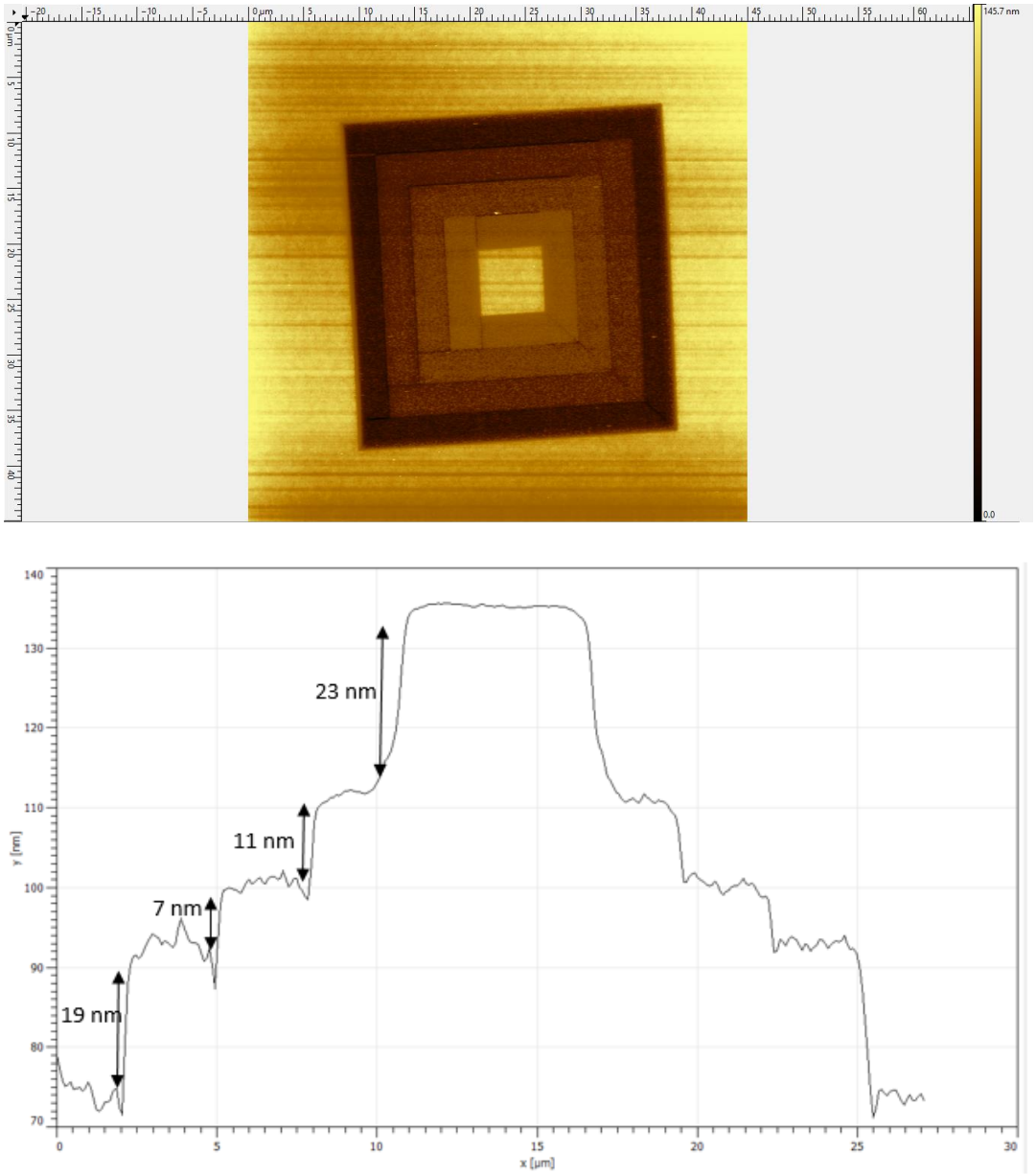

Figure 51. An AFM image (top) and a cross section (bottom) of a 4 step pyramid of a 300 nm thick resist developed thickness 60 nm.

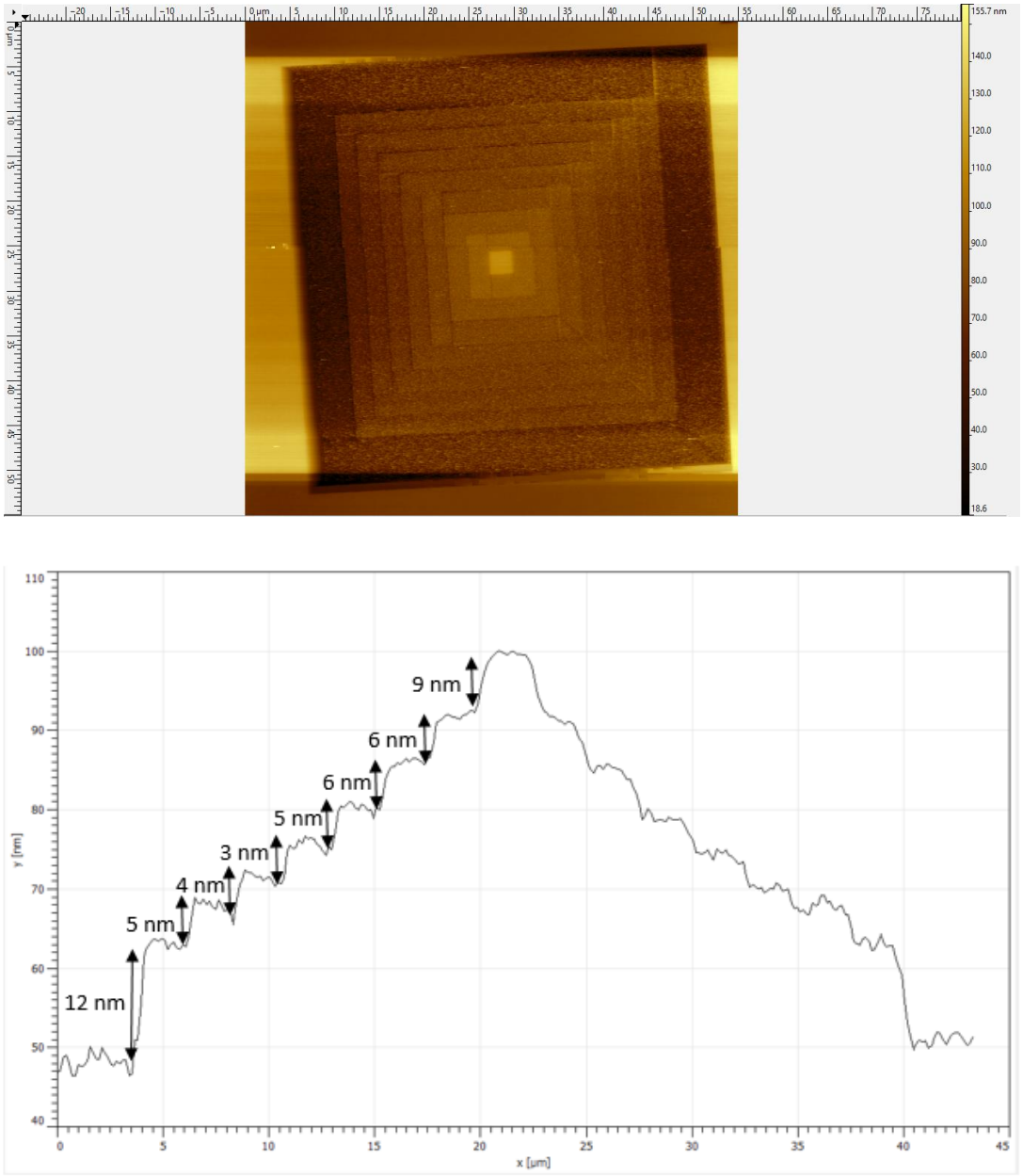

Figure 52. An AFM image (top) and a cross section (bottom) of an 8 step pyramid of a 300 nm thick resist developed thickness 60 nm.

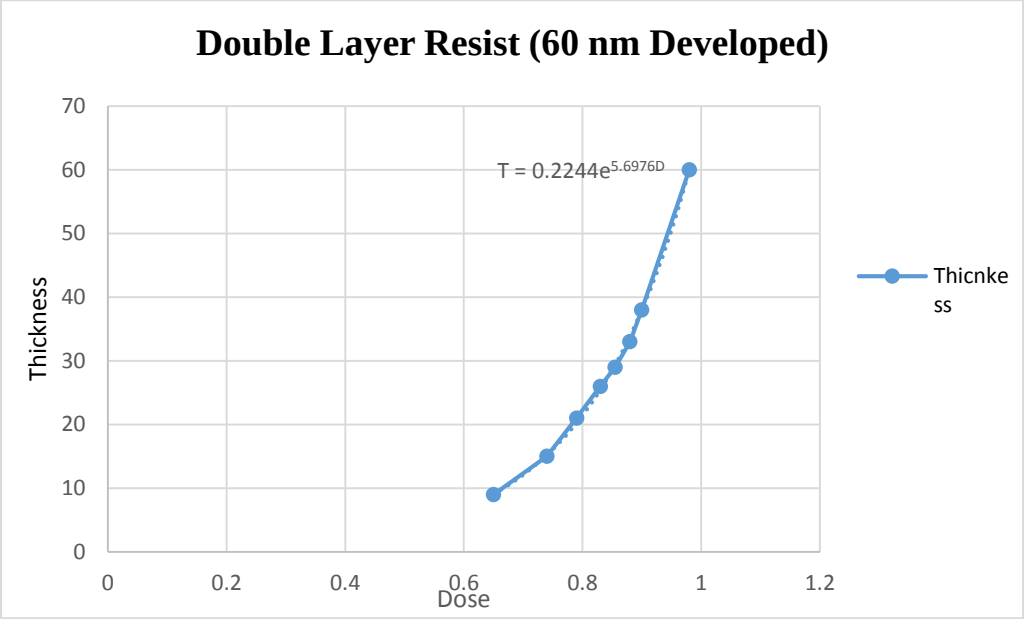

Figure 53. Thickness versus dosage relationship of a 60 nm developed double layer resist.

It turns out that the thickness is related to dosage exponentially according to the following formula:

$$T = 0.2244*e^{(5.6976*D)}$$

Where T is thickness in nanometers and D is the normalized dosage in μAs/cm².

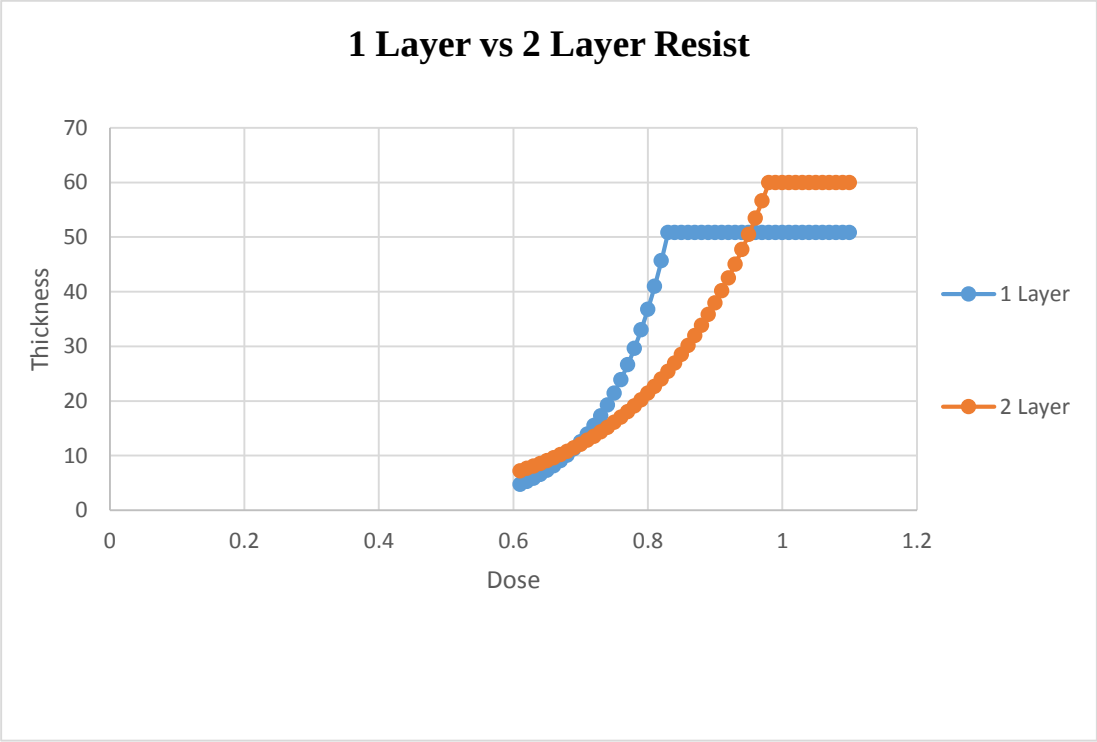

Figure 54. Comparison of dosage calibration of single layer resist versus double layer resist

6.2.6 Single Layer Resist 100 nm Developed (Results)

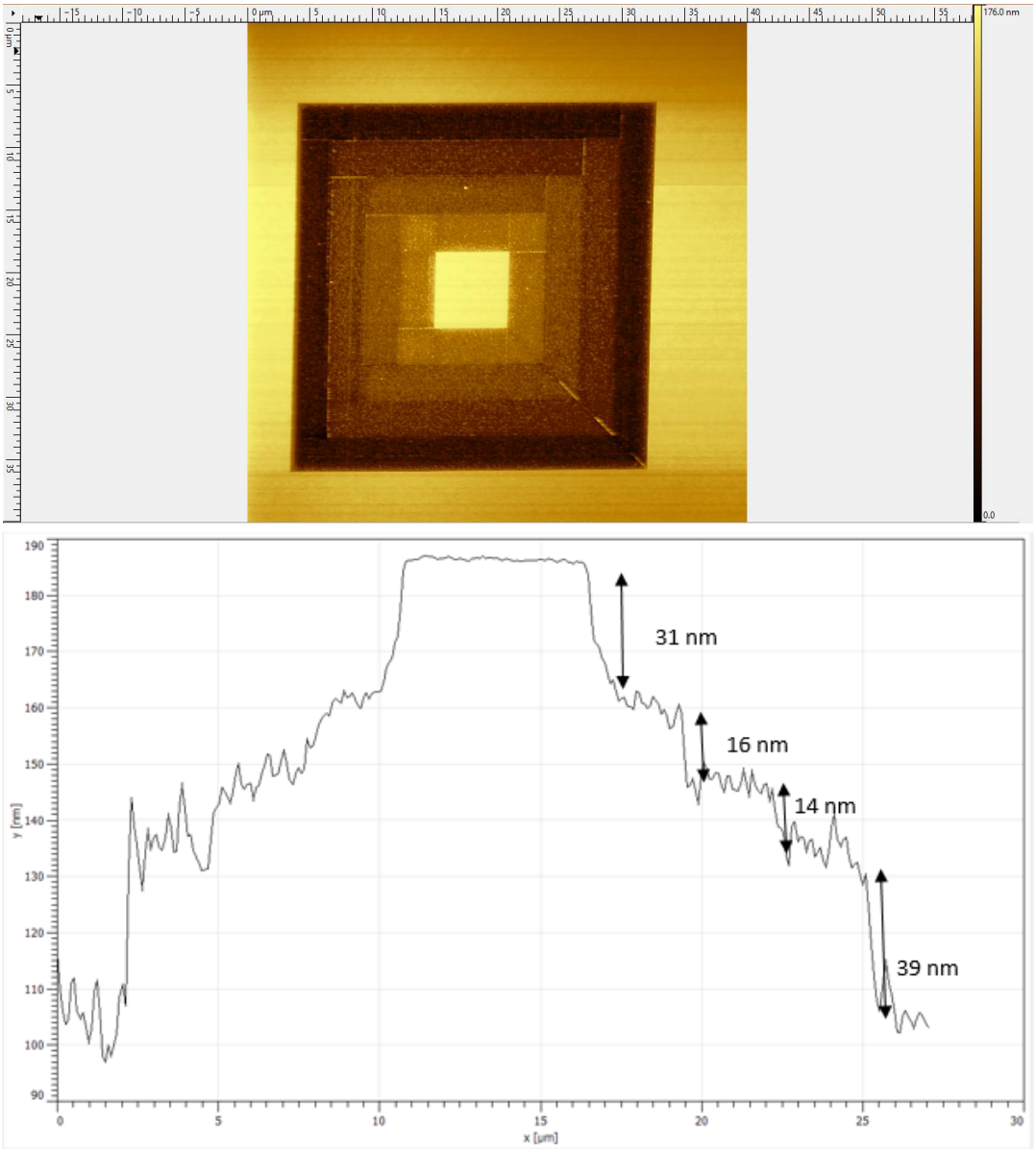

Figure 55. An AFM image (top) and a cross section (bottom) of a 4 step pyramid of a 200 nm thick resist developed thickness 100 nm.

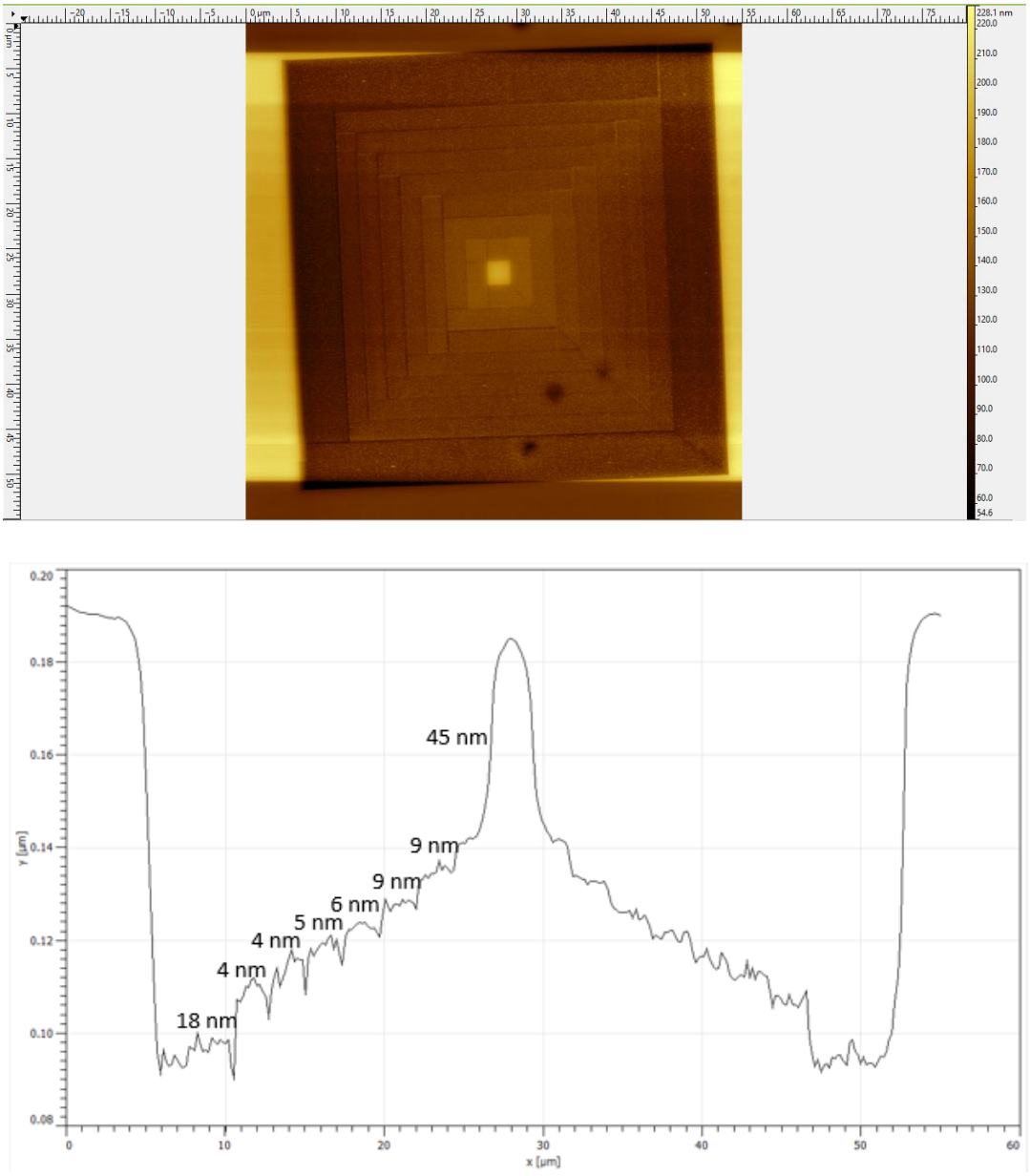

Figure 56. An AFM image (top) and a cross section (bottom) of an 8 step pyramid of a 200 nm thick resist developed thickness 100 nm.

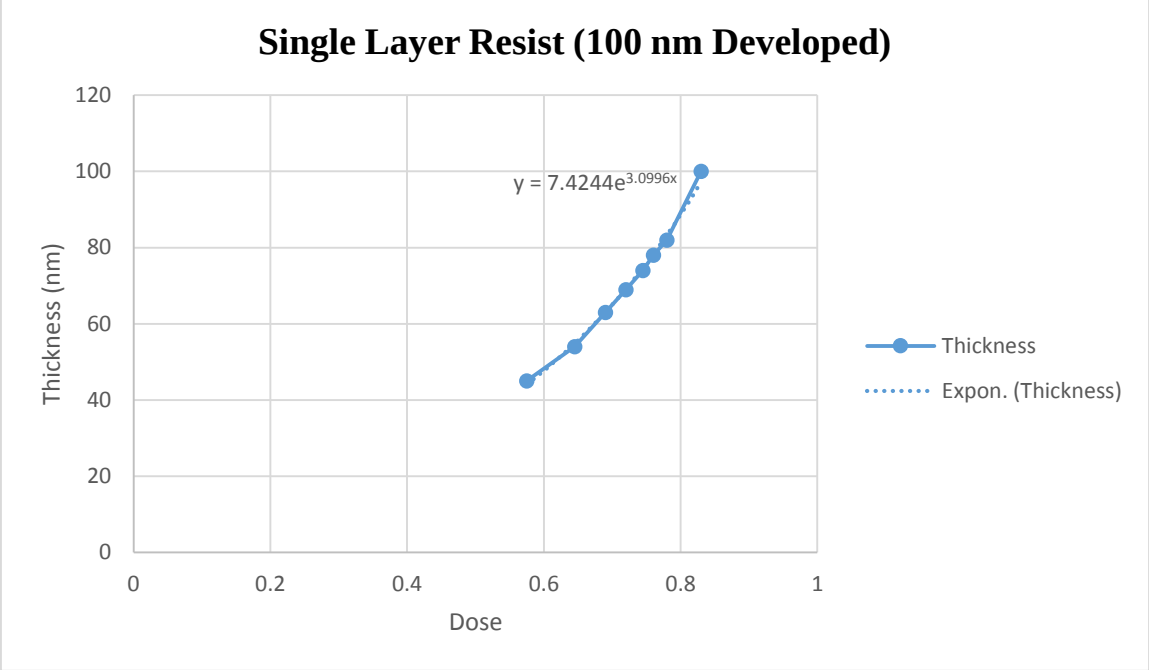

Figure 57. Thickness versus dosage relationship of a 100 nm developed single layer resist.

It turns out that the thickness is related to dosage exponentially according to the following formula:

$$T = 7.4244 * e^{(3.0996 * D)}$$

Where T is thickness in nanometers and D is the normalized dosage in μAs/cm².

6.2.7 Single Layer Resist 200 nm Developed (Results)

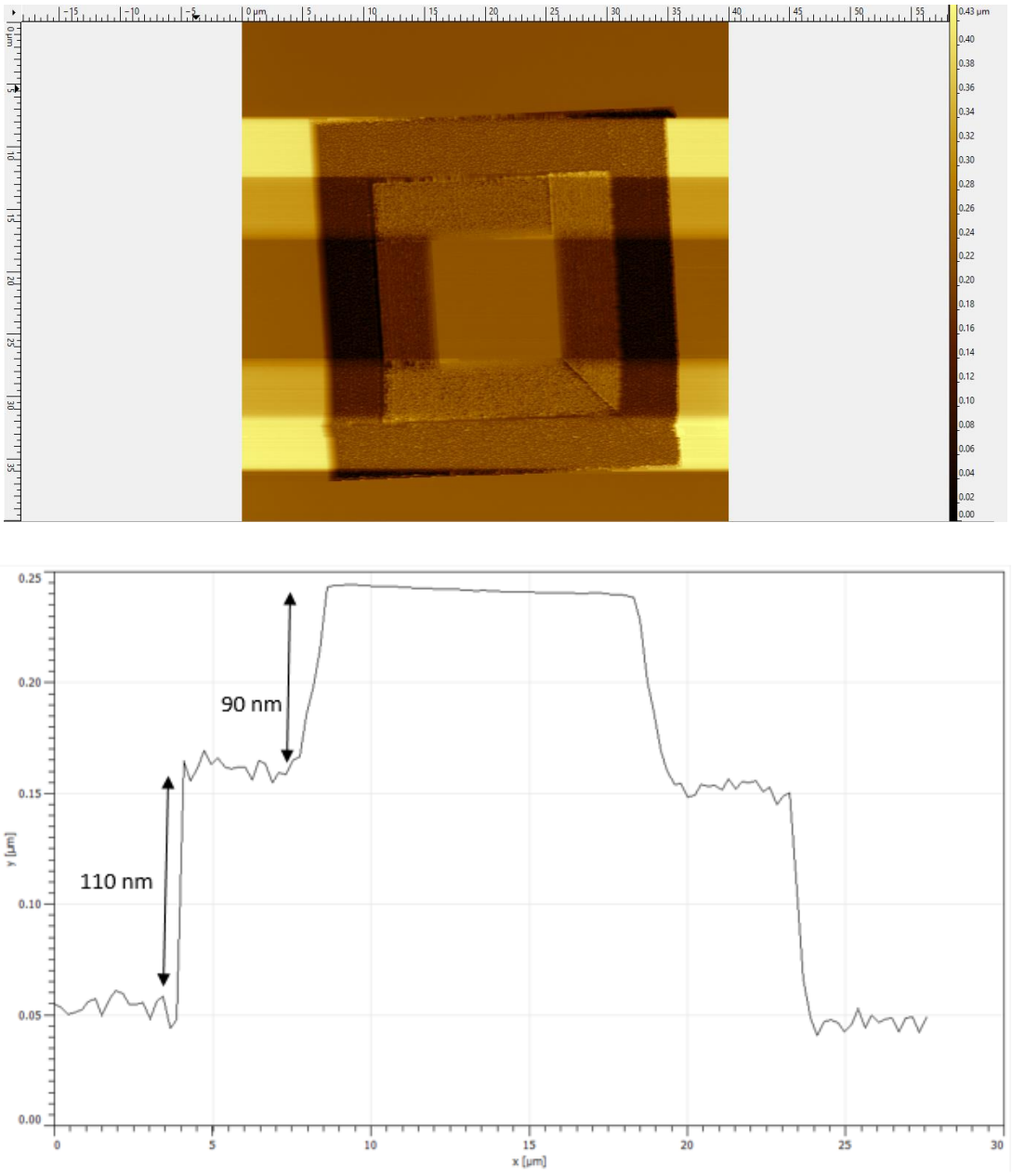

Figure 58. An AFM image (top) and a cross section (bottom) of a 2 step pyramid of a 200 nm thick resist developed thickness 200 nm.

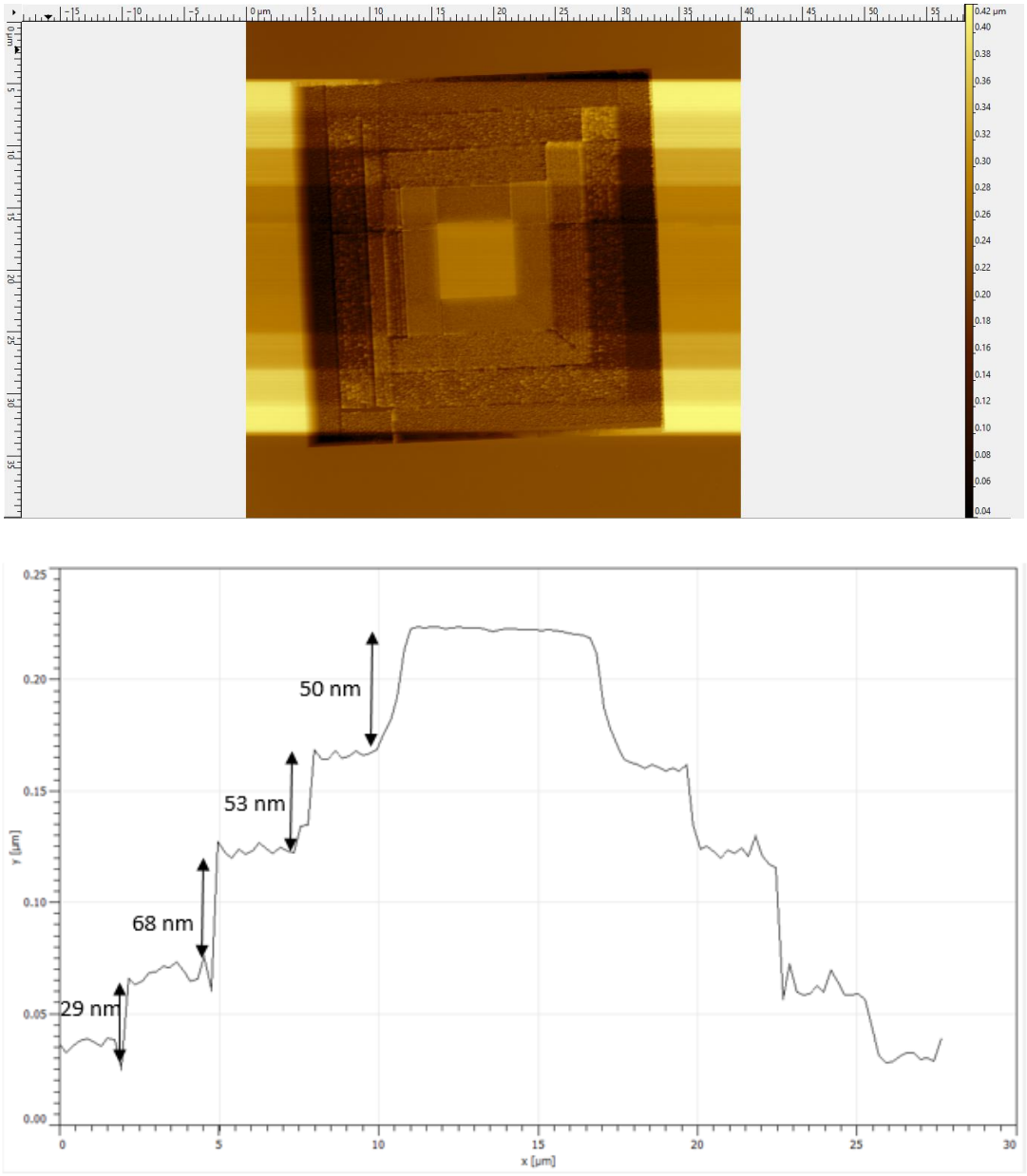

Figure 59. An AFM image (top) and a cross section (bottom) of a 4 step pyramid of a 200 nm thick resist developed thickness 200 nm.

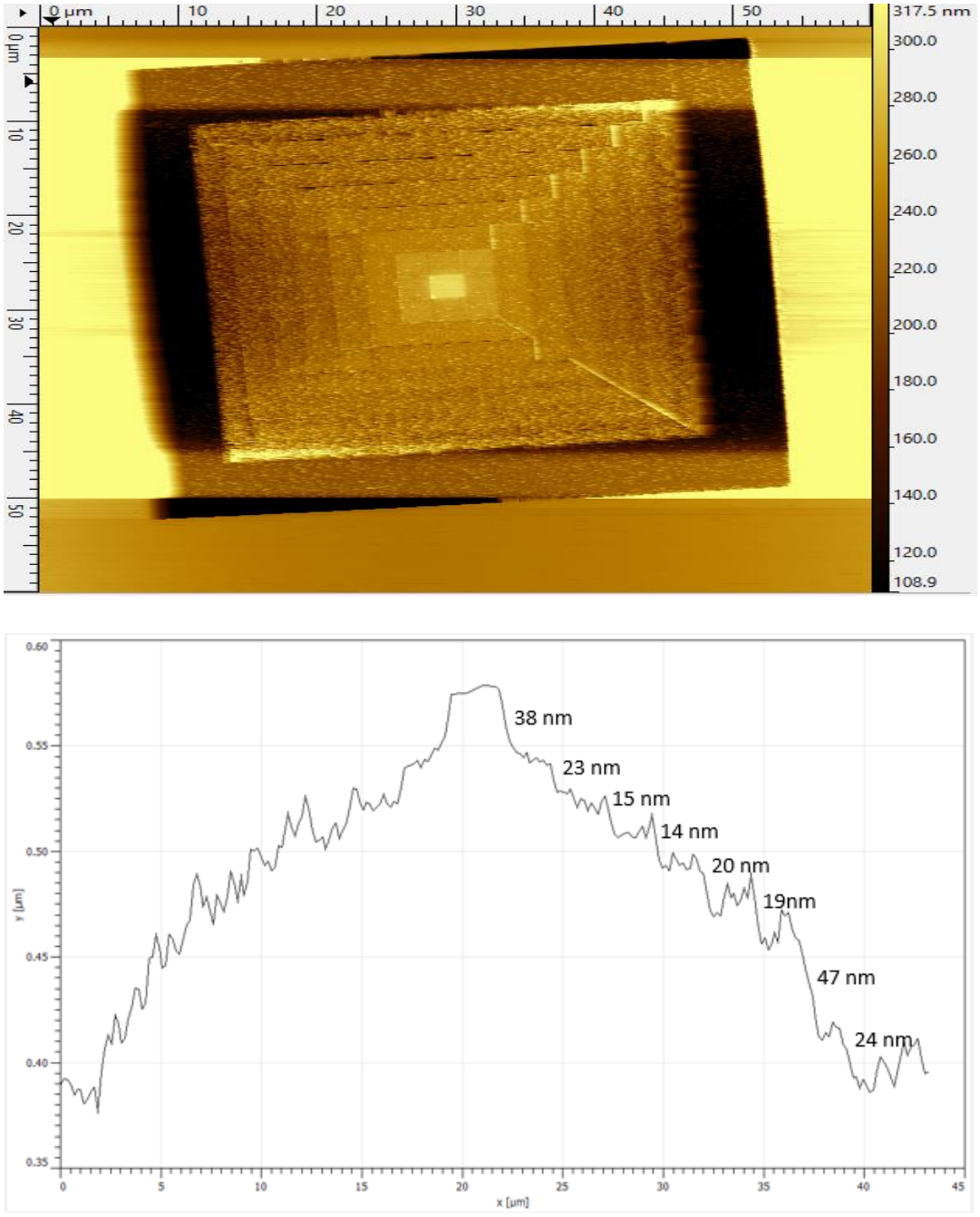

Figure 60. An AFM image (top) and a cross section (bottom) of a 8 step pyramid of a 200 nm thick resist developed thickness 200 nm.

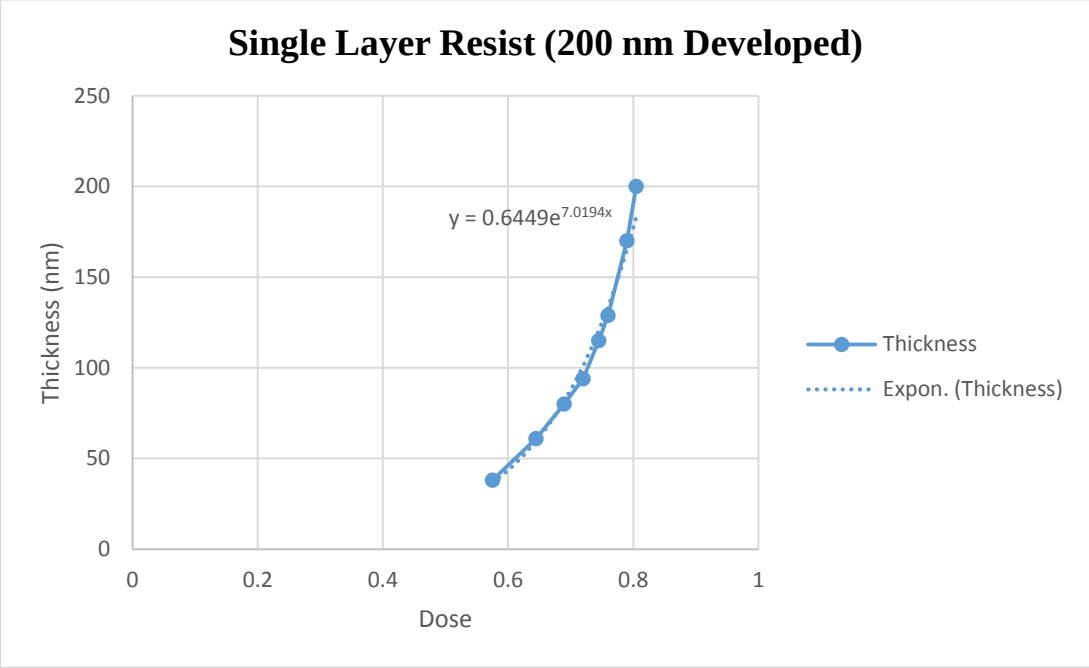

Figure 61. Thickness versus dosage relationship of a 200 nm developed single layer resist

It turns out that the thickness is related to dosage exponentially according to the following formula:

$$T = 0.6449 * e^{(7.0194 * D)}$$

Where T is thickness in nanometers and D is the normalized dosage in μAs/cm².

6.2.8 Double Layer Resist 300 nm Developed (Results)

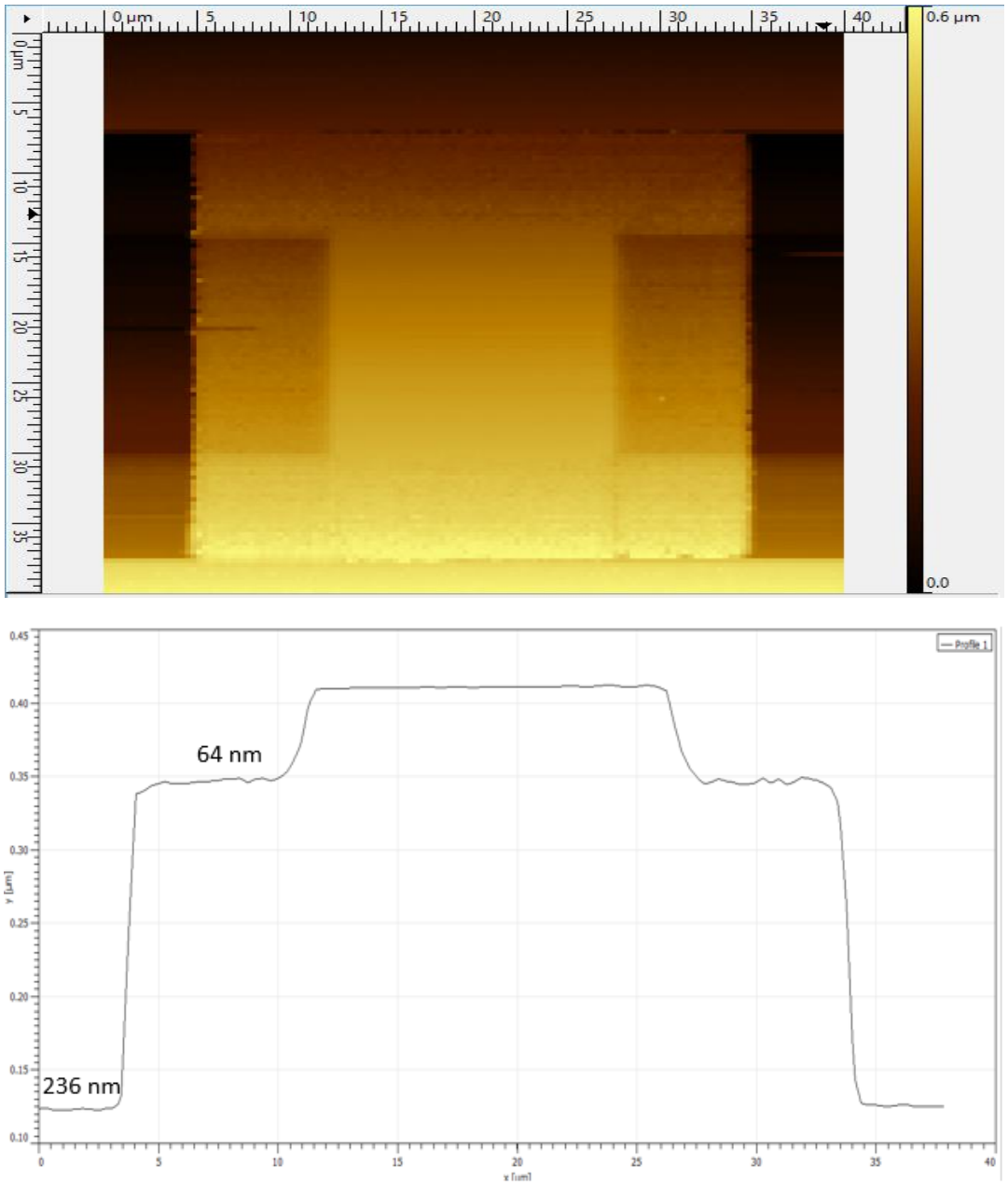

Figure 62. An AFM image (top) and a cross section (bottom) of a 2 step pyramid of a 300 nm thick resist developed thickness 300 nm, exposed with same dosage (83%) as that of a 2 step pyramid single layer resist.

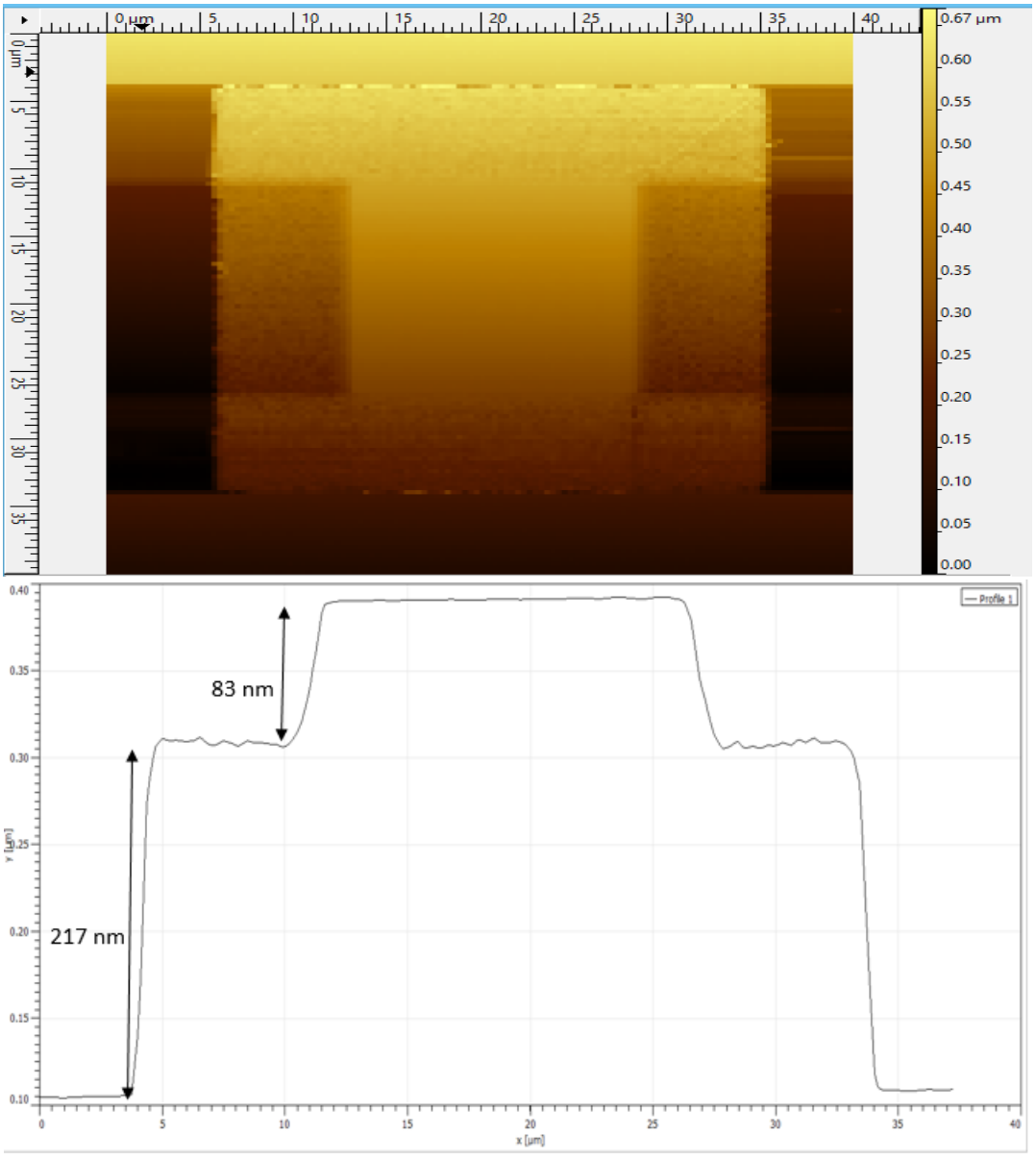

Figure 63. An AFM image (top) and a cross section (bottom) of a 2 step pyramid of a 300 nm thick resist developed thickness 300 nm, exposed with slightly higher dosage (87.2%) to that of a 2 step pyramid single layer resist.

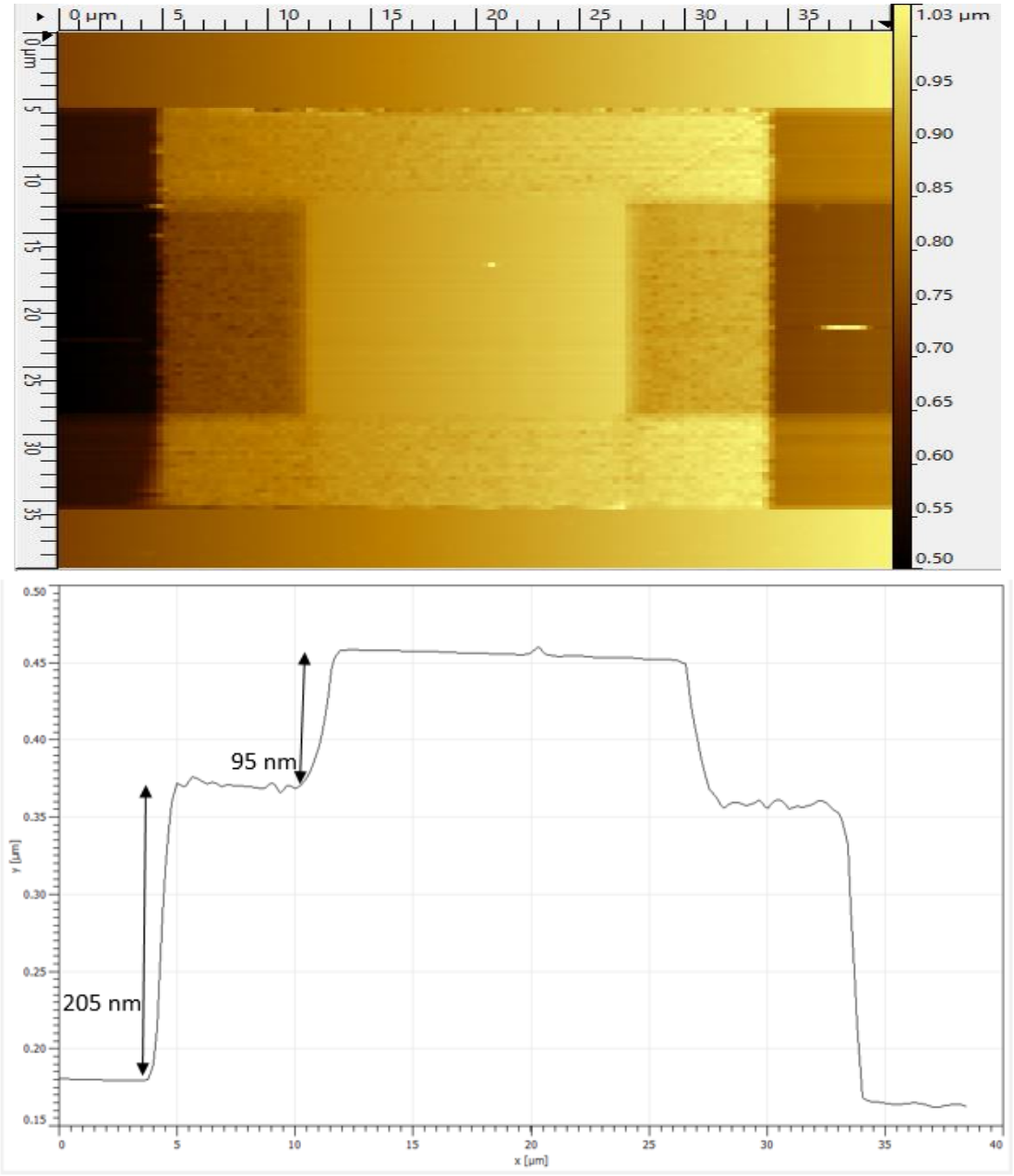

Figure 64. An AFM image (top) and a cross section (bottom) of a 2 step pyramid of a 300 nm thick resist developed thickness 300 nm, exposed with slightly higher dosage (89.6%) to that of a 2 step pyramid single layer resist.

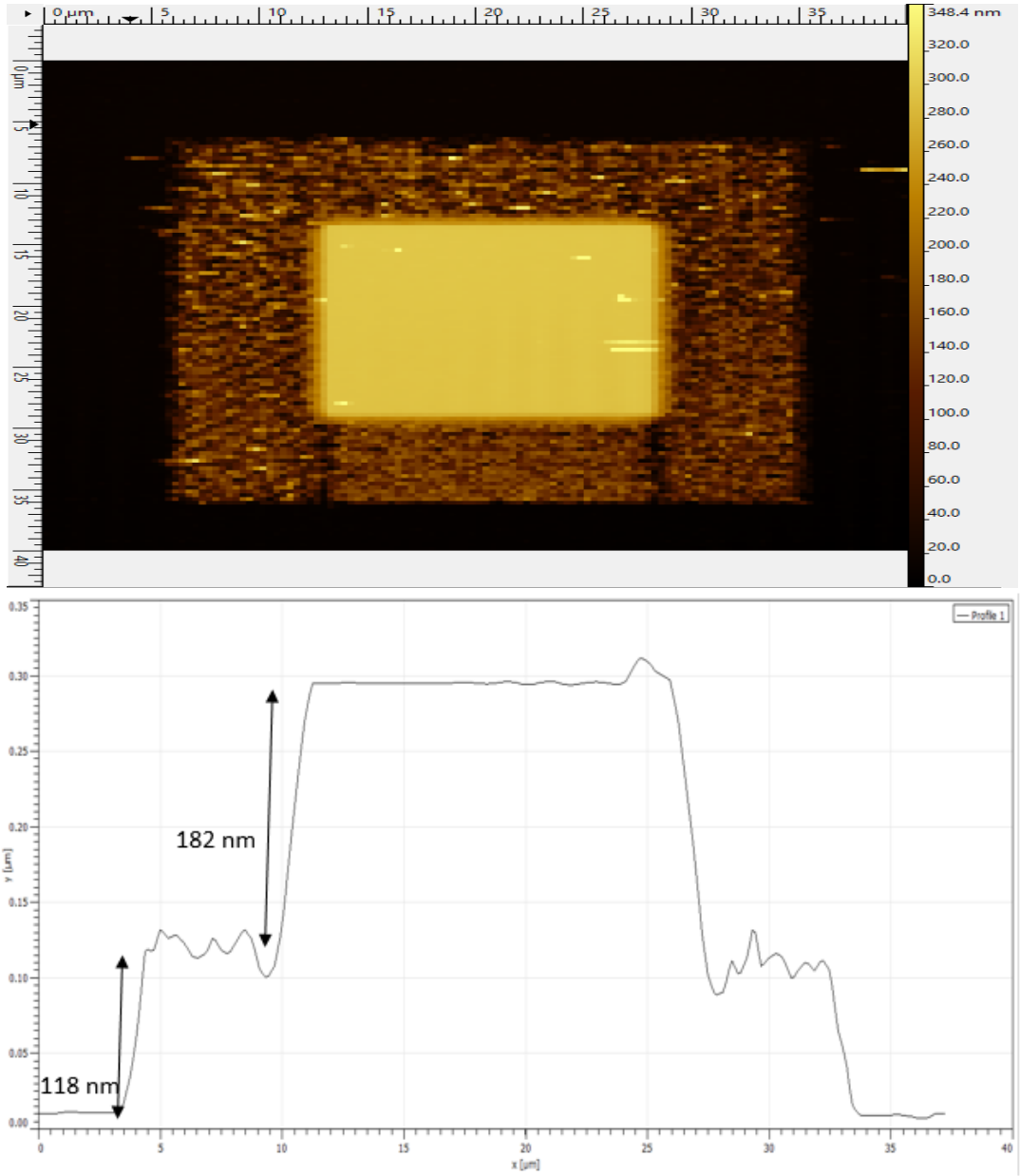

Figure 65. An AFM image (top) and a cross section (bottom) of a 2 step pyramid of a 300 nm thick resist developed thickness 300 nm, exposed with a higher dosage (99.5%) to that of a 2 step pyramid single layer resist.

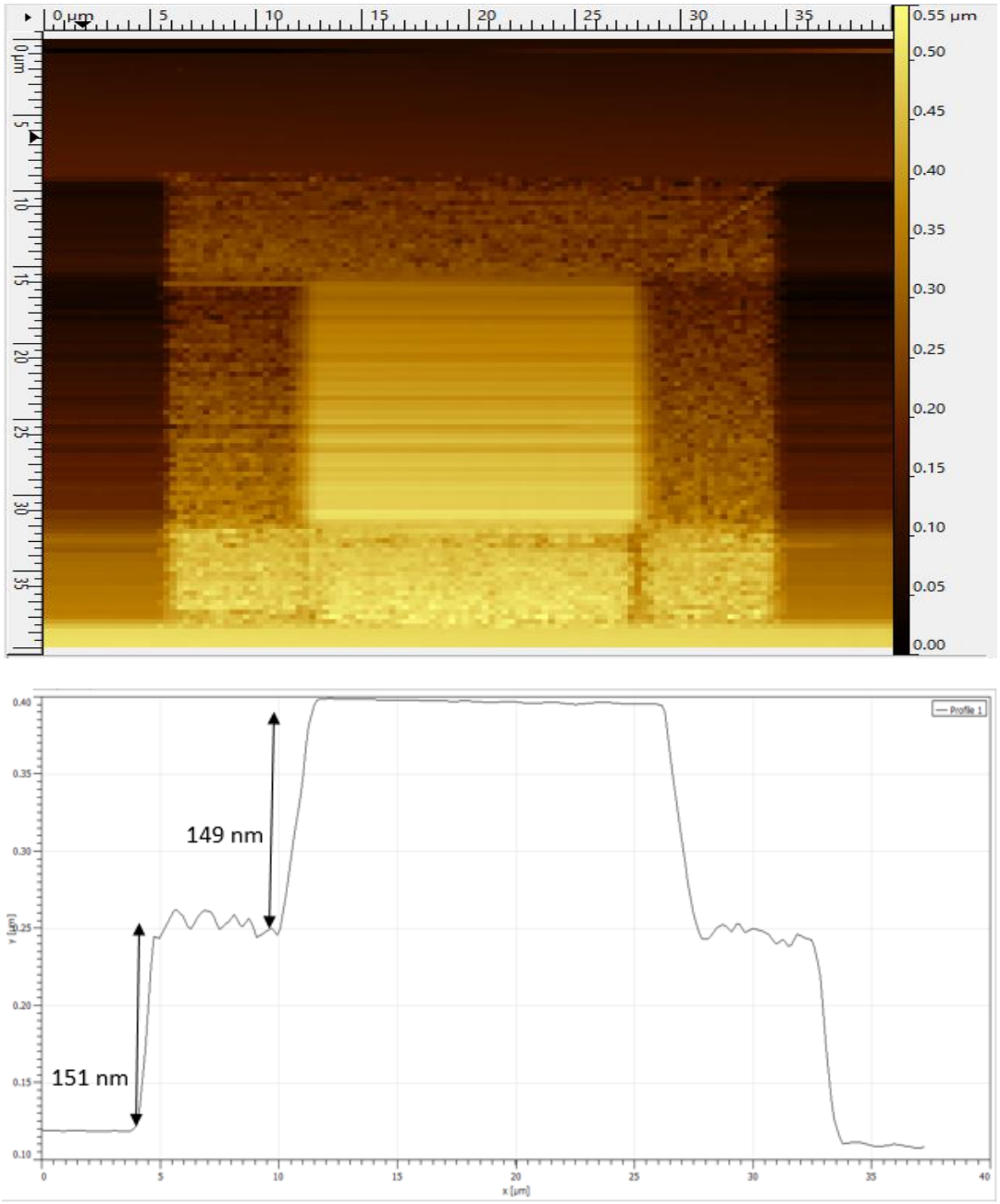

Figure 66. An AFM image (top) and a cross section (bottom) of a 2 step pyramid of a 300 nm thick resist developed thickness 300 nm.

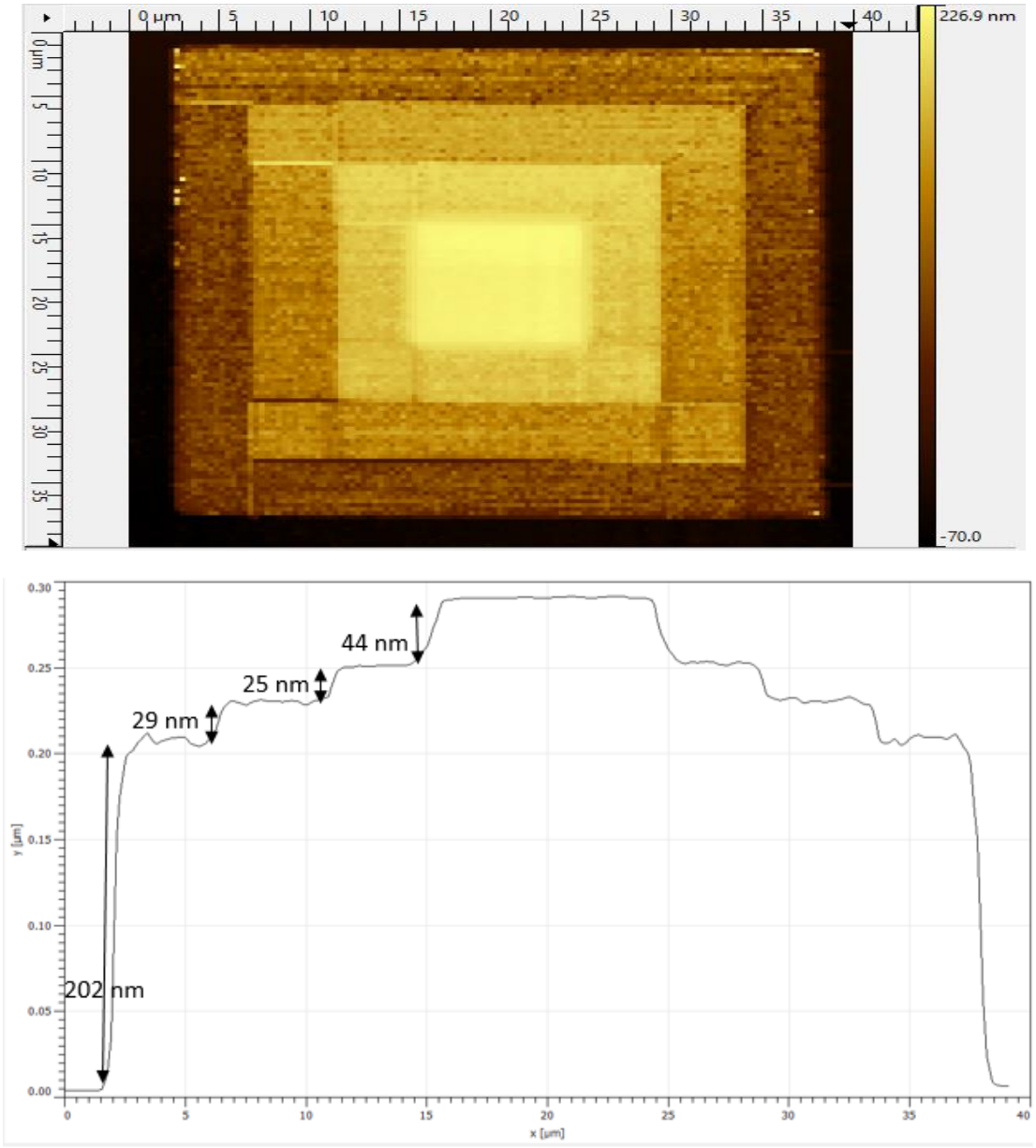

Figure 67. An AFM image (top) and a cross section (bottom) of a 4 step pyramid of a 300 nm thick resist developed thickness 300 nm, exposed with same dosage to that of a 4 step pyramid single layer resist.

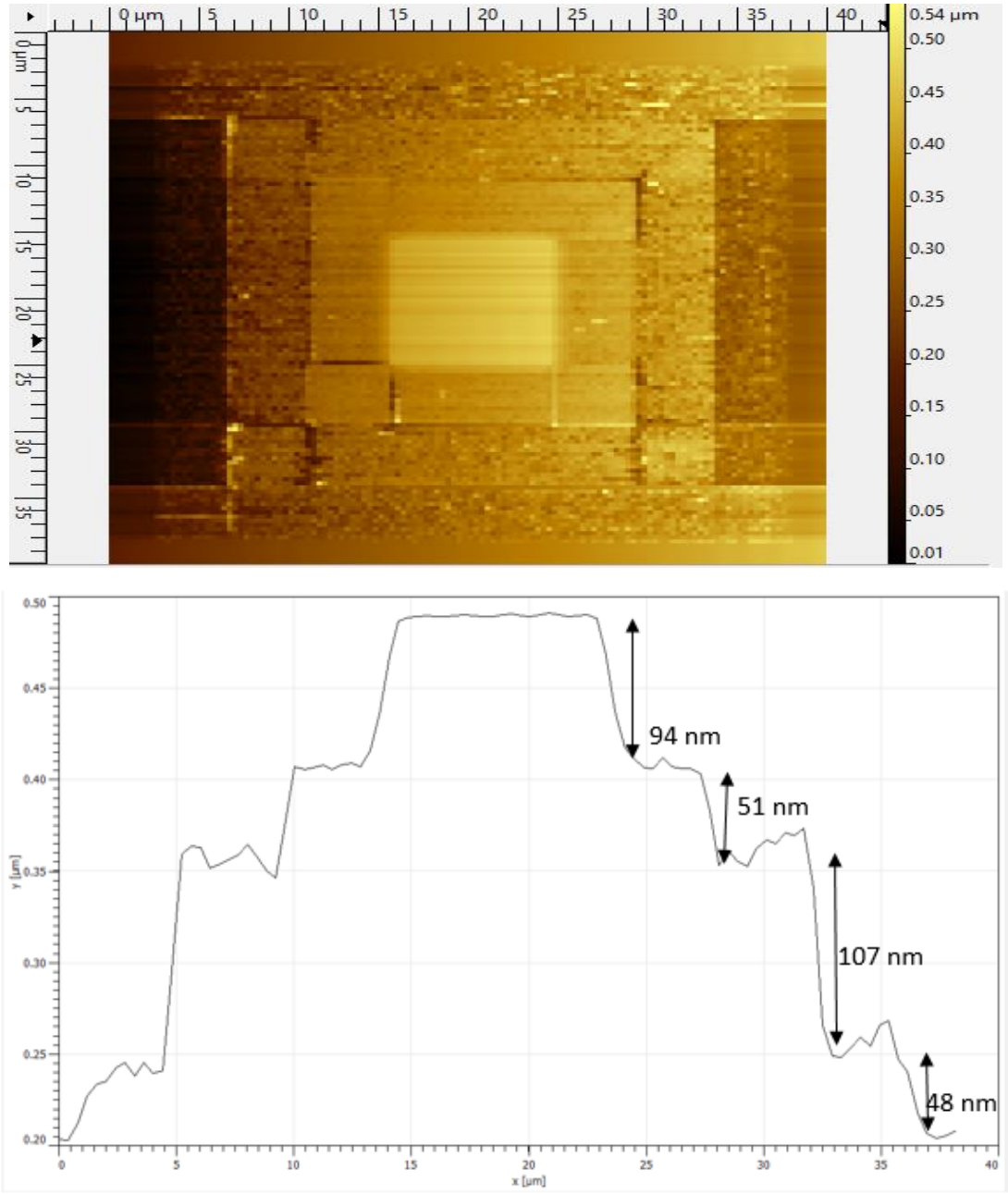

Figure 68. An AFM image (top) and a cross section (bottom) of a 4 step pyramid of a 300 nm thick resist developed thickness 300 nm, after dose modification.

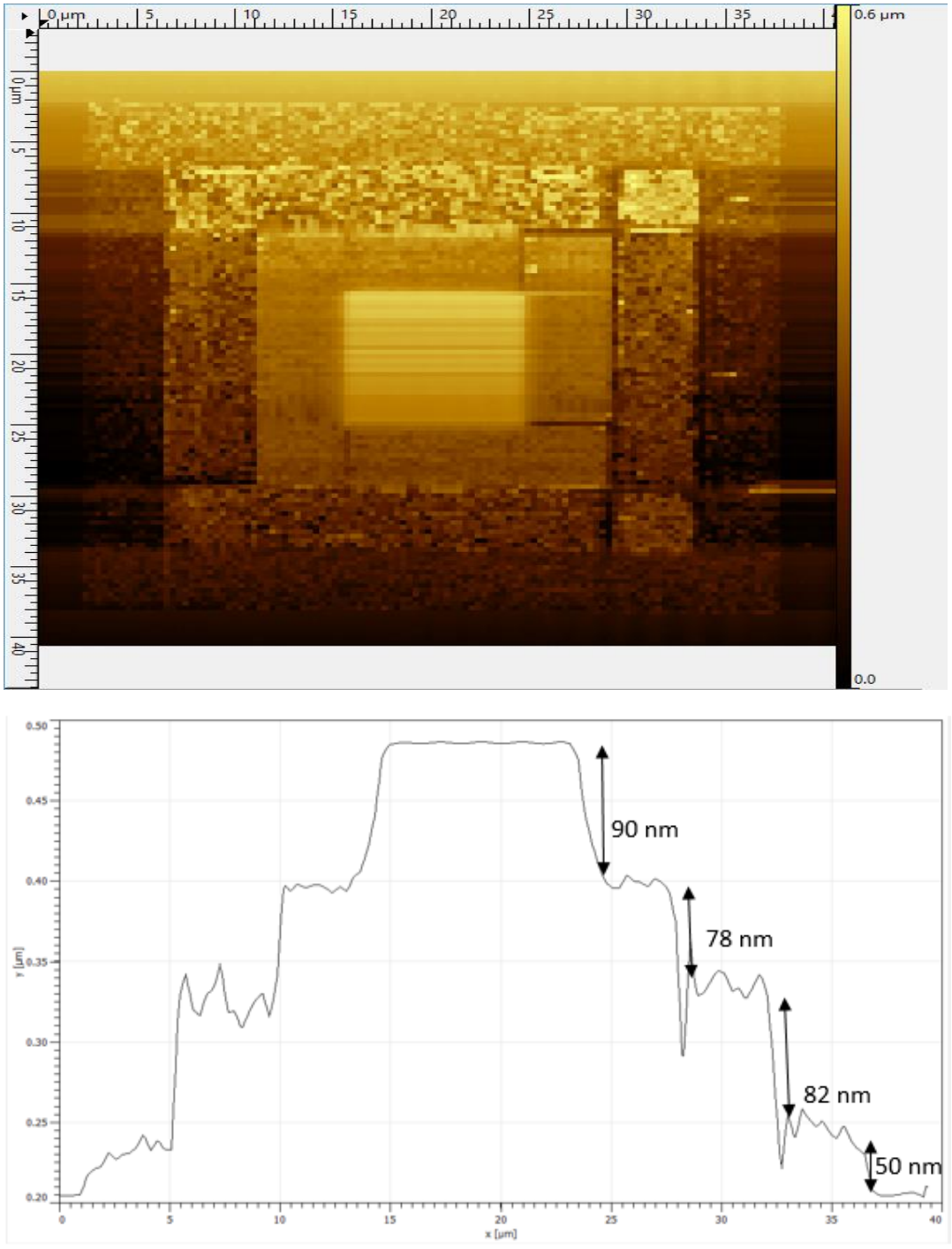

Figure 69. An AFM image (top) and a cross section (bottom) of a 4 step pyramid of a 300 nm thick resist developed thickness 300 nm, with further dosage calibration.

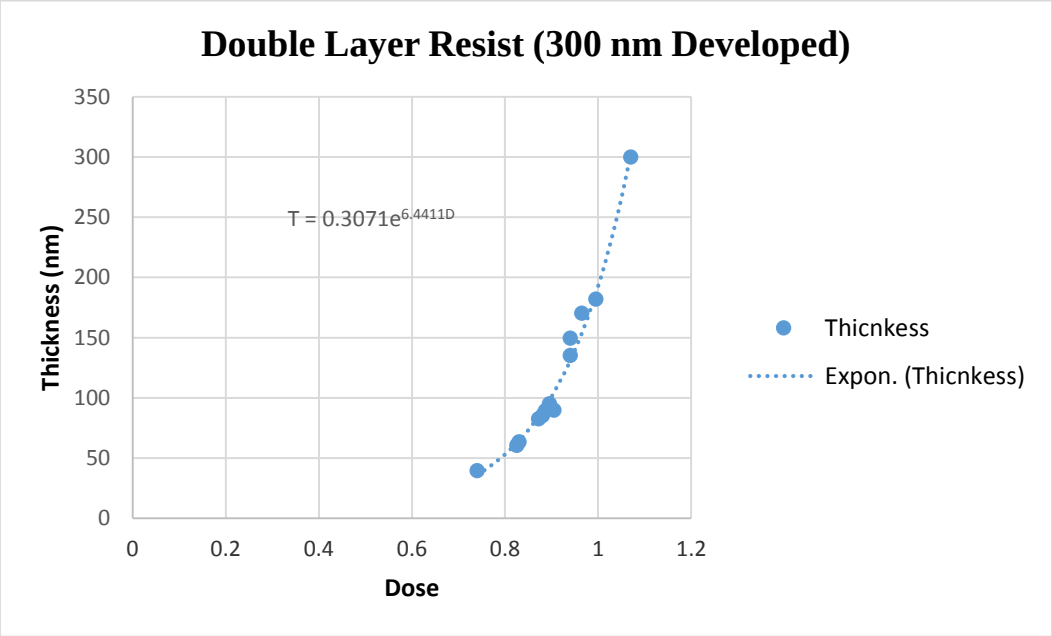

Figure 70. Thickness versus dosage relationship of a 300 nm developed double layer resist.

It turns out that the thickness is related to dosage exponentially according to the following formula:

$$T = 0.3071 * e^{(6.4411 * D)}$$

Where T is thickness in nanometers and D is the normalized dosage in µAs/cm².

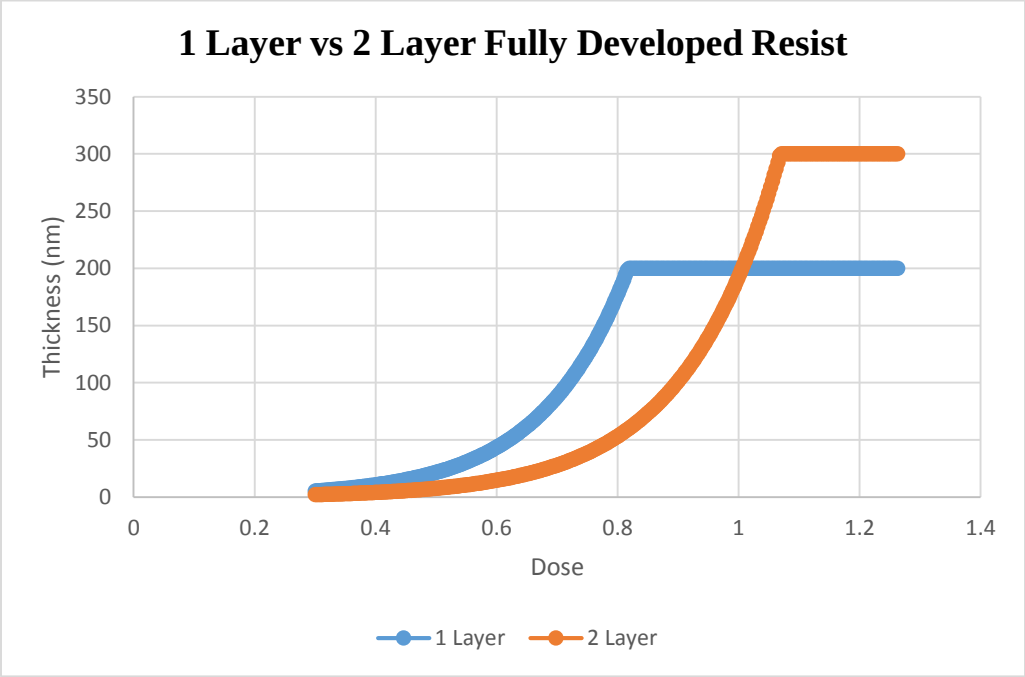

Figure 71. Comparison of dosage calibration of fully developed single layer resist versus double layer resist

It can be observed that both profiles has exponential dependence, moreover dosage depends on baking time and temperature.

6.2.9 Four Layer Resist 520 nm Developed (Results)

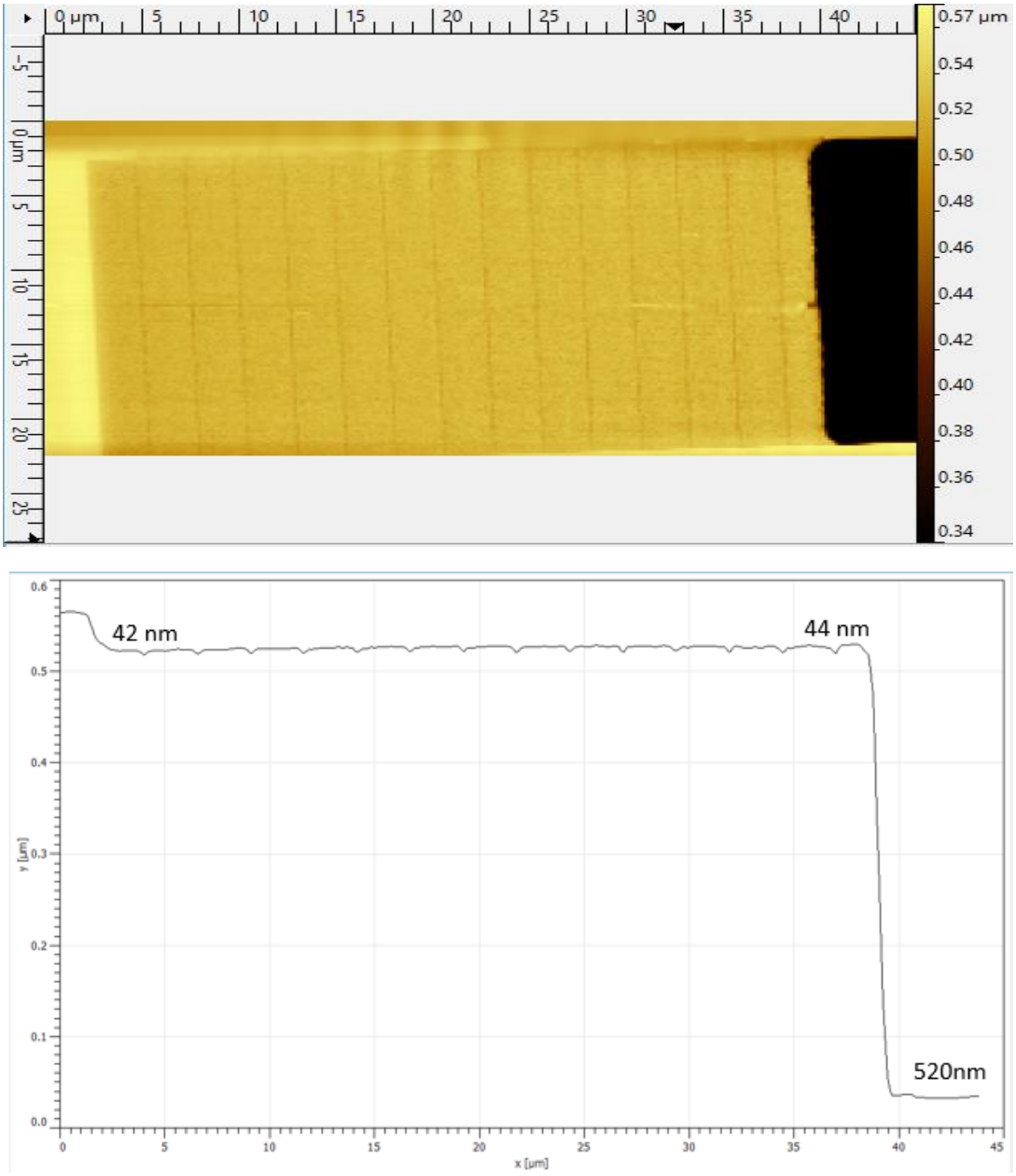

Figure 72. An AFM image (top) and a cross section (bottom) of a stair of a 520 nm thick 4 layer resist developed thickness 520 nm, varying dosage from 70% to 77% from left to right.

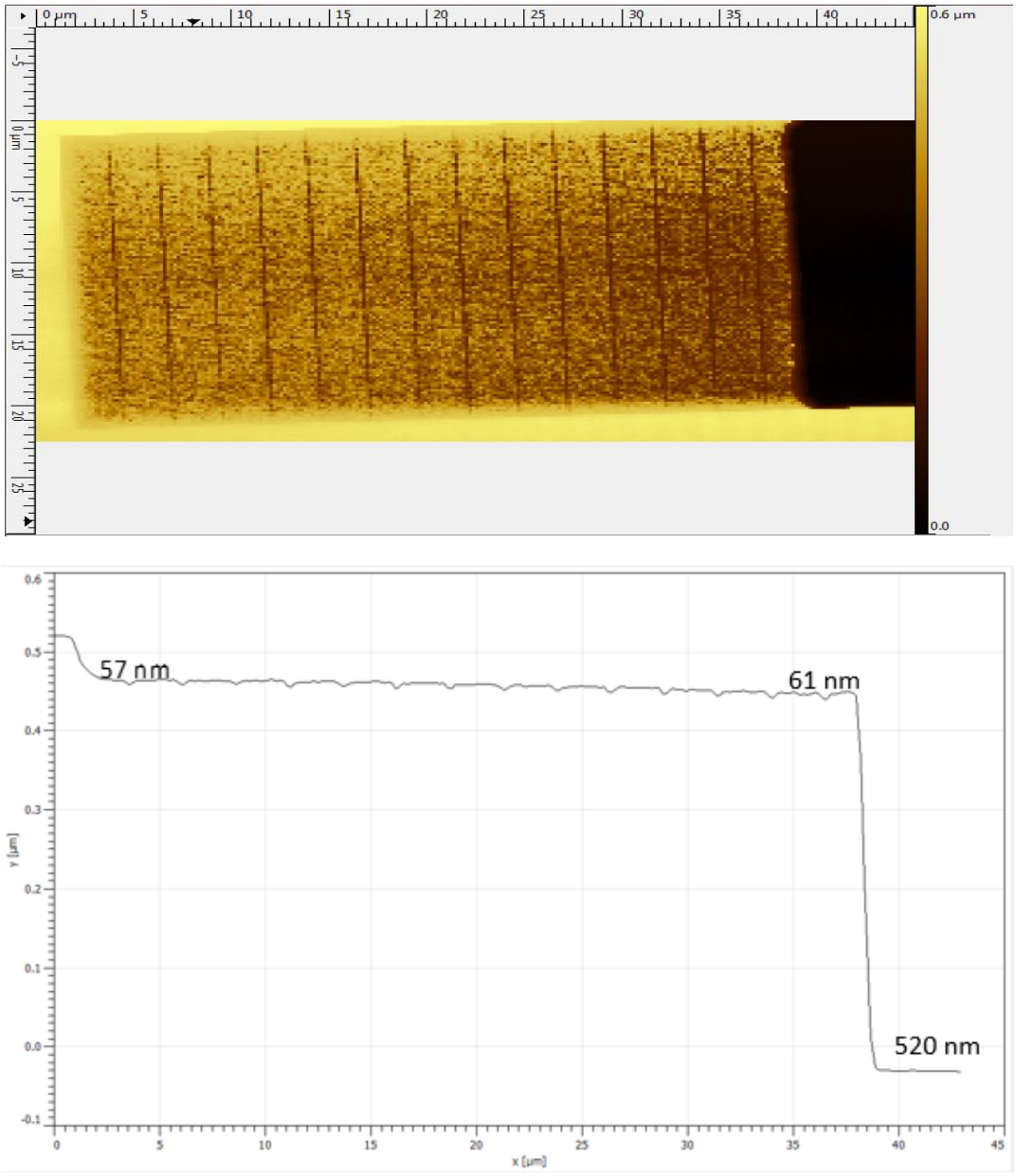

Figure 73. An AFM image (top) and a cross section (bottom) of a stair of a 520 nm thick 4 layer resist developed thickness 520 nm, varying dosage from 80% to 87% from left to right.

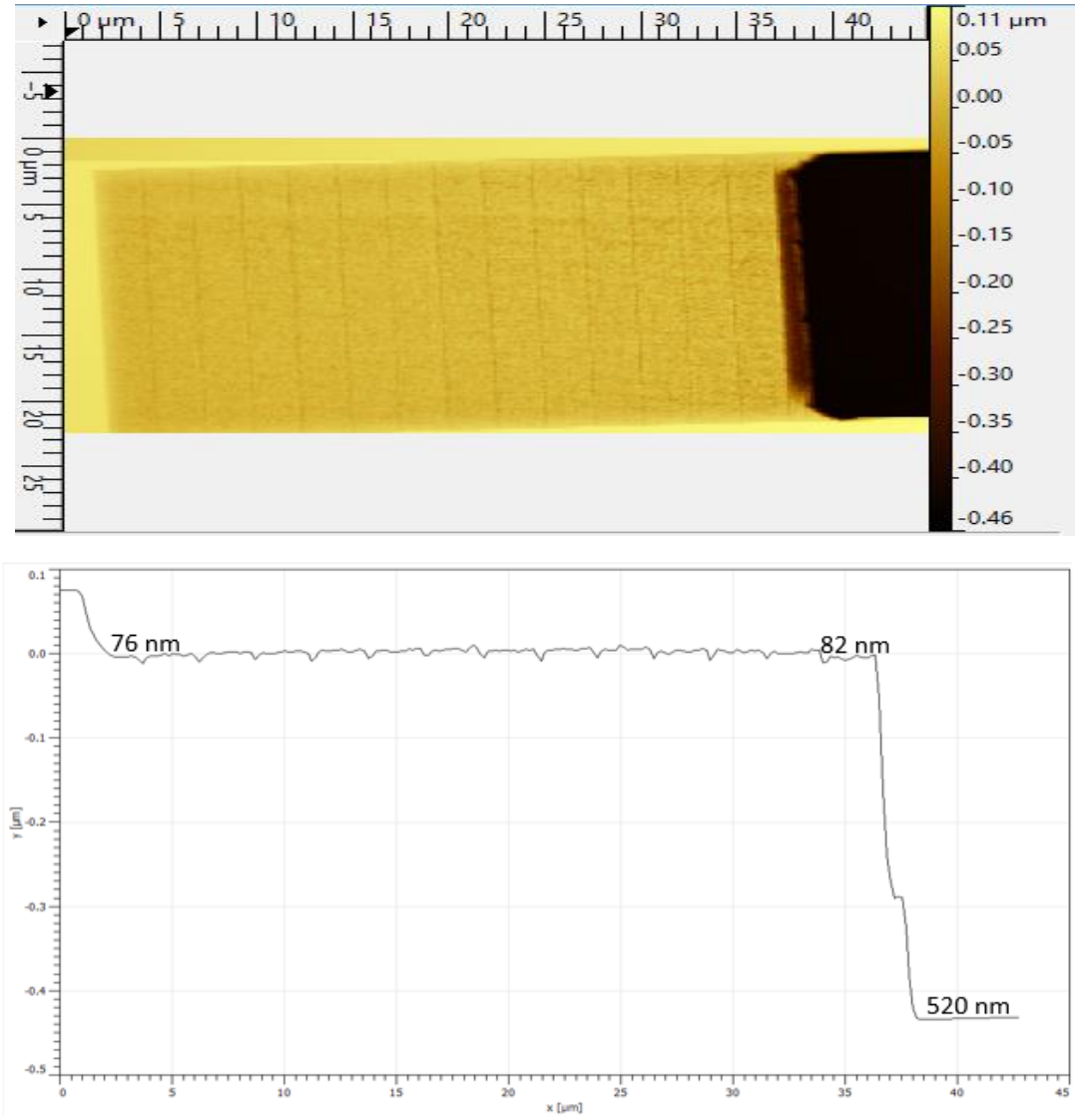

Figure 74. An AFM image (top) and a cross section (bottom) of a stair of a 520 nm thick resist developed thickness 520 nm, varying dosage from 90% to 97% from left to right.

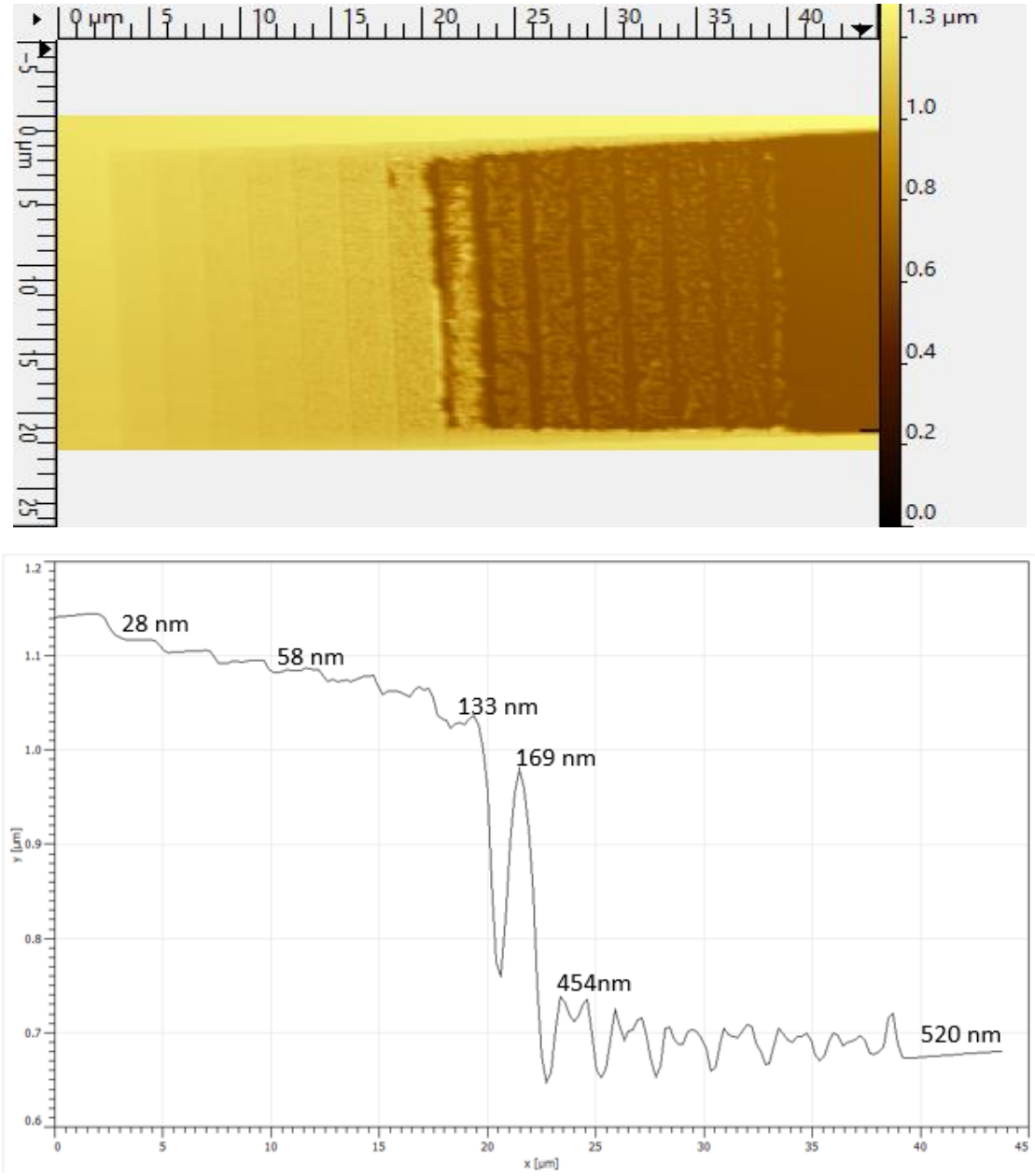

Figure 75 An AFM image (top) and a cross section (bottom) of a stair of a 520 nm thick resist developed thickness 520 nm, varying dosage from 60% to 130% from left to right.

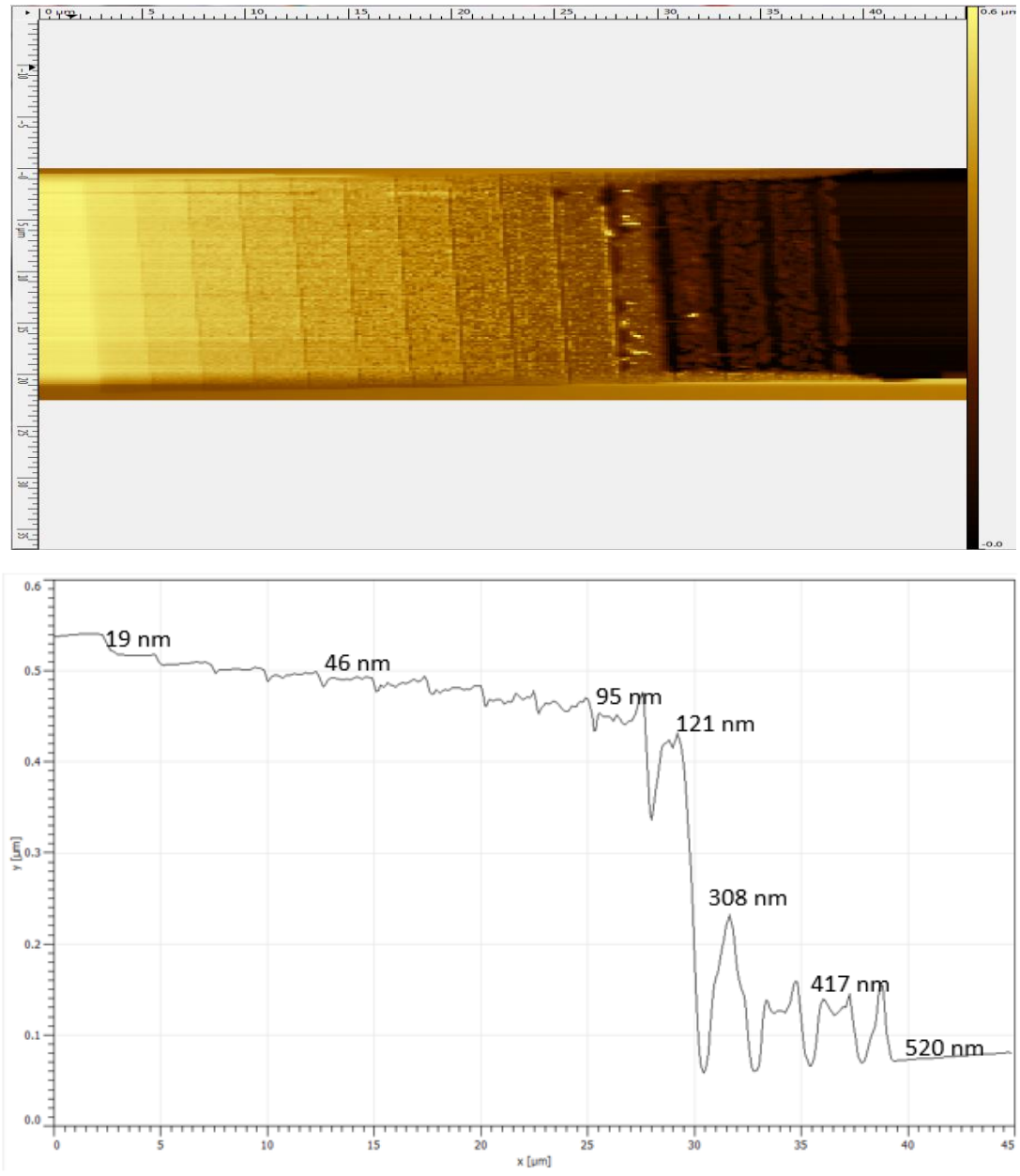

Figure 76. An AFM image (top) and a cross section (bottom) of a 2 step stair of a 520 nm thick resist developed thickness 520 nm, varying dosage from 50% to 120% from left to right.

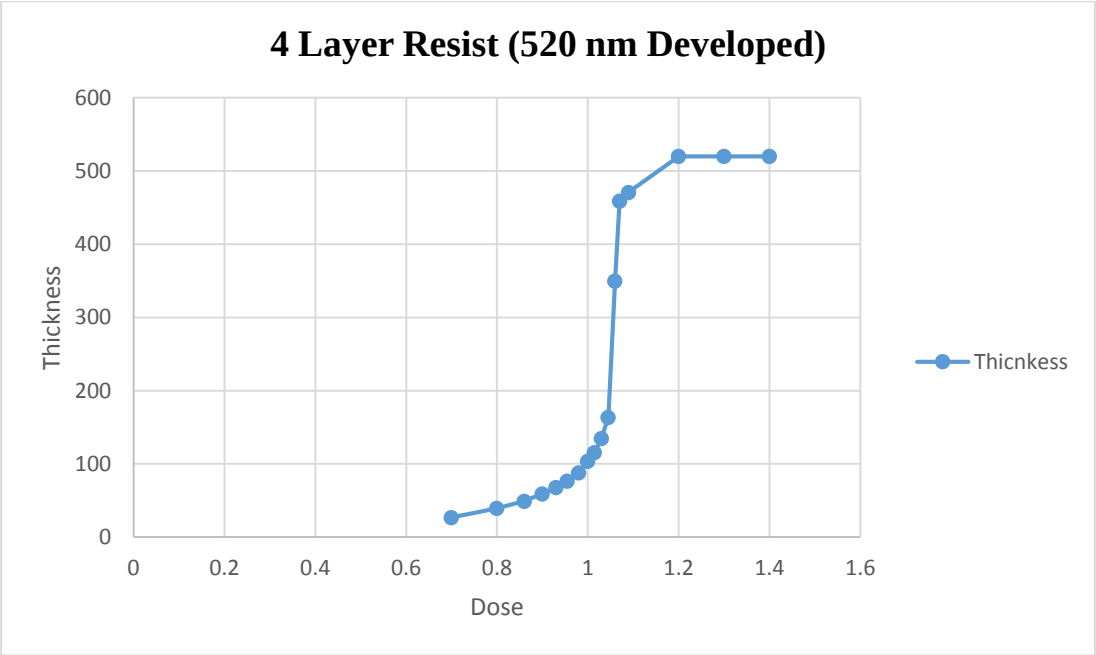

Figure 77. Thickness versus dosage relationship of a 520 nm developed double layer resist.

For four layer PMMA, the dosage versus thickness is no longer exponentially dependent. The resist which is baked several times becomes extremely sensitive to dosage.

The following images are the results of four layer resist varying the baking conditions for each layer.

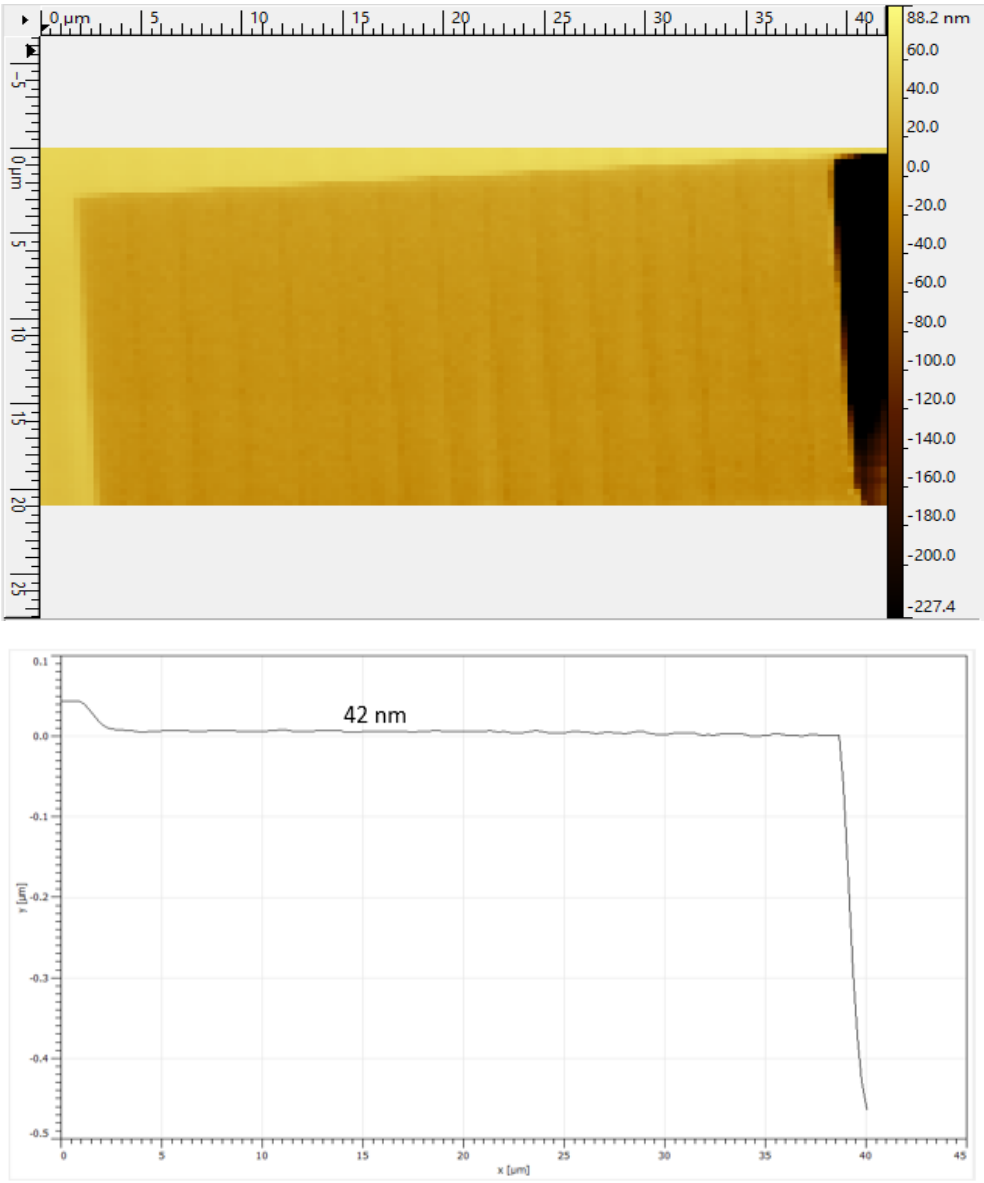

Figure 78. An AFM image (top) and a cross section (bottom) of a stair of a 520 nm thick resist developed thickness 520 nm, varying dosage from 70% to 78% from left to right.

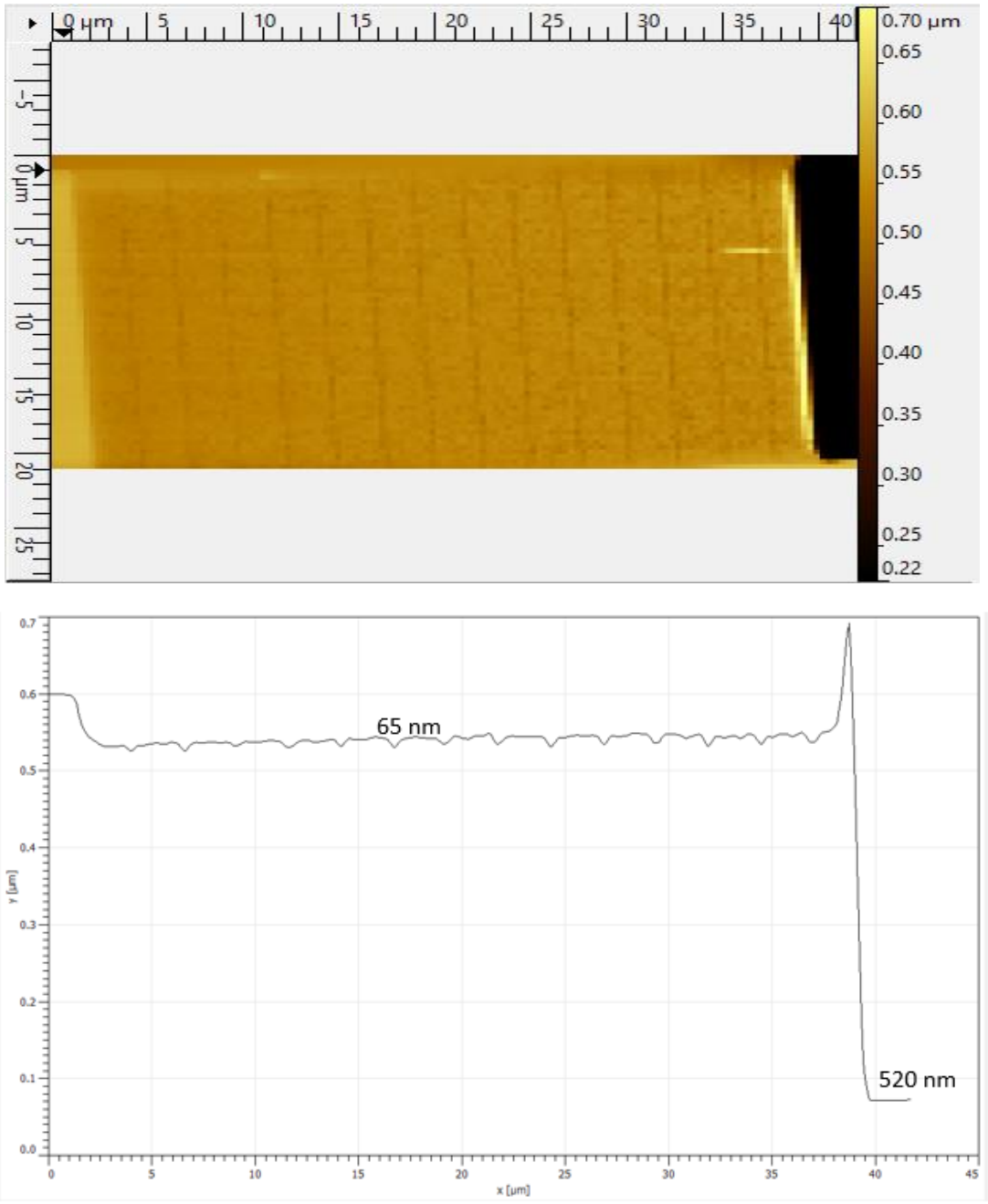

Figure 79. An AFM image (top) and a cross section (bottom) of a stair of a 520 nm thick resist developed thickness 520 nm, varying dosage from 85% to 92% from left to right.

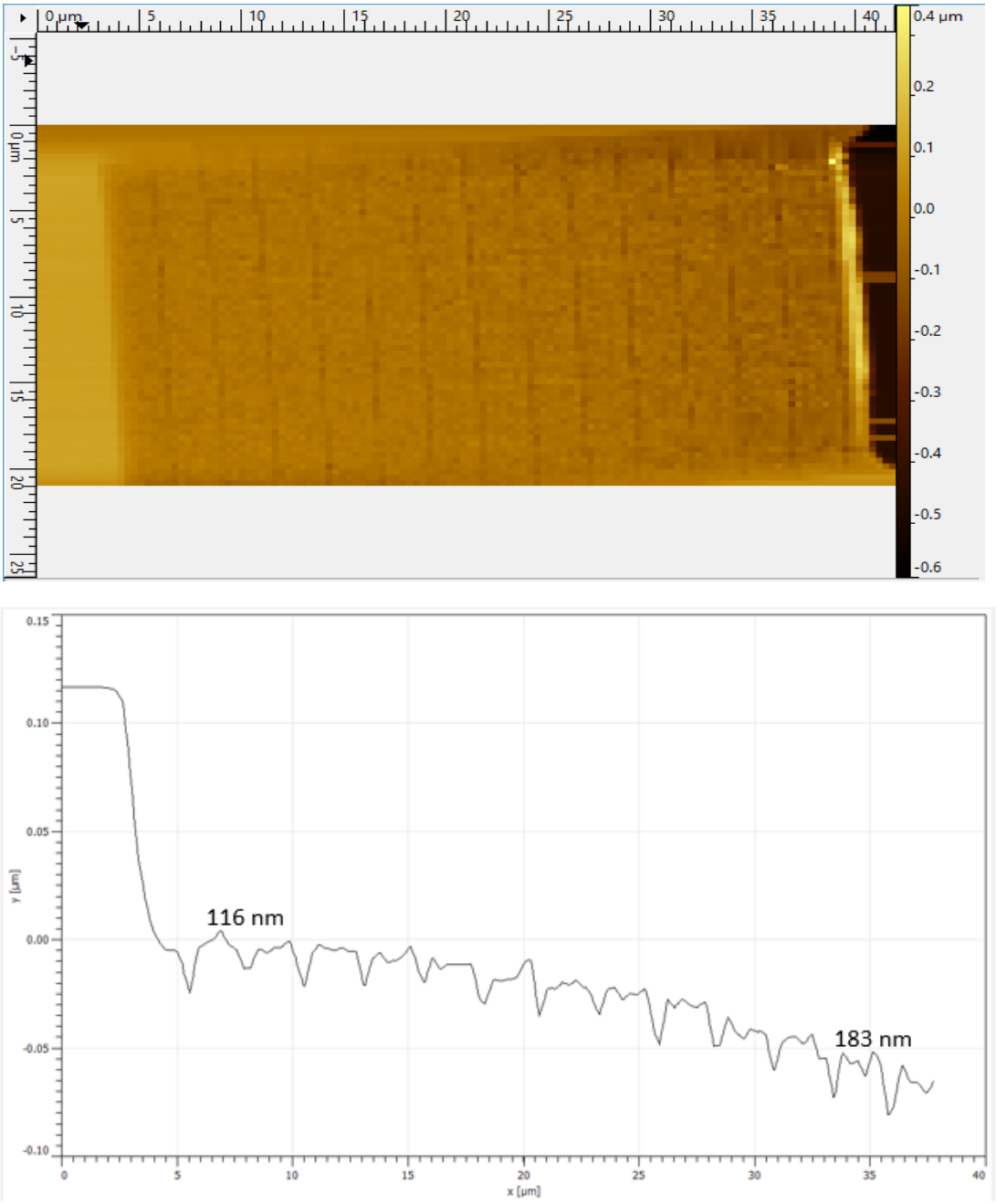

Figure 80. An AFM image (top) and a cross section (bottom) of a stair of a 520 nm thick resist developed thickness 520 nm, varying dosage from 101% to 108% from left to right.

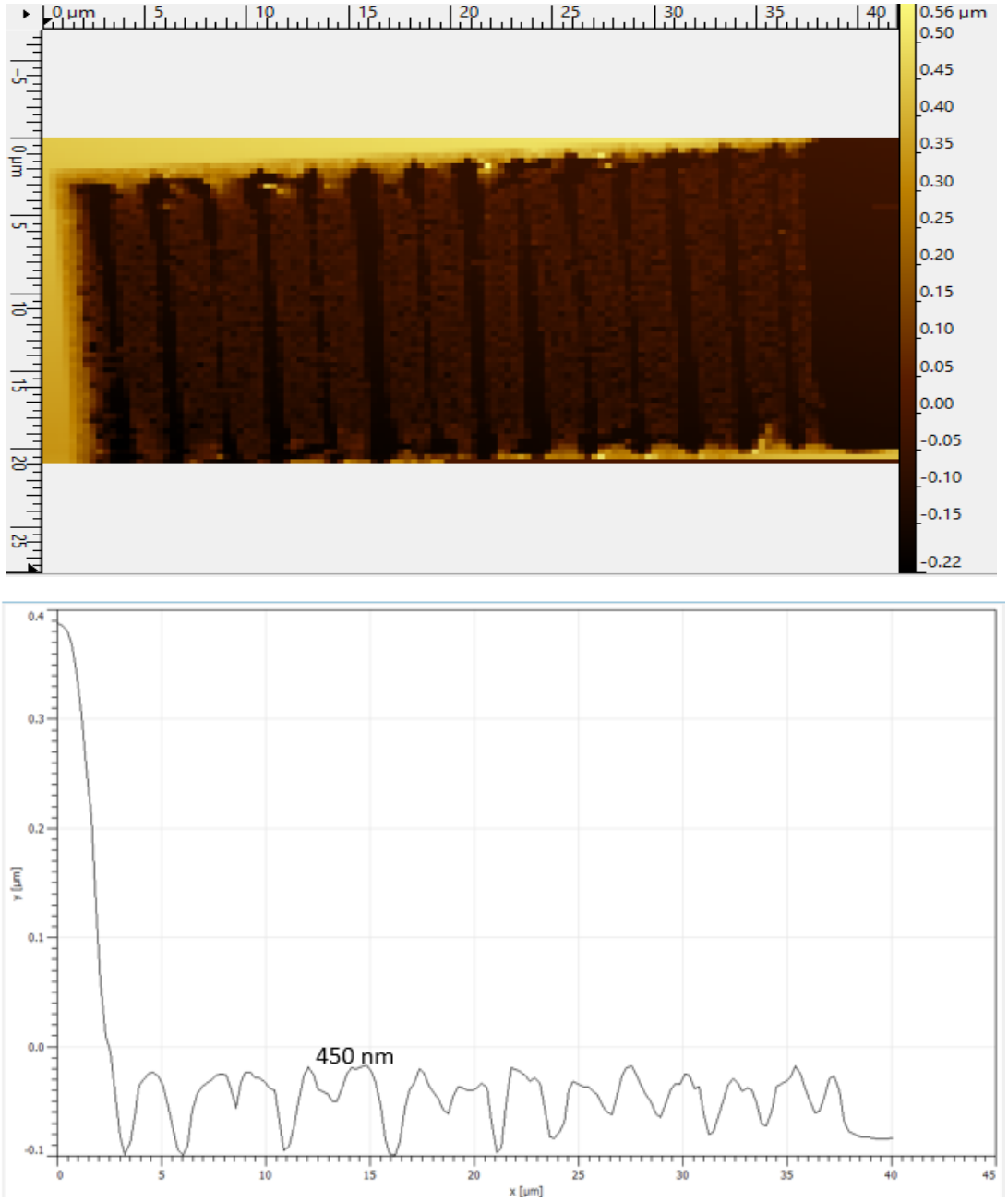

Figure 81. An AFM image (top) and a cross section (bottom) of a stair of a 520 nm thick resist developed thickness 520 nm, varying dosage from 110% to 115% from left to right.

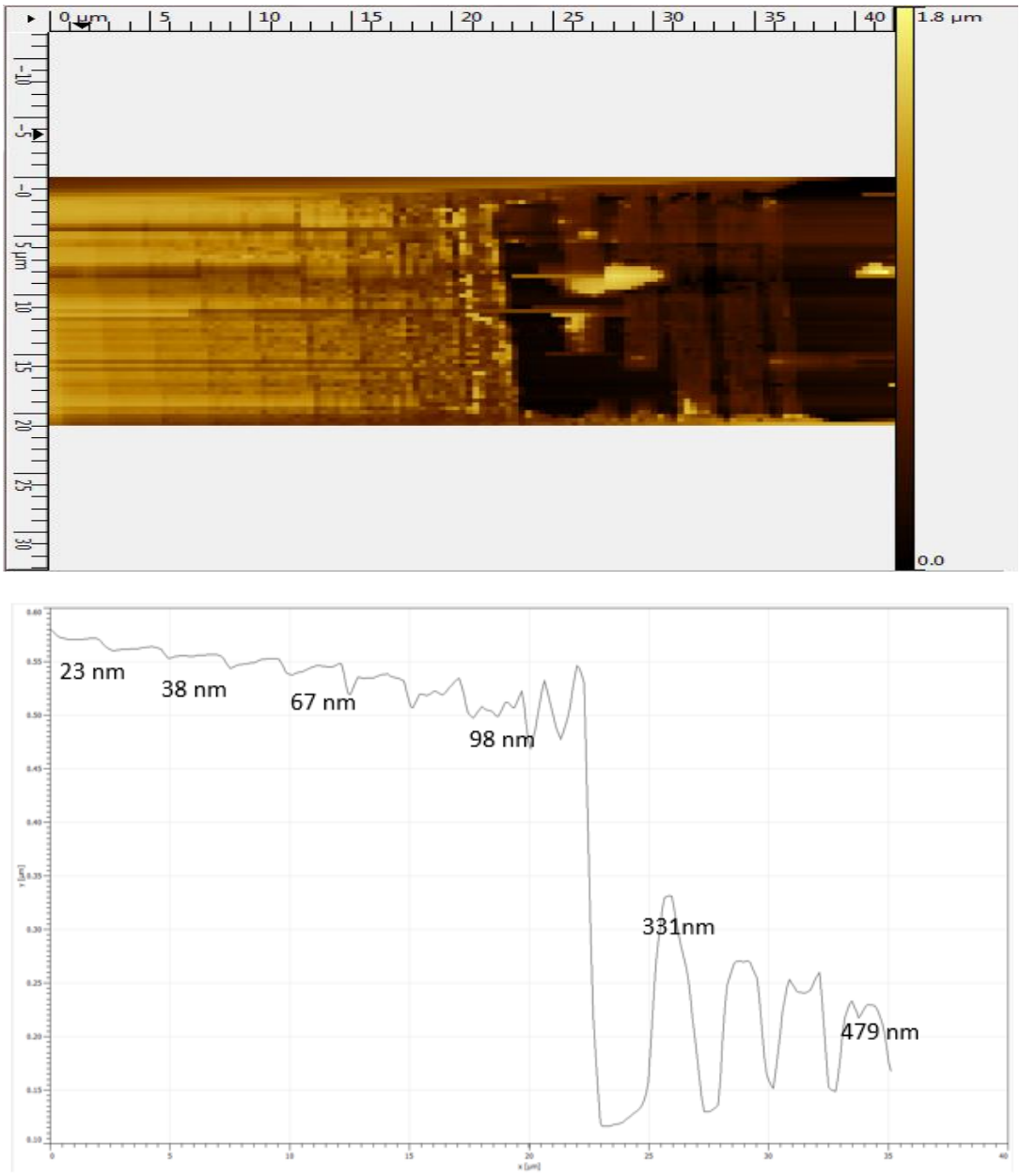

Figure 82. An AFM image (top) and a cross section (bottom) of a stair of a 520 nm thick resist developed thickness 520 nm, varying dosage from 60% to 120% from left to right.

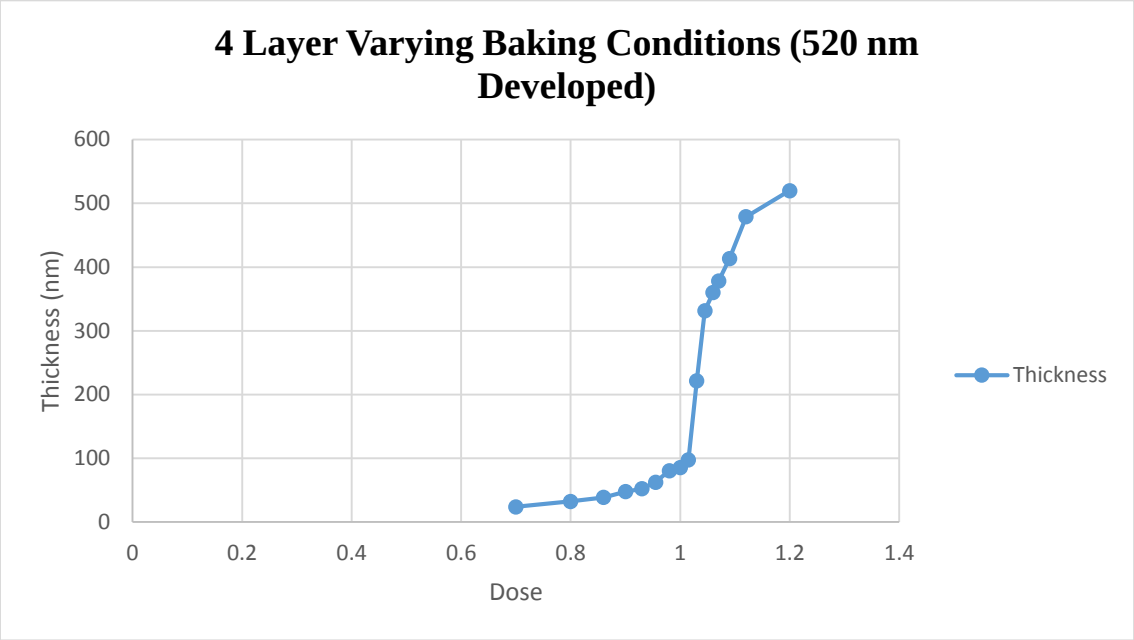

Figure 83. Thickness versus dosage relationship of a 520 nm developed double layer resist with varying baking conditions.

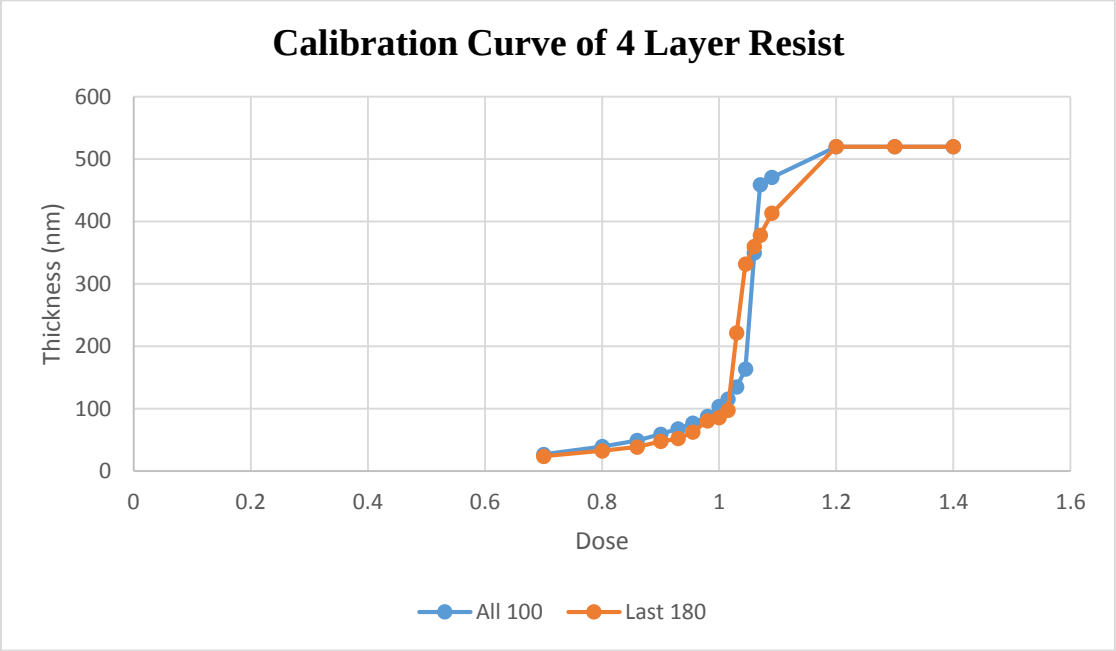

Figure 84. Thickness versus dosage relationship of a 520 nm developed four layer resist of different baking conditions.

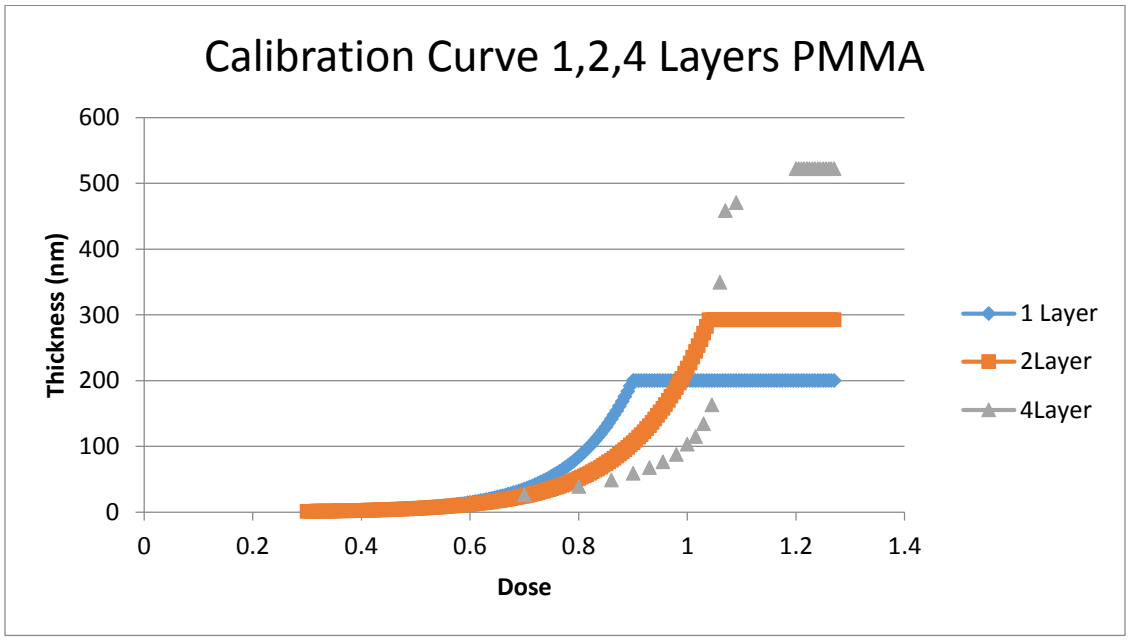

Figure 85. Thickness versus dosage relationship of a 1, 2,4 layer resist calibration curves.

CHAPTER 7

CONCLUSION

Baking condition is a critical factor that determines the resist's sensitivity to dosage exposure. When multi-layer resist is involved, backing condition becomes even more critical. Each layer must be baked at the optimal temperature and time in order to avoid over baking of the resist, yet the solvents in the resist must be completely evaporated in order to avoid the formation of bubbles from unreleased vapor in the bottom layer to the upper layer resist. Moreover, the bottom layer resist must be hard enough so that the upper layer resist wont mix and/or diffuse into the bottom layer resist. Lower temperatures could be used; however, it will take longer time to bake the resist. On the other hand, high temperatures can also be used, but when dealing with multi-layer resist the over baking of the bottom resist must be avoided. Over baking of the resist could cause cracking in the resist and/or degrades its chemical composition such that it requires further dosage modification to expose it. In addition, for each layer added a dosage recalibration and tuning of baking conditions must be performed in order to get the desired 3D structures. Moreover, the choice of the developer is also a critical factor that determines the topography of the 3D exposed structures. A strong developer might develop the top exposed resist and starts attacking the non-exposed resist by the time it starts to develop the bottom resist. On the other hand, a highly diluted developer could increase the developing time and reduce the contrast of the resist. Moreover, 3D proximity correction software must be used in order to avoid the double exposure of two neighboring structures.

CITED LITERATURE

1. I. Gibson, *Additive Manufacturing Technologies*. New York: Springer 2014.

2. B. Mueller, 'Additive Manufacturing Technologies – Rapid Prototyping to Direct Digital Manufacturing', *Assembly Automation*, vol. 32, no. 2, 2012.

3. A. Saxena and B. Sahay, *Computer aided engineering design*. New York: Springer, 2005.

4. ——, Marketsandmarkets.com, 'Additive Manufacturing Market - Forecasts 2012-17 | MarketsandMarkets', 2015. [Online]. Available:http://www.marketsandmarkets.com/Markets-Reports/additive-manufacturing-medical-devices-market-843.html.[Accessed:30-Mar-2015]

5. E. Sachs, M. Cima, P. Williams, D. Brancazio and J. Cornie, 'Three Dimensional Printing: Rapid Tooling and Prototypes Directly from a CAD Model', *Journal of Engineering for Industry*, vol. 114, no. 4, p. 481, 1992.

6. R. Guth, 'How 3-D Printing FiguresTo Turn Web Worlds Real', *WSJ*, 2007. [Online]. Available: http://www.wsj.com/articles/SB119742129566522283. [Accessed: 30- Mar- 2015].

7. A. Pilipović, P. Raos and M. Šercer, 'Experimental analysis of properties of materials for rapid prototyping', *Int J Adv Manuf Technol*, vol. 40, no. 1-2, pp. 105-115, 2007.

8. M. Göppert-Mayer, 'Über Elementarakte mit zwei Quantensprüngen', *Ann. Phys.*, vol. 401, no. 3, pp. 273-294, 1931.

9. W. Zhou, 'An Efficient Two-Photon-Generated Photoacid Applied to Positive-Tone 3D Microfabrication', *Science*, vol. 296, no. 5570, pp. 1106-1109, 2002.

10. K. Lee, R. Kim, D. Yang and S. Park, 'Advances in 3D nano/microfabrication using two-photon initiated polymerization', *Progress in Polymer Science*, vol. 33, no. 6, pp. 631-681, 2008.

11. K. Lee, D. Yang, S. Park and R. Kim, 'Recent developments in the use of two-photon polymerization in precise 2D and 3D microfabrications', *Polym. Adv. Technol.*, vol. 17, no. 2, p p. 72-82, 2006.

12. S. Maruo, O. Nakamura and S. Kawata, 'Three-dimensional microfabrication with two-photon-absorbed photopolymerization', *Opt. Lett.*, vol. 22, no. 2, p. 132, 1997.

CITED LITERATURE (Continued)

13. Y. Zhang, Q. Chen, H. Xia and H. Sun, 'Designable 3D nanofabrication by femtosecond laser direct writing', *Nano Today*, vol. 5, no. 5, pp. 435-448, 2010.

14. K. Ikuta, T. Ogata, M. Tsubio and S. Kojima, 'Development of mass productive micro stereo lithography (Mass-IH process)', *Proceedings of Ninth International Workshop on Micro Electromechanical Systems*, 1996.

15. L. Li, M. Hong, M. Schmidt, M. Zhong, A. Malshe, B. Huis in't Veld and V. Kovalenko, 'Laser nano-manufacturing – State of the art and challenges', *CIRP Annals - Manufacturing Technology*, vol. 60, no. 2, pp. 735-755, 2011.

16. Shi-Che Lo and Homg-Nian Wang, 'Near-field photolithography by a fiber probe', *Proceedings of the 2001 1st IEEE Conference on Nanotechnology. IEEE-NANO 2001 (Cat.No.01EX-516)*, 2001.

17. A. Tseng, 'Recent developments in micromilling using focused ion beam technology', *Journal of Micromechanics and Microengineering*, vol. 14, no. 4, pp. R15-R34, 2004.

18. S. Reyntjens and R. Puers, 'A review of focused ion beam applications in microsystem technology', *Journal of Micromechanics and Microengineering*, vol. 11, no. 4, pp. 287-300,2001.

19. J. Taniguchi, K. Koga, Y. Kogo and I. Miyamoto, 'Rapid and three-dimensional nanoimprint template fabrication technology using focused ion beam lithography', *Microelectronic Engineering*, vol. 83, no. 4-9, pp. 940-943, 2006.

20. ——, 'Atomic force microscope for 3-D resolution', *Precision Engineering*, vol. 12, no. 2, p.123, 1990.

21. D. Eigler and E. Schweizer, 'Positioning single atoms with a scanning tunnelling microscope', *Nature*, vol. 344, no. 6266, pp. 524-526, 1990.

22. C. Vieu, F. Carcenac, A. Pépin, Y. Chen, M. Mejias, A. Lebib, L. Manin-Ferlazzo, L. Couraud and H. Launois, 'Electron beam lithography: resolution limits and applications', *Applied Surface Science*, vol. 164, no. 1-4, pp. 111-117, 2000.

23. V. Manfrinato, L. Zhang, D. Su, H. Duan, R. Hobbs, E. Stach and K. Berggren, 'Resolution Limits of Electron-Beam Lithography toward the Atomic Scale', *Nano Letters*, p.1303211-02652000, 2013.

CITED LITERATURE (Continued)

24. S. Sun and G. Leggett, 'Matching the Resolution of Electron Beam Lithography by Scanning Near-Field Photolithography', *Nano Letters*, vol. 4, no. 8, pp. 1381-1384, 2004.

25. D. Bates, *Atomic and molecular processes*. New York: Academic Press, 1962.

26. Hyperphysics.phy-astr.gsu.edu, 'Mean Free Path, Molecular Collisions', 2015. [Online]. Available: http://hyperphysics.phy-astr.gsu.edu/hbase/kinetic/menfre.html#c3. [Accessed : 4 - Mar- 2015].

27. G. Elert, 'Dielectric Strength of Air', *Hypertextbook.com*, 2015. [Online]. Available: http://hypertextbook.com/facts/2000/AliceHong.shtml. [Accessed: 31- Mar- 2015].

28. S. Giere, M. Kurrat and U. Schumann, 'HV dielectric strength of shielding electrodes in vacuum circuit-breakers', *20th International Symposium on Discharges and Electrical Insulation in Vacuum*, 2002.

29. R. Gomer, 'Field, thermionic, and secondary electron emission spectroscopy', *Journal of Colloid and Interface Science*, vol. 102, no. 1, p. 311, 1984.

30. P. Cochems, M. Runge and S. Zimmermann, 'A current controlled miniaturized non-radioactive electron emitter for atmospheric pressure chemical ionization based on thermionic emission', *Sensors and Actuators A: Physical*, vol. 206, pp. 165-170, 2014.

31. J. Wittke, 'Electron Microprobe Techniques Class Notes', *Www4.nau.edu*, 2015. [Online]. Available: http://www4.nau.edu/microanalysis/Microprobe/ProbeNotes.html. [Accesseed: 31- Mar- 2015].

32. I. Appuhamilage, D. Adjei, S. Alatabi, R. Alnaimi, A. Michette and S. Pfauntsch, 'Development of a Soft X-ray Microprobe for Radiobiology Studies', *Acta Phys. Pol. A*, vol.125, no. 4, pp. 882-885, 2014.

33. D. Ye, S. Moussa, J. Ferguson, A. Baski and M. El-Shall, 'Highly Efficient Electron Field Emission from Graphene Oxide Sheets Supported by Nickel Nanotip Arrays', *Nano Letters*, vol. 12, no. 3, pp. 1265-1268, 2012.

34. J. Mutus, L. Livadaru, R. Urban, J. Pitters, A. Peter Legg, M. Salomons, M. Cloutier and R. Wolkow, 'Nanoscale structuring of tungsten tip yields most coherent electron point-source', *New J. Phys.*, vol. 15, no. 7, p. 073038, 2013.

CITED LITERATURE (Continued)

35. M. Schenk, M. Krüger and P. Hommelhoff, 'Strong-Field Above-Threshold Photoemission from Sharp Metal Tips', *Phys. Rev. Lett.*, vol. 105, no. 25, 2010.

36. P. Rai-Choudhury, *Handbook of microlithography, micromachining , and microfabrication*. Bellingham, Wash., USA: SPIE Optical Engineering Press, 1997.

37. W. Knauer, 'Boersch effect in electron-optical instruments', *J. Vac. Sci. Technol.*, vol. 16, no. 6, p. 1676, 1979.

38. S. Kim, B. Marelli, M. Brenckle, A. Mitropoulos, E. Gil, K. Tsioris, H. Tao, D. Kaplan and F. Omenetto, 'All-water-based electron-beam lithography using silk as a resist', *Nature Nanotech*, vol. 9, no. 4, pp. 306-310, 2014.

39. M. Gschrey, R. Schmidt, J. Schulze, A. Strittmatter, S. Rodt and S. Reitzenstein, 'Resolution and alignment accuracy of low-temperature in situ electron beam lithography for nanophotonic device fabrication', *Journal of Vacuum Science & Technology B, Nanothechnology and Microelectronics: Materials, Processing, Measurement, and Phenomena*,vol. 33, no. 2, p. 021603, 2015.

40. S. Okazaki, 'High resolution optical lithography or high throughput electron beam lithography: The technical struggle from the micro to the nano-fabrication evolution', *Microelectronic Engineering*, vol. 133, pp. 23-35, 2015.

41. J. Smith, N. Crosland, S. Doran, R. Dowling, J. Hartley, P. Hoyle, D. King, L. Kutcher, A.McClelland and M. Turnidge, 'Increased throughput, determined by a suite of benchmark patterns, in a Gaussian electron-beam lithography tool with a 100 MHz writing rate', *Alternative Lithographic Technologies VI*, 2014.

42. O. Yavas, C. Ochiai, M. Takai, A. Hosono and S. Okuda, 'Maskless fabrication of field emitter array by focused ion and electron beam', *Applied Physics Letters*, vol. 76, no. 22, p. 3319, 2000.

43. J. Sanabia, K. Burcham, J. Klingfus, G. Piaszenski, M. Kahl and R. Jede, 'Fixed Beam Moving Stage Electron Beam Lithography of Waveguide Coupling Device Structures', *Conference on Lasers and Electro-Optics 2012*, 2012.

44. R. Kendall, 'A servo guided X–Y–theta stage for electron beam lithography', *Journal of Vacuum Science & Technology B: Microelectronics and Nanometer Structures*, vol. 9, no. 6, p. 3019, 1991.

CITED LITERATURE (Continued)

45. I. Utke, S. Moshkalev and P. Russell, *Nanofabrication using focused ion and electron beams*. Oxford: Oxford University Press, 2011.

46. M. Cao, N. Zhang, T. Hu, F. Wang and W. Cui, 'Secondary electron emission from rough metal surfaces: a multi-generation model', *Journal of Physics D: Applied Physics*, vol.48, no. 5, p. 055501, 2015.

47. L.I. Aparshina, S.V. Dubonos, S.V. Maksimov, A.A. Svintsov, S.I. Zaitsev, *Energy dependence of proximity parameters investigated by fitting before measurement test*, Journal of Vacuum Science Technology B, 15(6), 2298-2302, 1997

48. H. Ibach and D. Mills, *Electron energy loss spectroscopy and surface vibrations*. New York: Academic Press, 1982.

49. M. Walz, F. Vollnhals, F. Rietzler, M. Schirmer, H. Steinrück and H. Marbach, 'Investigation of proximity effects in electron microscopy and lithography', *Applied Physics Letters*, vol. 100, no. 5, p. 053118, 2012.

50. T. Hoshino and K. Mabuchi, 'Closed-looped in situ nano processing on a culturing cell using an inverted electron beam lithography system', *Biochemical and Biophysical Research Communications*, vol. 432, no. 2, pp. 345-349, 2013.

51. ——, Www4.nau.edu, 'Electron Interaction with Matter: Volume', 2015. [Online]. Available: https://www4.nau.edu/microanalysis/Microprobe/Interact-Volume.html. [Accessed: 07- Apr- 2015].

52. Z. Ruan, P. Zhang, S. Mao, H. Li and Z. Ding, 'Monte Carlo Study of the Influence of Electron Beam Focusing to SEM Image Sharpness Measurement', *e-Journal of Surface Science and Nanotechnology*, vol. 12, no. 0, pp. 247-251, 2014.

53. D. Landau and K. Binder, *A guide to Monte Carlo simulations in statistical physics*. Cambridge: Cambridge University Press, 2000.

54. P. Rai-Choudhury, *Handbook of microlithography, micromachining, and microfabrication*. Bellingham, Wash.: SPIE Optical Engineering Press, 1997.

55. Nanolithography.gatech.edu, 'Proximity Effect in E-beam Lithography', 2015. [Online]. Available: http://nanolithography.gatech.edu/proximity.htm. [Accessed: 31- Mar- 2015].

CITED LITERATURE (Continued)

56. Soo-Young Lee and B. Cook, 'PYRAMID-a hierarchical, rule-based approach toward proximity effect correction. I. Exposure estimation', *IEEE Trans. Semicond. Manufact.*, vol. 11, no. 1, pp. 108-116, 1998.

57. T. Chang, 'Proximity effect in electron-beam lithography', *J. Vac. Sci. Technol.*, vol. 12, no.6, p. 1271, 1975.

58. R. Murali, 'Nanolithography', *MEMS Reference Shelf*, pp. 37-62, 2008.

59. S. Aya, K. Kise, H. Yabe and K. Marumoto, 'Validity of Double and Triple Gaussian Functions for Proximity Effect Correction in X-ray Mask Writing', *Japanese Journal of Applied Physics*, vol. 35, no. 1, 3, pp. 1929-1936, 1996.

60. G. Watson, 'A background dose proximity effect correction technique for scattering with angular limitation projection electron lithography implemented in hardware', *Journal of Vacuum Science & Technology B: Microelectronics and Nanometer Structures*, vol. 13, no. 6, p. 2504, 1995.

61. G. Owen, 'Methods for proximity effect correction in electron lithography', *Journal of Vacuum Science & Technology B: Microelectronics and Nanometer Structures*, vol. 8, no. 6, p. 1889, 1990.

62. P. Kotula, G. Rohrer and M. Marsh, 'Focused ion beam and scanning electron microscopy for 3D materials characterization', *MRS Bull.*, vol. 39, no. 04, pp. 361-365, 2014.

63. Y. Shi, S. Gao, M. Lu, W. Li and X. Xu, 'Segmental calibration for commercial AFM in vertical direction', *Eighth International Symposium on Precision Engineering Measurement and Instrumentation*, 2013.

64. F. Mohn, B. Schuler, L. Gross and G. Meyer, 'Different tips for high-resolution atomic force microscopy and scanning tunneling microscopy of single molecules', *Applied Physics Letters*, vol. 102, no. 7, p. 073109, 2013.

CITED LITERATURE (Continued)

65. H. Butt, K. Graf and M. Kappl, *Physics and chemistry of interfaces*. Weinheim: Wiley-VCH 2003.

66. J. Zhang, P. Chen, B. Yuan, W. Ji, Z. Cheng and X. Qiu, 'Real-Space Identification of Intermolecular Bonding with Atomic Force Microscopy', *Science*, vol. 342, no. 6158, pp.6-11-614, 2013.

67. J. Cox, *Fundamentals of linear electronics*. Albany: Delmar Thomson Learning, 2002.

68. S. Grutzik, R. Gates, Y. Gerbig, D. Smith, R. Cook and A. Zehnder, 'Accurate spring constant calibration for very stiff atomic force microscopy cantilevers', *Rev. Sci. Instrum.*,vol. 84, no. 11, p. 113706, 2013.

69. F. Giessibl, 'Advances in atomic force microscopy', *Reviews of Modern Physics*, vol. 75, no. 3, pp. 949-983, 2003.

70. J. Masajada, A. Popiołek-Masajada, I. Augustyniak and B. Sokolenko, 'Towards superresolition imaging with optical vortex scanning microscope',*Optical Measurement Systems for Industrial Inspection VIII*, 2013.

71. S. Santos, V. Barcons, H. Christenson, J. Font and N. Thomson, 'The Intrinsic Resolution Limit in the Atomic Force Microscope: Implications for Heights of Nano-Scale Features', *PLoS ONE*, vol. 6, no. 8, p. e23821, 2011.

72. V. Manfrinato, L. Zhang, D. Su, H. Duan, R. Hobbs, E. Stach and K. Berggren, 'Resolution Limits of Electron-Beam Lithography toward the Atomic Scale', *Nano Letters*, p.130-321102652000, 2013.

73. Microchem.com, 'PMMA: FAQs :: MicroChem', 2015. [Online]. Available: http://www.microchem.com/pmma_faq.htm. [Accessed: 01- Apr- 2015].

74. E. Tolstosheeva, E. Barborini, E. Meyer, M. Shafi, S. Vinti and W. Lang, 'Micropatterning of nanoparticle films by bilayer lift-off', *Journal of Micromechanics and Microenginee*ring vol. 24, no. 1, p. 015001, 2013.

CITED LITERATURE (Continued)

75. G. Research, *Polymethyl Methacrylate (PMMA) Market Analysis By Application (Construction, Electronics, Automotive, Signs & Display), By Product (Extruded Sheets, Cell Cast Sheet & Blocks, Pellets, Beads) And Segment Forecasts To 2020*. San Francisco: Grand View Research, 2014.

76. C. Wolf-Brandstetter, S. Roessler, S. Storch, U. Hempel, U. Gbureck, B. Nies, S. Bierbaum and D. Scharnweber, 'Physicochemical and cell biological characterization of PMMA bone cements modified with additives to increase bioactivity', *J. Biomed. Mater. Res.*, vol. 101, no. 4, pp. 599-609, 2012.

77. C. Thorne, W. Grabb and J. Smith, *Grabb and Smith's plastic surgery*. Philadelphia: Wolters Kluwer Health/Lippincott Williams & Wilkins, 2007.

78. P. Manson, W. Crawlgy, J. Hoopes and S. Wolfe, 'Frontal Cranioplasty', *Plastic and Reconstructive Surgery*, vol. 77, no. 6, pp. 901-904, 1986.

79. W. Zhang, A. Abang, D. Webb and G. Peng, 'Wavelength Drift of PMMA-Based Optical Fiber Bragg Grating Induced by Optical Absorption', *IEEE Photonics Technology Letters*, vol. 27, no. 4, pp. 336-339, 2015.

80. ——, Swicofil.com, 'Polymethyl methacrylate PMMA polymer monofilaments and fibers', 2-015. [Online]. Available:http://www.swicofil.com/products/278polymethylmethacrylate.html.[Accessed: 01- Apr- 2015].

81. S. Mac Rae, M. Matsuda, S. Shellans and L. Rich, 'The Effects of Hard and Soft Contact Lenses on the Corneal Endothelium', *American Journal of Ophthalmology*, vol. 102, no. 1, pp. 50-57, 1986.

82. L. Upadhyaya, J. Singh, V. Agarwal and R. Tewari,'The implications of recent advances in carboxymethyl chitosan based targeted drug delivery and tissue engineering applications', *Journal of Controlled Release*, vol. 186, pp. 54-87, 2014.

83. ——, Microchem.com, 'SU-8 Negative Epoxy Series Resists - MicroChem', 2015. [Online]. Available: http://www.microchem.com/Prod-SU8_KMPR.htm. [Accessed: 01- Apr-20-2015].

CITED LITERATURE (Continued)

84. R. Joyce, K. Singh, S. Varghese and J. Aktar, 'Effective cleaning process and its influence on on surface roughness in anodic bonding for semiconductor device packaging', *Materials Science in Semiconductor Processing*, vol. 31, pp. 84-93, 2015.

85. ——, Microchem.com, 'BioMEMS and microfluidic applications through SU-8 Surface Modification', 2015. [Online]. Available: http://www.microchem.com/Appl-MEMs-Surface-Mod.htm. [Accessed: 01- Apr- 2015].

86. S. Huang, S. Wang, C. Hsieh, Y. Lin, C. Lai and M. Wu, 'An integrated microfluidic cell culture system for high-throughput perfusion three dimensional cell culture based assays: effect of cell culture model on the results of chemosensitivity assays', *Lab on a Chip*, vol. 13, no. 6, p. 1133, 2013.

87. Y. Yoon, D. Lee and J. Lee, 'Surface modified nano-patterned SU -8 pillar array optically transparent super-hydrophobic thin film', *Journal of Micromechanics and Microengineering*, vol. 22, no. 3, p. 035012, 2012.

88. Q. Hamid, C. Wang, J. Snyder and W. Sun, 'Surface modification of SU-8 for enhanced cell attachment and proliferation within microfluidic chips', *J. Biomed. Mater. Res.*, vol. 103, no. 2, pp. 473-484, 2014.

89. ——, Householdproducts.nlm.nih.gov, 'Household Products Database - Health and Safety Information on Household Products', 2015. [Online]. Available: http://householdproducts.nlm.nih.gov/cgi-bin/household/brands?tbl=brands&id=21003001. [Accessed:01-Apr-2015].

90. P. Kim, W. Adorno-Martinez, M. Khan and J. Aizenberg, 'Enriching libraries of high aspect-ratio micro- or nanostructures by rapid, low-cost, benchtop nanofabrication', *Nature Protocols*, vol. 7, no. 2, pp. 311-327, 2012.

91. Y. Barrandon and H. Green, 'Cell size as a determinant of the clone-forming ability of human keratinocytes.', *Proceedings of the National Academy of Sciences*, vol. 82, no. 16, pp.5390-5394, 1985.

VITA

NAME: Khodr Maamari

EDUCATION: B.S., Electrical Engineering, University of Illinois at Chicago, Chicago, Illinois, 2012.

M.S., Electrical Engineering, University of Illinois at Chicago, Chicago, Illinois, 2014.

Ph.D., Electrical Engineering, University of Illinois at Chicago, Chicago, Illinois, 2015.

EXPERIENCE: Graduate Research Assistant, University of Illinois at Chicago, Chicago; Nanotechnology Core Facility, Summer 2012 - Summer 2015.

Teaching Assistant, University of Illinois at Chicago, Chicago; Network Analysis, Fall 2012; Filter Synthesis, Spring 2013.

PUBLICATIONS: J. Sautner et al., "Vortex Transformation in 3-D Nano-structures", MTI and ITS FALL Workshop 2013: Coherent Hybrid Structures on the Mesoscale, Evanston, Illinois (2013).

M. Purahmad et al., "A MEMS-based Resistive Vacuum Gauge with Voltage Readout", 26th International Vacuum Nanoelectronics Conference (IVNC), Roanoke, Virginia (2013).

K. Maamari et al., "3D Electron Beam Lithography for Biomedical Applications", International Workshop Nanoscale Spectroscopy and Nanotechnology, Chicago, Illinois (2014).

T. Grzebyk et al., "Integration of a MEMS-type Vacuum Pump with a MEMS-type Pirani Pressure Gauge", Journal of Vacuum Science and Technology B, Nanotechnology and Microelectronics: Materials, Processing, Measurement, and Phenomena, vol. 33, no. 3, pp. 03C103 (2015).